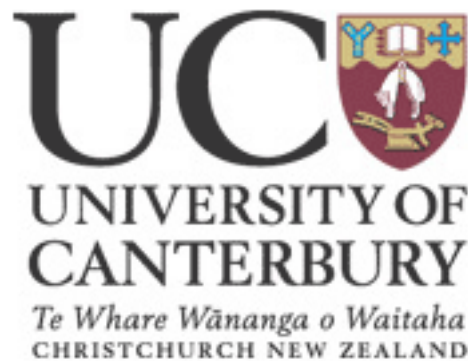


A Battery Equalisation System for Electric Vehicle

A thesis submitted in partial fulfillment
of the requirements for the degree of
Master of Engineering
at the
University of Canterbury
Christchurch, New Zealand



**Department of
Electrical and Computer Engineering**

By
Ming-Kuang(Leo) HSIEH, BE (Hons)
09 July 2007

Abstract

In 1999, the Electrical and Computer Engineering Department at the University of Canterbury started building their third electric vehicle (EV3) based on a TOYOTA MR2 with the goal of building a higher performance vehicle to match present combustion engine vehicles. The car is powered by 26 12volt sealed lead-acid batteries connected in series to achieve a nominal 312V DC source.

A battery voltage equaliser is a device that draws energy from a higher charged battery, then discharges into a lower charged battery. The need for a voltage equaliser is principally due to the differences in cell chemistry, temperature gradients along the battery string and the ages of the batteries. During the charging or discharging process, some batteries reach their nominal voltage or reach deep discharge states before the others. Then if the charger keeps charging the batteries or the load keeps drawing energy from these batteries, it results in damage to the batteries. Therefore maintaining the charge level on each battery becomes important. In addition, it also improves the battery life and vehicle travelling range.

This thesis details the analysis of three different types of battery equaliser, which are based on a 24W buck-boost converter, 192W buck-boost converter and 192W flyback converter. In this design, all converters are designed to work under current mode control with average of 2A. To make each converter install without significant effect on the performance and the cost, each converter is also built with the goals of being small, lightweight, cost effective, flexible for mounting, maintenance free and highly efficient.

At the end, the prototype battery equalisation converters were designed, constructed and tested, and the efficiencies from each converter are measured around 90 ~ 92%. The experimental results show two banks of series connected batteries can be successfully equalised by the designed equaliser. This thesis covers the design, simulation and the construction procedures of this battery equaliser system, and also details on some considerations and possible future improvement that were found during the experimental test.

Acknowledgment

First and foremost, I would like to express my gratitude to my supervisors, Associate Professor Richard Duke and Dr. Simon Round for their advice, guidance, encouragement and being very patient throughout this project.

I would also like to thank all the members in the Power Electronics Research Group (William Chen, Si-Kuok Ting, Irene Ting, John and Ari) for giving me good advice and being as a good family in this research group. Special thanks to technician Ron Battersby, Ken Smart, Dudley Berry, Scott Lloyd and Nick Smith in the laboratory and sharing their practical experiences.

To my family in Taiwan and in New Zealand, I like to express my appreciation to all my family members, especially my parents and brother in Taiwan who supported me during my entire study period. For my boarding family in New Zealand, Brian Baker and Veronica Baker, who always look after my living and health over the years. Last but not least, I would also like to say thank you to Pastor Albert Tang for being a great teacher, a brother and being a great spiritual supporter to me.

Table of contents

| | |
|---|------|
| Abstract | i |
| Acknowledgment | ii |
| Table of contents | iii |
| Table of Figures | v |
| Table of Tables | vii |
| Publication arising from this thesis | viii |
| | |
| 1 Introduction..... | 1 |
| 1.1. Project overview..... | 1 |
| 1.2. Thesis structure..... | 4 |
| | |
| 2 Battery Monitoring and Equaliser Topologies..... | 6 |
| 2.1. Battery monitoring..... | 7 |
| 2.2. Common bus topology..... | 7 |
| 2.3. Common core topology..... | 10 |
| 2.4. Ring topology..... | 11 |
| 2.5. Selection of voltage equaliser configuration for EV3..... | 13 |
| | |
| 3 Converter design..... | 17 |
| 3.1. The 24W buck-boost converter..... | 17 |
| 3.1.1. The PWM controller..... | 18 |
| 3.1.2. Average current mode control..... | 19 |
| 3.1.3. The gate drive..... | 20 |
| 3.1.4. The power converter of the 24W buck-boost converter..... | 21 |
| 3.2. The 192W buck-boost converter..... | 31 |
| 3.3. The 192W flyback converter..... | 32 |
| 3.3.1. PWM controller for the 192W flyback converter..... | 33 |
| 3.3.2. 192W flyback transformer..... | 34 |
| 3.3.3. Reducing the voltage stress on MOSFETs..... | 37 |
| 3.4. Summary..... | 39 |

| | | |
|----------|--|----|
| 4 | Converters simulations..... | 40 |
| 4.1. | 24W buck-boost converter..... | 41 |
| 4.2. | 192W buck-boost converter..... | 43 |
| 4.3. | 192W flyback converter..... | 45 |
| 4.4. | Summary..... | 48 |
| 5 | The system construction..... | 49 |
| 5.1. | The 24W Buck-boost converter..... | 49 |
| 5.1.1. | Inductor design..... | 49 |
| 5.1.2. | MOSFET selection..... | 52 |
| 5.2. | The 192W Buck-boost converter..... | 54 |
| 5.3. | The 192W Flyback converter..... | 55 |
| 5.4. | Summary..... | 59 |
| 6 | Performance records..... | 57 |
| 6.1. | Battery equalisation between non-isolated banks..... | 59 |
| 6.2. | Battery equalisation between isolated banks..... | 63 |
| 6.3 | Summary..... | 58 |
| 7 | Conclusion..... | 70 |
| Appendix | | 73 |
| | The schematics of 24W buck-boost converter..... | 74 |
| | The schematics of 192W buck-boost converter..... | 75 |
| | The schematics of 192W flyback converter..... | 76 |
| | The PCB of 24W buck-boost converter..... | 77 |
| | The PCB of 192W buck-boost converter..... | 78 |
| | The PCB of 192W flyback converter..... | 79 |
| | The data sheet of E32 planar inductor..... | 80 |
| | The data sheet of E43 planar inductor | 81 |
| | The data sheet of SUD35N05-26L MOSFET..... | 82 |
| | The data sheet of IRF740 MOSFET..... | 84 |

Table of Figures

| | |
|---|----|
| Figure 1.1. Battery location..... | 2 |
| Figure 2.1. The common bus equaliser..... | 8 |
| Figure 2.2. The common core equaliser..... | 10 |
| Figure 2.3. The ring equaliser..... | 11 |
| Figure 2.4. The proposed voltage equaliser structure..... | 13 |
| Figure 2.5. The efficiency comparison of buck-boost and Cuk converters..... | 14 |
| Figure 2.6. The proposed voltage equaliser structure..... | 15 |
| Figure 3.1. The Buck-boost converter..... | 17 |
| Figure 3.2. The block diagram of SG3526..... | 18 |
| Figure 3.3. The average current mode control circuit..... | 19 |
| Figure 3.4. The RM core power rating curve..... | 23 |
| Figure 3.5. 3C90 B-H curve..... | 25 |
| Figure 3.6. The construction of the planar inductor..... | 27 |
| Figure 3.7. The track width versus temperature rise diagram..... | 28 |
| Figure 3.8. The construction of the integrated inductor..... | 29 |
| Figure 3.9. The flyback converter..... | 32 |
| Figure 3.10. The PWM controller for the 192W flyback converter..... | 33 |
| Figure 3.11 Flyback converter with clamping circuit..... | 38 |
| Figure 4.1. 24W non-isolated buck-boost converter..... | 41 |
| Figure 4.2. The switching waveforms of the 24W buck-boast converter..... | 42 |

| | |
|---|----|
| Figure 4.3. 24W buck-boost converter equalisation..... | 43 |
| Figure 4.4. 192W buck-boost converter..... | 44 |
| Figure 4.5. 192W buck-boost converter switching waveforms..... | 44 |
| Figure 4.6. 192W buck-boost converter equalisation..... | 45 |
| Figure 4.7. The schematic of the 192W flyback converter..... | 46 |
| Figure 4.8. 192W flyback converter switching waveforms..... | 46 |
| Figure 4.9. 192W flyback converter equalisation..... | 47 |
| | |
| Figure 5.1. RM, planar inductor and integrated inductors efficiency comparison..... | 50 |
| Figure 5.2. The inductor for the 24W buck-boost converter..... | 52 |
| Figure 5.3. The photo of the 24W Buck-boost battery equaliser..... | 53 |
| Figure 5.4. 24W buck-boost converter action waveforms..... | 53 |
| Figure 5.5. The 192W buck-boost converter..... | 55 |
| Figure 5.6. The frequency response curve of the 192W flyback converter..... | 56 |
| Figure 5.7 The switching waveform with/without the clamping circuit..... | 57 |
| Figure 5.8 The photo of the 192W flyback converter..... | 57 |
| Figure 5.9. The switching waveform of the 192W flyback converter..... | 58 |
| | |
| Figure 6.1. The equalisation setup..... | 60 |
| Figure 6.2. Equalisation procedure..... | 62 |
| Figure 6.3. The setup diagram for non-isolated bank equalisation..... | 63 |
| Figure 6.4. Battery equalisation process for an eight series connected batteries..... | 65 |
| Figure 6.5. The setup diagram for isolated bank equalisation..... | 66 |
| Figure 6.6. Equalisation process for the isolated battery banks..... | 68 |

Table of Tables

| | |
|---|----|
| Table 2.1. Comparison of equaliser topologies..... | 13 |
| Table 4.1. The open-circuit voltages after 30A of 60 minutes discharge..... | 40 |
| Table 6.1. The measured battery open-circuit voltages..... | 63 |
| Table 6.2. The measured battery open-circuit voltages..... | 67 |

Publication arising from this thesis

Ming-Kuang(Leo) HSIEH, Simon Round, Richard Duke, “*An Investigation Of Battery Voltage Equalization Topologies For An electric Vehicle*”, accepted to be published at the Australian Universities Power Engineering Conference (AUPEC 2004). Christchurch, New Zealand, September 2004

1. Introduction

1.1. Project overview

The first electric car was invented by Thomas Davenport in 1834. At that time, the battery used in the car was not rechargeable. In the next few decades, numbers of electric cars and rechargeable battery technologies were developed, which brought more attention to investigate electric vehicle (EV) development. In the late 1890s EVs outsold gasoline cars ten to one. EVs dominated the roads and dealer showrooms. Some automobile companies, like Oldsmobile and Studebaker actually started out as successful EV companies, only later transitioning to gasoline-powered vehicles. In fact, the first car dealerships were exclusively for EVs[1].

Early production of EVs, like all cars, was accomplished by hand assembly. In 1910, volume production of gasoline powered cars was achieved with the motorised assembly line. This breakthrough manufacturing process killed off all but the most well-financed car builders. Independents, unable to buy components in volume died off. The infrastructure for electricity was almost non-existent outside of city boundaries, limiting EVs to city-only travel. Another contributing factor to the decline of EVs was the addition of an electric motor (called the starter) to gasoline powered cars, finally removing the need for the difficult and dangerous crank to start the engine. Due to these factors, by the end of World War I, production of electric cars stopped and EVs became niche vehicles, serving as taxis, trucks, delivery vans, and freight handlers[1].

In the late 1960s and early 1970s, there was a rebirth of EVs, which was prompted by concerns about air pollution and the OPEC oil embargo. In the early 1990s, a few major automakers resumed production of EVs, prompted by California's landmark Zero Emission Vehicle (ZEV) mandate. Those EVs were produced in very low volumes, essentially hand-built like their early predecessors. However, as the ZEV mandate was weakened over the years, the automakers stopped making EVs and Toyota was the last major manufacturer to stop EV production in 2003[1].

In the past thirty years, the University of Canterbury has also been investigating and developing its own EVs. The original EV was developed to test motor speed control ideas for AC induction motors.[2] In 1982, the second EV was developed, and that was based on a Austin Farina and powered by 20 series connected lead-acid batteries to form a nominal 240V dc bus. In 1999 the development of the third EV started with the goal of building a higher performance vehicle to match present combustion engined vehicles.

The third electric vehicle (EV3) produced by the Electrical and Computer Engineering Department at the University of Canterbury is based on a TOYOTA MR2. It is powered by 26 Hawker Genesis 12volt 26A-hour sealed lead-acid batteries connected in series to achieve a nominal 312V DC source and these batteries are conveniently divided into four banks by the constraints of their location in the car. The first bank consists of 8 batteries, which are located under the front bonnet of the MR2. The second bank consists of 6 batteries and is placed in the engine bay at the back. The third and the fourth banks consist of 6 batteries each and are located in the rear boot. These battery locations are shown in *Figure 1.1*.

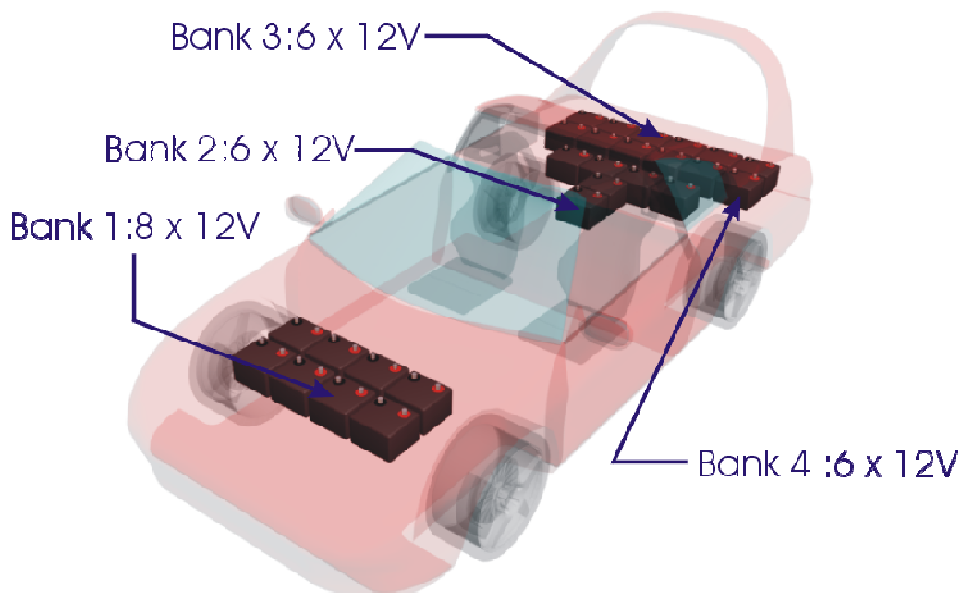


Figure 1.1. Battery location

Maintenance of cells at an equalised charge level is critical for enhancing battery life[1]. The need for a voltage equaliser is principally due to the differences in cell chemistry, temperature gradients along the battery string and the ages of the batteries. During the charging process, some batteries will consequently reach full charge before others and before the overall battery terminal voltage reaches its nominal value[1]. Therefore, if the charger continues to charge the remaining batteries, it would result in overheating the fully charged batteries, thus reducing their useful life. The same principle can also be applied to the discharging process. Any over-discharge would lead a battery into deep discharge, which can also reduce the life of the battery and decrease the travelling range of the electric vehicle.

The idea of a basic battery equaliser is to balance the charge level of two batteries by drawing energy from the one with the higher charge and transferring it to the other. To achieve this, a high frequency dc-dc converter is used. In power electronics, every converter has its own energy storage, which can be an inductor, a capacitor, a transformer or some combination of these. By controlling the switching signal, this energy storage capacity can be charged from the source and then discharged to the load. In a battery equaliser, the overcharged battery can be considered as the source and the undercharged battery as the load.

The objective of this thesis is to investigate various battery equalisation topologies that could be implemented into the EV3 to equalise the charge level of each individual battery within the entire battery string. Since there is a total of 26 batteries that need to be equalised, a number of equalisers have to be built for the entire battery string. Therefore, the design of each equaliser must be small, lightweight, cost effective, easy to interface, flexible for mounting, maintenance free and highly efficient.

An additional complication arises from the fact that these 26 batteries are not all located in a single compartment of the vehicle. In addition to having an equaliser capable of transferring energy between adjacent batteries, energy must also be able to be transferred between the battery banks (*Figure 1.1*) and between the top and bottom of the entire string.

1.2. Thesis structure

In this thesis; various types of voltage equaliser topologies, which include the common core, common bus and ring equalisers are investigated. In Chapter two the principles of each equaliser topology are described. It demonstrates how the dc-dc converter can be used to interface between two batteries or two banks of batteries and then transfer the energy from one to the other. To design the most suitable equaliser for the EV3, the advantages and disadvantages of each topology, based on this construction, cost and future upgradeability are listed.

In Chapter three the design procedures of the dc-dc converters making up the equaliser are detailed. To minimise the converter size and to increase the manufacturability, various type of inductors, such as RM core, planar core and integrated inductor are also investigated. In this chapter, all electric specifications including the power rating, current ripple and the strategy of the control circuit of each converter are also defined.

In chapter four the simulations of all dc to dc converters making up the chosen equaliser topology are described. To achieve realistic results of simulations, discharging test measurements over eight series connected lead-acid batteries was first carried out. The result of these tests gives an indication of the possible voltage variations for each battery. The simulation is carried out by Pspice simulator and each rechargeable battery is modelled as a 1F capacitor. The simulation results demonstrate that the selected converters can be successfully used in the battery equalisation system.

In Chapter five the construction of each converter and their control circuits are detailed. In this battery equalisation system, each converter is designed to operate at a fixed current rate of 2A. Therefore current mode control is implemented into every converter. In the design of the power converter, the performance comparison of the RM cored inductor, the integrated inductor and the planar inductor are also investigated in order to determine the best solution for each converter to meet the requirement of light weight and low profile format.

In Chapter six, two sets of equalisation results for the battery equalisation system are obtained. These equalisation tests are based on equalising two banks of four series connected batteries. Before each equalisation test, all batteries are equally charged to 13V. In the first equalisation test, the two banks are connected in series, which forms an eight series connected batteries string. Then the equalisation of individual batteries is done by seven buck-boost converters after the entire string battery has been discharged for an hour at a rate of 30A. After that, the 192W non-isolated buck-boost converter equalises the two banks of batteries to ensure each bank has an equal charge level. In the second equalisation test, the two banks of four series connected batteries are isolated from each other and the equalisation between each bank is done by an isolated flyback converter.

In Chapter seven, the conclusion finalises the overall design process and summarises the outcome. The difficulties and some considerations from the design of each converter are also described. In addition, some possible future investigations are also pointed out.

References:

- [1] Electric Vehicle History. May 2005. Electric Auto Association (EAA),
<http://www.eaaev.org/Flyers/eaaflyer-evhistory.pdf>
- [2] Richard Duke, “Construction and Performance of an Electric Toyota MR2”,
Departmental seminar, 2005

2. Battery Monitoring and Equaliser Topologies

The idea of a battery equaliser is to balance the charge level of two or more batteries by drawing energy from the one with the higher charge and then discharging to a lower level battery. The most efficient means of achieving this transfer is by using a high frequency dc-dc converter. In power electronics, every converter has an energy storage, which may be an inductor, a capacitor, a transformer or some combination of these. By controlling the converter's switching signal, this energy storage capacity is normally charged from the source then discharged to the load. In a battery equaliser the overcharged battery can be considered as the source and the undercharged battery as the load.

To design the most suitable voltage equaliser for the EV3, there are a number of concerns that have to be addressed. Due to the limited space in the car, the battery equaliser has to be compact. Further, since there are 26 lead-acid batteries in the car, a large number of battery equalisers are required in order to efficiently balance each individual battery. This makes the cost, construction, manufacturability and efficiency of the battery equaliser important aspects to consider.

The batteries used in the EV3 are rated at 26Ahr, and the equalisation rate is proportional to the operational current of the equalisation system. Unfortunately higher operational current brings larger power losses from the system, which results in increased switching losses. In order to achieve a reasonably fast equalisation rate and to minimise the power loss from the converter, the average operational current for this equalisation system is set to 2A.

In this Chapter, Section 2.1 describes two common battery monitoring techniques; the coulometric and the open-circuit battery monitoring techniques, and how these techniques could be implemented into the EV3. In Sections 2.2, 2.3 and 2.4; three battery equalisation topologies common bus, common core and ring are detailed. Their construction, the component counts, and the operating principles are also discussed. In Section 2.5 a summary of these three topologies is given, and a decision is made to identify the best solution for constructing a suitable battery equalisation network for the EV3.

2.1. Battery monitoring

The maintenance of cells at an equalised charge level is critical for enhancing battery life[1]. There are numbers of ways to monitor the charge level of a lead-acid battery, and the most common techniques are Coulometric measurement and open-circuit voltage measurement. Coulometric measurement counts the ampere-hours either coming out of or going into the battery bank. In its most basic form the battery capacity is assumed to be fixed, and then a sensor has to be used for every battery in order to determine how much energy has been drawn from or has flowed into the battery. In reality the total battery capacity varies with the discharge current, the type of discharge, temperature and the age of the battery[2]. Open-circuit voltage can be used to determine the state of charge and is more suited to battery monitoring in an electric vehicle, since the open-circuit voltage can be measured directly from standard battery terminals. The open-circuit voltage of a sealed lead-acid battery also relates directly to the battery's state of charge[3]. The main drawback of the open circuit voltage monitoring technique is that the open-circuit voltage must stabilise before a reliable measurement can be made, and this can take from half an hour to several hours depending on the type of battery[3].

2.2. Common bus topology

The common bus equaliser topology is shown in *Figure 2.1*. There are two different types of common bus equaliser topologies. For both common bus equaliser topologies; energy transformation for each battery is done using an isolated DC-DC converter, which can be a flyback, push-pull, half-bridge or full-bridge converter.

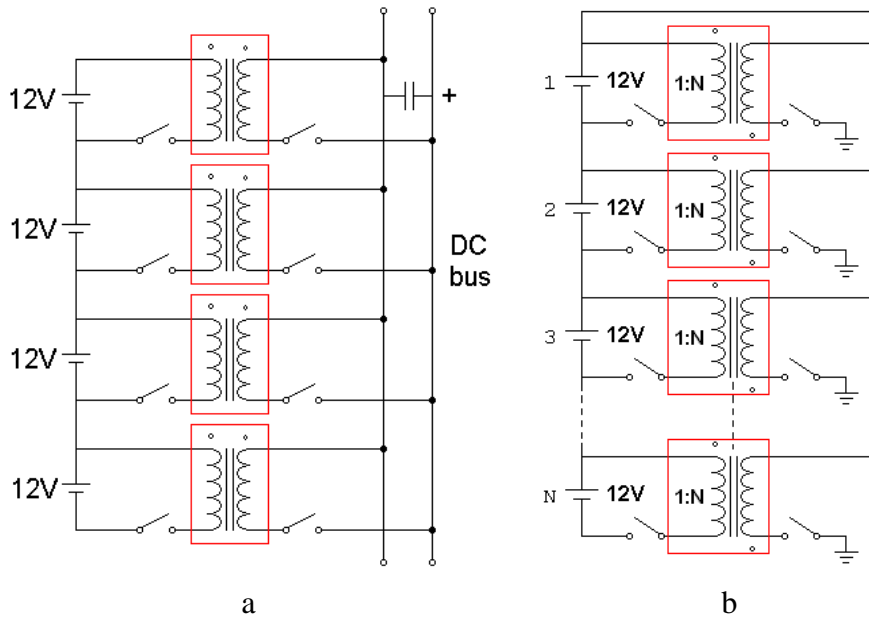


Figure 2.1. The common bus equaliser

In the first common bus equaliser shown in *Figure 2.1.a*, the temporary energy storage is the common bus, which can be made up from a capacitor bank or a separate rechargeable battery. Energy transformation between any batteries in the series connected battery string is done by using the isolated converter to draw the energy from the higher charged battery, store the energy onto the common bus, and then using the other isolated converter to discharge this energy into the lower charged battery[1].

In the second common bus equaliser shown in *Figure 2.1.b*, there is no intermediate energy storage unit. When one battery is overcharged; the associated isolated converter will draw the energy from this overcharged battery, and then recharge the entire battery string [1]. On the other hand, if one battery is under-charged, the battery equalisation system would take the energy from the whole battery string to recharge the under-charged battery via its associated isolated converter.

Both common bus topologies would be good for a single long string of batteries, because the converters are all individually attached to the common bus, and the batteries and common bus are isolated from each other. Therefore only two steps are required to transfer energy between any two batteries. Probably the most negative aspect of this topology is that each and every converter requires a transformer to provide electrical isolation between the battery and the common bus.

Comparing these two common bus equalisers, the first common bus equaliser shown in *Figure 2.1.a* has the advantage of flexibility of the transformer ratio and is better for future expansion. Since the voltage rating on each side of the transformer is identical, the transformer ratio of the primary and secondary windings can be made as 1:1, which means the transformer ratio is not affected by the total number of the series string battery. So if any battery is required to be added to or removed from the electric vehicle, this common bus topology is very flexible for future expansion. However the major drawback of this common bus equaliser topology is due to the extra set of capacitors or battery used on the common bus side as the temporary energy storage, which brings an additional cost.

The second common bus equaliser does not require any additional capacitor or battery bank as the temporary energy storage, therefore the component count is less than the first common bus topology. Although this equaliser has the advantage of a low component count, the transformer primary to secondary turns ratio for each converter has to be kept as 1:N, where N is the total number of batteries in the whole series string. Therefore if the total number of batteries is large, the weight of the transformer would be relatively heavier compared with the first common bus topology, because the number of turns on one side of the transformer has to be N times larger than the other side. This may also require the converter to use larger transformer, since these extra turns require more winding space. The other disadvantage of this common bus topology is because the turns ratio N has to be made equal to the total number of batteries, therefore this restricts the possibility of future changes such as adding some extra batteries to or withdrawing some battery from the battery string. Further, since one side of the transformer is always connected to the high voltage battery string and if batteries are spread in different compartments of the vehicle, the high common bus voltage would be required to be routed throughout the vehicle, which brings an additional safety concern.

2.3. Common core topology

The common core topology is shown in *Figure 2.2*. Compared with the common bus topology, the common core topology uses identical numbers of isolated dc-dc converters to equalise every battery. The difference is that in the common core topology all windings have to be coupled to the common core, which is the energy storage unit in this topology. The principle of this topology is that once the overcharged battery is detected; the converter will charge the common core by drawing the energy from the overcharged battery. Then distributing the stored energy in the common core to every battery along the series connected string battery via the diode, where the largest portion of the stored energy will be directed to the lowest voltage battery without any additional control [1].

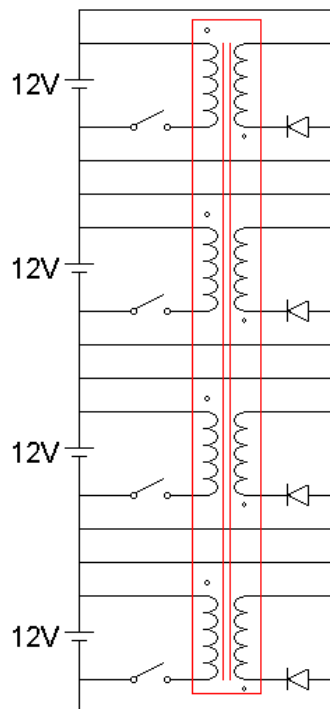


Figure 2.2. The common core equaliser

The common core topology is a good solution for a long string of batteries. However the problem with this topology is that this scheme has a fairly high sensitivity to the leakage inductance between secondary windings. Any slight mismatch of the secondary windings would lead the charge on each battery to remain unbalanced after the equalisation process [1]. To minimise this problem; the obvious requirement is that all batteries must be located in the same compartment and the transformer winding all have to be wound on the same

core in order that all the secondary windings have identical inductance. In the EV3; the 26 batteries are divided into four banks and placed in three different compartments, which makes the common core topology difficult to implement. The other problem with this topology is that when dealing with large numbers of batteries in the string, a larger transformer core is required, which makes the equaliser difficult to mount, especially if space is a concern [1].

2.4. Ring topology

The ring equaliser topology is shown in *Figure 2.3*. In this topology, the entire series string of batteries is considered as a ring. Within the string of batteries; every two adjacent batteries are linked by a non-isolated dc-dc converter and where the top and the bottom batteries are linked by an isolated converter to overcome the potential difference [1].

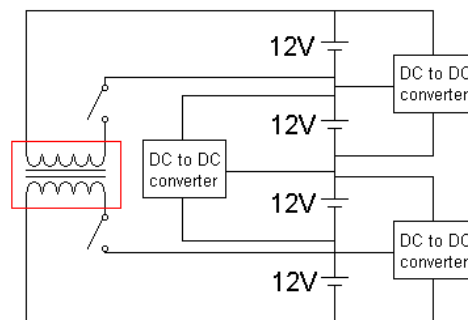


Figure 2.3. The ring equaliser

The principal attraction of this topology over the other topologies is that only one converter needs to be isolated. The non-isolated converters can be constructed in compact, lightweight and low profile formats. However the disadvantage of this topology is because each converter can only transfer the energy to or from adjacent batteries. Therefore for any two batteries separated a few batteries away from each other, the equalisation system has to draw the energy from the higher charged battery, and then transfer the energy through each individual battery between them to charge the lower charged battery, which can make the overall system inefficient.

The non-isolated converters used in this topology could be either buck-boost or Cuk converters. In terms of manufacturability, the buck-boost converter has the advantage of a low component count, therefore the cost and the size of the converters can be kept to a minimum. By comparing the converter efficiency, due to the lower current ripple, the Cuk converter has higher efficiency than the buck-boost converter, which is important for high power transformation. To choose the most suitable non-isolating converter for the ring equaliser is dependent on how much power the converter needs to transfer. If the power rating is small, the extra power loss from the buck-boost converter could be negligible, and using fewer components could also reduce the manufacturing cost.

The isolated converter in this equaliser is used to provide electrical isolation and achieve energy transformation between the top and the bottom batteries of the string. Unlike the previous topologies, the ring topology only requires one isolated converter, and the turns ratio of the transformer is 1:1. This makes the isolated converter relatively easy to design, because this converter can work independently with no need to take the other converters into account.

The advantage of the ring topology is that all the converters work independently and the non-isolated converters can be made in a compact lightweight and low profile format. Since any battery and converter can be added on or taken off the battery string without affecting the others, this topology becomes easy for future expansion and mounting.

2.5. Selection of voltage equaliser configuration for EV3

A summarised comparison table of equaliser topologies is shown in *Table 2.1*.

| | Common bus | Common core | Ring |
|----------------|---|--|---|
| For | <ul style="list-style-type: none"> • Good for long battery string • Easy for future expansion | <ul style="list-style-type: none"> • Good for long battery string • Simple control | <ul style="list-style-type: none"> • Can be made in small size and light weight • Easy for future expansion |
| Against | <ul style="list-style-type: none"> • Converter requires transformer | <ul style="list-style-type: none"> • Converter requires transformer • Inflexible for future expansion • Inflexible for mounting | <ul style="list-style-type: none"> • Inefficient to transfer the energy to the remote battery |

Table 2.1. Comparison of equaliser topologies

For the EV3 application, the ring structure is the most appropriate because most of the converters can satisfy the requirement of being small, non-isolated and easily manufacturable. In fact only one converter connected between the top and bottom of the battery string needs transformer isolation, and the proposed configuration is shown in *Figure 2.4*.

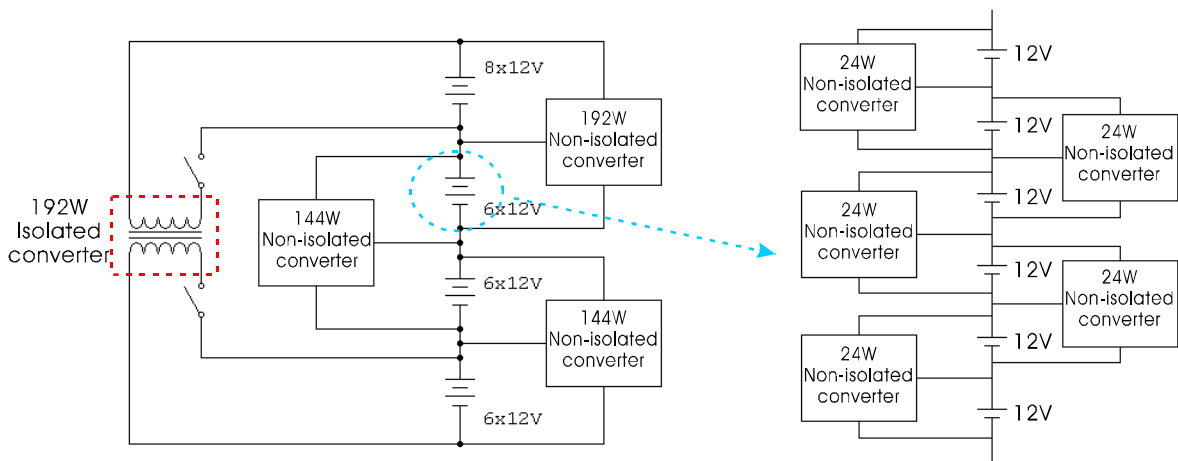


Figure 2.4. The proposed voltage equaliser structure

In *Figure 2.4*, the overall battery string is divided into four banks. Inside each bank, a number of 24W non-isolated converters are used to equalise the batteries inside the bank. The batteries inside each bank would be equalised first by the 24W non-isolated converters, then the bank equalisation would be done by the 144W or 192W converters.

The key points for selecting the types of converters are the cost, manufacturability and efficiency. Unfortunately there is no single solution to satisfy all the requirements. For the non-isolated converters, the buck-boost configuration has the advantage of a low component count, therefore the buck-boost would have the advantages of high manufacturability and low cost. The Cuk converter has theoretically the highest efficiency when the converter is used for transferring energy between any adjacent batteries, but the drawback of the Cuk converter is if the converter is desired to have bi-directional energy transformation capability, the component count would be double that of the buck-boost converter. Therefore in order to decide which converter is the best choice, the converter efficiency comparison of the buck-boost and the Cuk converters was calculated through simulation. In this performance test both converters have a fixed input voltage of 12V, and by changing the input current, the efficiency of each converter over a range of power rating from 10W to 50W was measured. The results of these simulations are shown in *Figure 2.5*, which indicate there is no significant efficiency improvement when using the Cuk converter. Therefore the buck-boost converter was chosen as the non-isolated converter of the equaliser.

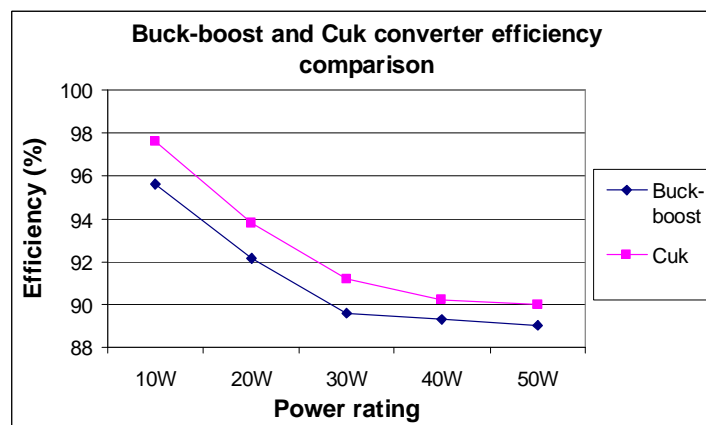


Figure 2.5. The efficiency comparison of buck-boost and Cuk converters

The isolated converter provides the electrical isolation between the top and bottom bank. Various isolated converters can be selected, such as flyback, push-pull, forward, half-bridge and full-bridge converters. By comparing both electrical and mechanical characteristics, the decision for the isolated converter was made. Due to the significantly low component counts over the others, the single switch flyback converter was chosen because only one MOSFET is required on each side of the transformer to achieve bi-directional energy

transformation. However the price to pay for the single switch flyback converter is that the single switch flyback converter must dissipate the energy stored in the leakage inductance of the transformer in either the switch or a snubber associated with the switch. Other isolated converters with more than one switch such as the two switch flyback converter or half bridge forward converter perform better because the energy stored in the leakage inductance does not need to be dissipated.

The disadvantages of the isolated converter are the size, cost and the manufacturability of the transformer. For any converter that uses transformer as its energy transfer unit, if the operational voltage is low, the required minimum number of turns would be low, and the ratio of the primary leakage inductance to the primary inductance becomes too high, reducing the converter efficiency. Increasing the turns of the winding can solve this problem, but it would increase the size of the transformer and winding resistance.

The proposed ring voltage equaliser structure is shown in *Figure 2.6*. Within this structure, three 192/144W non-isolated buck-boost are used to balance the banks from the top to the bottom, and a isolated flyback converter is used to balance the energy between the top and the bottom bank. Inside each bank, the adjacent batteries are equalised by 24W non-isolated buck-boost converters. In this design, all the converters are designed for bi-directional energy transfer, with average currents selected as 2A, so that approximately 10% of total charge can be balanced in an hour.

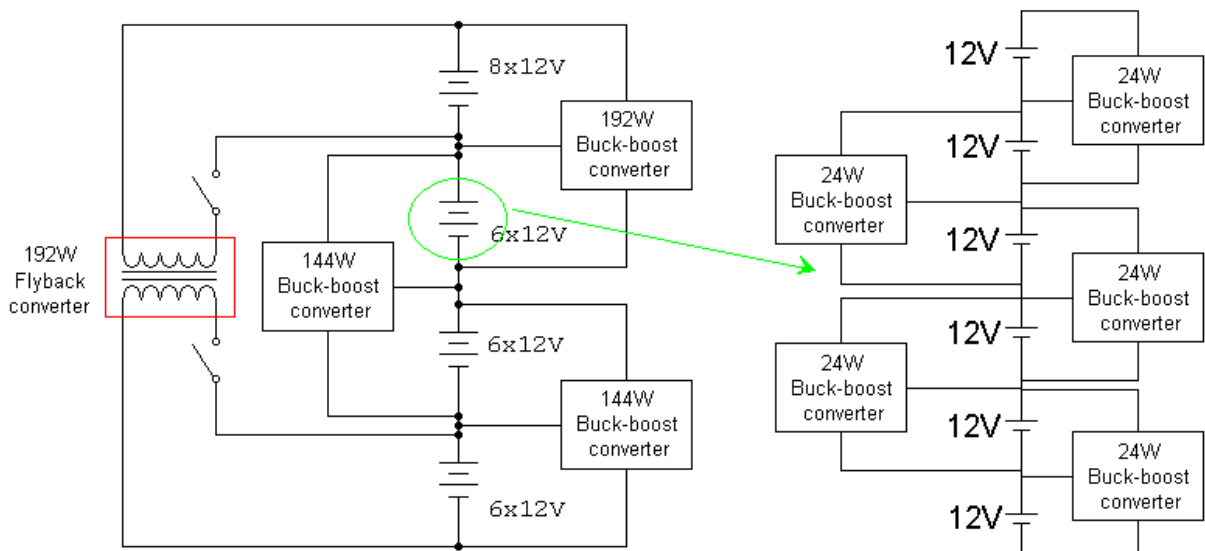


Figure 2.6. The proposed voltage equaliser structure

In the next chapter, the design procedures of each converter are detailed. This includes the control strategy, and the design of each controller and converter. The calculations of each required component values are listed and several inductor core construction technologies are also introduced to achieve a more compact design.

References:

- [1] PowerDesigner, “*Dynamic Equalization Techniques For Series Battery Stacks*”
http://www.powerdesigners.com/InfoWeb/design_center/articles/NDCD/ndcd.shtm
- [2] Linden, D., *Handbook of Batteries*, 2nd ed. 1995, USA: McGraw-Hill.
- [3] Sinclair P., Duke R.M. and Round S.D. “*An Adaptive Battery Monitoring System for an Electrical Vehicle*”. Proc. Intl. Conf. on Power Electronics, Drives and Energy Systems, Perth, Australia, 1998

3. Converter design

In Chapter 2, the ring equaliser topology was chosen as the proposed equaliser structure for the EV3, and the primary reason for choosing this topology is that fewer isolated converters are required to make up a low profile, low cost and easily expandable voltage equalisation system. This battery equalisation system requires three different types of converter to be built, the 24W buck-boost converter, the 192W buck-boost converter and the 192W flyback converter.

In this chapter, the detailed design procedures of each converter are demonstrated, and the key factors of each converter are also discussed. The operational current for all converters are limited at 2A, and the target efficiency for all converters are 90%.

3.1. The 24W buck-boost converter

In the EV3, all 26 batteries are connected in series and divided into four banks. Within any bank, a 24W buck-boost converter is used to interconnect any two adjacent batteries. The design of this converter can be split into two parts: the controller and the power converter. The controller includes the PWM generator and the gate drive, which is used to drive the buck-boost power converter. The schematic diagram of the buck-boost converter for the 24W battery equaliser is shown in *Figure 3.1*.

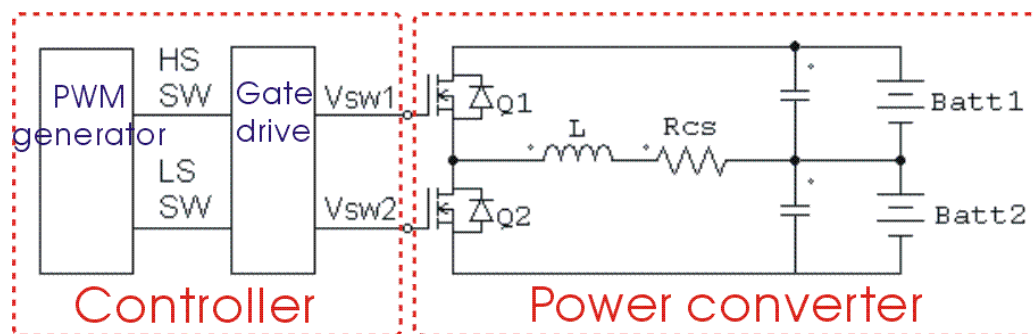


Figure 3.1. The Buck-boost converter

3.1.1. The PWM controller

The PWM controller is the heart of the converter. In this design, the two main functions that the controller provides are:

- Generating the PWM switching signals to drive the power converter.
- Sensing the pulse by pulse current signal from the converter, and converting this pulsed current signal into an average current signal, which is used to adjust the duty-cycle of the PWM signal to switch the MOSFETs.

The selected PWM control IC is SG3526 and its block diagram is shown in *Figure 3.2*. The SG3526 is a high performance monolithic pulse width modulator circuit designed for fixed-frequency switching regulators and other power control applications. Included in the 18-pin dual-in-line package are a temperature compensated voltage reference, sawtooth oscillator, error amplifier, pulse width modulator, and two low impedance power drivers. Also included are protective features such as soft-start and undervoltage lockout, digital current limiting, double pulse inhibit, a data latch for single pulse metering, adjustable deadtime, and provision for symmetry correction inputs. For ease of interface, all digital control ports are TTL and B-series CMOS compatible. Active LOW logic design allows wired-OR connections for maximum flexibility. This versatile device can be used to implement single-ended or push-pull switching regulators of either polarity, both transformerless and transformer coupled. The SG3526 is characterized for operation from 0°C to +125°C, and it is capable of generating PWM signals up to 350kHz with a duty cycle from 10 to 95%. [1]

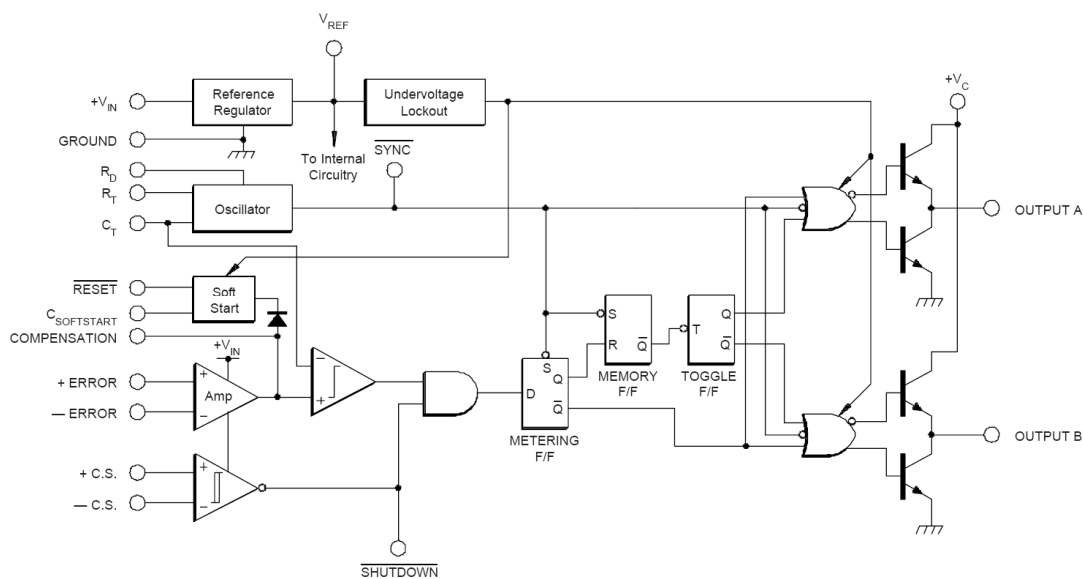


Figure 3.2. The block diagram of SG3526

As mentioned in the previous chapter, the operational current of this battery equalisation system is set to 2A. To achieve this, all the PWM controllers will be designed to operate under average current mode control.

3.1.2. Average current mode control

The control strategy for the operation of any converter can be either voltage mode or current mode. In voltage mode, the output voltage of the converter is regulated. Therefore if the output impedance is high, the output current would be low, but if the load impedance is low, the output current would be high. Alternatively, with current mode control the output current from the converter is regulated, and the output voltage varies in response to load impedance changes. In this project, every converter was designed to transfer the energy at a constant rate of 2A; therefore, current mode control was employed.

A small shunt resistor or a current transformer are the common choices for current sensing. The shunt resistor is easier and cheaper to apply, but when a large current is involved, the shunt resistor generates larger conduction loss than the current transformer. In this design, since the regulated average current is only 2A, the shunt resistor has been chosen to sense the current signal.

To ensure current mode control functions properly, choosing a suitable value for the current sensing resistor is also important. If the resistance is too small, the current signal may be too small and easily affected by noise, thus reducing the accuracy of the measurement. Alternatively if the resistance value is too high, the power loss from the current sensing resistor affects the converter overall efficiency. In this battery equaliser design, since some converters are placed close to the motor and other high power electronic circuit, it is important to ensure the measured current signal is accurate enough for the rest of control circuit. According to the experimental results, a 40m Ω shunt resistor can provide a good quality current signal and keep the efficiency degradation at an acceptable level.

As shown in *Figure 3.1*, the current sensing resistor R_{CS} is placed in series with the inductor with neither end connected to ground. Therefore, a differential amplifier with a common mode range greater than 12V is required to accurately measure the current signal across R_{CS} , and in this design the CA3140E op-amp was chosen, and the average current mode control circuit is shown in *Figure 3.3*. This current mode control circuit can only measure one way of current flow. Therefore for this bi-directional battery equaliser, another set of this current mode control circuit is required.

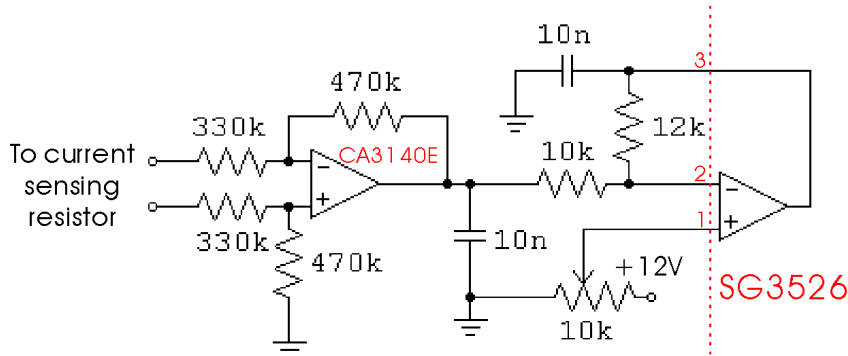


Figure 3.3. The average current mode control circuit

This current mode control circuit can be divided into two parts. The first part is the differential amplifier, which is the current sensing part, and this is made up by CA3140E op-amp. The second part is the current limiting part, which is made up by the internal error amplifier of the SG3526 PWM controller. The operating principle of this current mode control circuit is first of all, the differential amplifier measures the signal from current sensing resistor. Then the 10nF capacitor will smooth the current signal, which makes it more like a dc voltage for the following current limiting circuit. In *Figure 3.3*, the 10k Ω potentiometer set the average operational current level, and in this application the average current is limited to 2A.

3.1.3. The gate drive

To efficiently drive the MOSFET in a power converter, minimising the turn on/turn off time of the MOSFET is important. To reduce the switching time, sufficient driving current must be supplied to charge the gate capacitor in the MOSFET. During the turn off time, the MOSFET also requires a fast path to discharge the energy in the gate capacitor. Therefore, a gate drive is used in order to reduce the switching time, minimising the switching loss.

The IR2112(S) is a high voltage, high speed, power MOSFET and IGBT driver with independent high and low side referenced output channels. Logic inputs are compatible with standard CMOS or LSTTL outputs, down to 3.3V logic. The output drivers feature a high pulse current buffer stage designed for minimum driver cross-conduction. Propagation delays are matched to simplify use in high frequency applications. The floating channel can be used to drive an N-channel power MOSFET or IGBT in the high side configuration, which can operate at up to 600 volts.[2]

3.1.4. The power converter of the 24W buck-boost converter

The design of the 24W buck-boost converter is characterised by two key components, the inductor and the MOSFET. The inductor is the energy storage unit in the buck-boost converter, and the MOSFET is the switching device of this converter. In the following section, the detailed inductor design procedure is listed, and to improve the manufacturability, the technology of the planar inductor and the integrated inductor are also investigated.

A - Inductor design on RM core

This inductor design procedure is carried out by the standard RM core, and the design consideration includes the core size, core material, required inductance and airgap. However, this design procedure can also be applied to other types of inductor cores.

Step 1: Select core material and core size

Different materials have different magnetic characteristics. An inductor's magnetic core is made of specially formed material with “soft” magnetic properties. Although physically hard, a magnetic core is said to be “soft” when it does not retain significant magnetism. Silicon steel, iron powder and ferrite are common core materials for inductor design.

Silicon steel is relatively inexpensive and easy to form. In addition, silicon steel is a metal with low resistivity. Low-core resistivity means silicon steel readily conducts electrical current. The result is that undesirable eddy currents can flow in the core material. Eddy currents contribute to heating and core loss. In addition, a silicon steel core tends to reach the point of saturation rather easily. When saturated, a core is unable to store additional magnetic energy. Rapid saturation results in reduced operating range[4].

Iron powder has higher resistivity than silicon steel. By special processing, iron particles are insulated from each other. The particles are mixed with a binder. The cores are then pressed into their final shape. Next, a baking process is used to cure the cores. After curing, many tiny air gaps combine to provide a distributed air gap effect, which also serves to insulate the particles from one another thereby reducing eddy current flow in the core. This extends the useful frequency range, but there is a trade-off. The binding material adds a distributed air gap to the core. The distributed air gap reduces the permeability of the core [4].

Ferrite is a crystalline magnetic material made of iron oxide and other elements. The mixture is processed at a high temperature and formed into a crystalline molecular structure. Unlike the other material, ferrites are ceramic materials with magnetic properties. Ferrites have high magnetic permeability and high electrical resistivity. Consequently, undesirable eddy currents are greatly reduced by ferrite cores. With their high resistivity, ferrites are ideal for use as inductors. For example, ferrite beads are frequently used to reduce parasitic oscillations and for general filtering at the component lead level. This type of broadband component requires a broadband low-Q in order to provide high impedance over a wide frequency range[4].

By comparing the characteristics of each core material, ferrite becomes the better choice for inductor design. However there are a numbers of different ferrite cores that can be chosen. Considering the cost, availability, the frequency and the flux density, the 3C90 material is selected.

There are many possible inductor core geometries. A core's geometry depends on various factors, including the application, the available mounting area and volume, the allowable radiation, the limitations on windings, the operating temperature, and how the inductor will

be mounted. Consequently, a core's geometrical shape can take the form of a cylinder, bobbin, toroid or several other complex shapes[4]. In the beginning of the inductor design the standard RM core is used to carry out the design process. Then the planar inductor and the integrated inductor technology will be demonstrated later on.

The selection of the core size depends on the power that the converter is designed to deliver. If the core is too small, the inductor would be saturated during the operation. However there is harm to the converter efficiency when using a large inductor core, but choosing the right core size can reduce the manufacturing cost, size and the weight of the converter. The power rating to the core size curve is shown in *Figure 3.4* [2], for this 24W buck-boost converter, the RM10 core is chose.

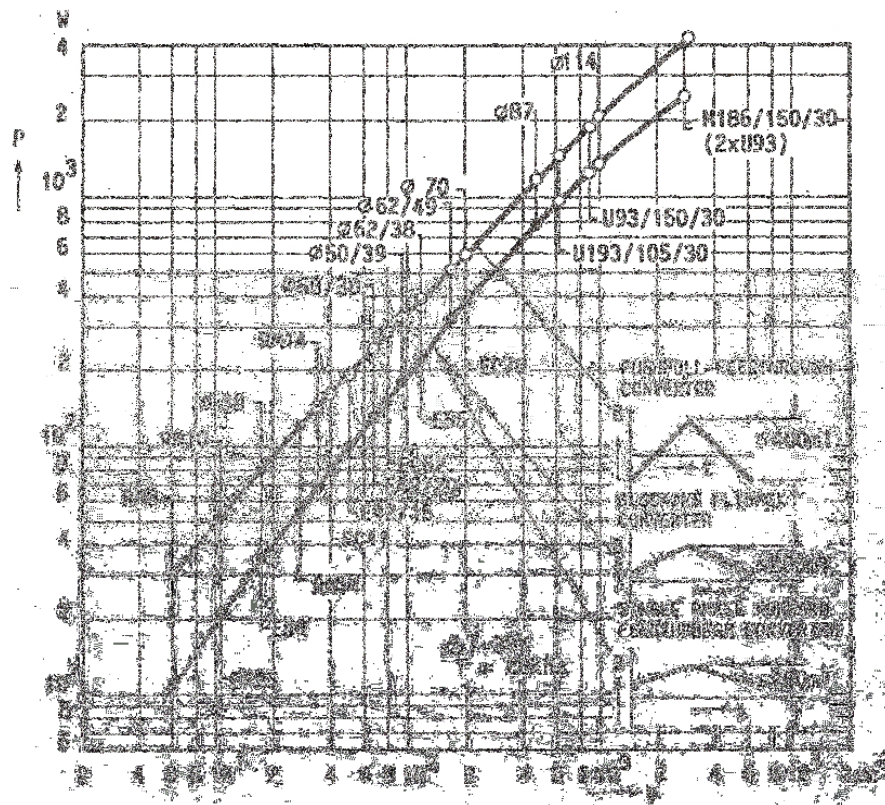


Figure 3.4. The RM core power rating curve.

Step 2, Calculating the minimum inductance.

The minimum inductance is required to maintain the continuous conduction of the converter when the maximum input voltage is applied. However it is also important not to make the inductance too large, because a larger inductance requires more turns, which leads

to higher conduction loss during operation. The standard terminal voltage of the battery is 12V, but when the battery is fully charged, the battery voltage can go up to 13V. Assuming the duty-cycle of the switching signal is 50%, if the converter operates at average current of 2A, the allowable peak current would be 8A in order to maintain the converter operates under continuous conduction.

However this assumption can only be made when the converter has 100% efficiency, but in reality it is not possible to achieve this. To make the design more practical, the maximum current ripple is set to 6A and the minimum inductance can be calculated by *Equation 3.1*.

$$L = \frac{V \cdot DT}{\Delta I} \quad \text{Equation 3.1}$$

L = minimum inductance

V = maximum input voltage

D = duty-cycle

T = switching period

ΔI = allowable ripple current flow through the inductor

Assuming the maximum input voltage is 13V, switching frequency is 100kHz, 50% duty-cycle and 6A of ripple current. The minimum inductance is calculated as 11.9 μ H.

Step 3, Selecting maximum “on” period

Since the charge level of the battery is proportional to the terminal voltage of the battery, the input voltage of the converter will not stay at 13V at all times, as mentioned in the previous step. Therefore, in order to maintain the constant power flow when low input voltage occurs, the duty-cycle of the switching signal has to be increased, and the maximum “on” period is defined when the lowest input voltage occurs.

The minimum inductance was calculated from Step 2. If the input voltage drops to 11.5V, and the switching frequency and the current ripple remain unchanged, the maximum duty-cycle can be calculated as 62% from *Equation 3.1*.

Step 4: Calculating the air gap

For every dc to dc converter that uses an inductor, a sufficient air gap has to be carefully calculated. The air gap is used for storing energy from the dc source. An insufficient air gap would lead the inductor to saturate, which decreases the converter efficiency. Alternatively, if the air gap is too large, the inductance will be small, which leads the converter to operate in discontinuous conduction, which can also affect the converter efficiency. The air gap size can be calculated by *Equation 3.2*.

$$\alpha = \frac{\mu_r \cdot N^2 \cdot A_e}{2 \cdot L} \quad \text{Equation 3.2}$$

$$\mu_r = 4\pi \times 10^{-7}$$

N = number of turns

A_e = area of the core, mm²

L = inductance, mH

From Step 1 and 2, the RM10 core was selected as the initial core size and the minimum inductance 11.9μH was also calculated. Assuming the number of turns N is equal to 10, the required air gap can be calculated as 0.507mm.

Step 5: Check core flux density and saturation margin

After calculating the required inductance, number of turns and the air gap size, it is necessary to check the maximum flux density in the core to ensure an adequate margin between the maximum working value. *Figure 3.4* shows the B-H curve of the 3C90 core, and the flux density must not reach the saturation region.

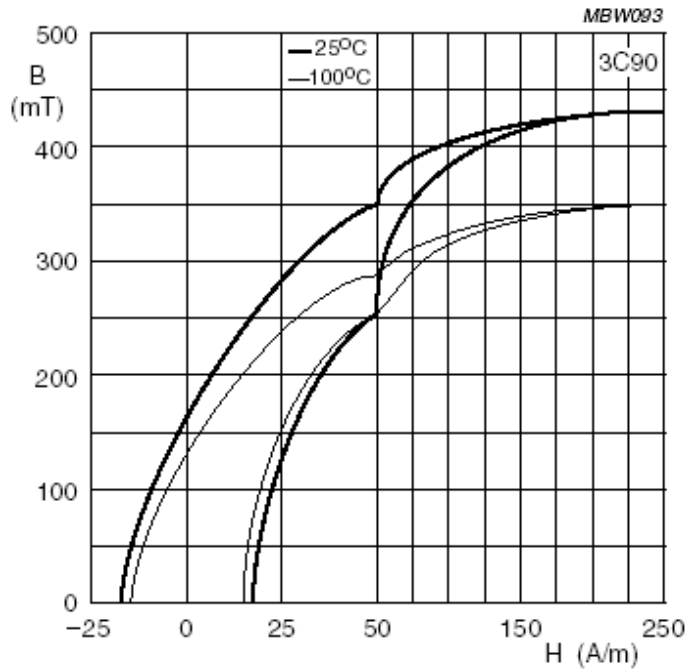


Figure 3.5. 3C90 B-H curve

The flux density consists of the ac flux density B_{ac} and dc flux density B_{dc} . The sum of the ac and dc flux densities is the maximum flux density of the core, where the ac and dc flux density can be calculated by *Equation 3.3* and *3.4*.

$$B_{ac} = \frac{V \cdot t}{N \cdot A_e} \quad \text{Equation 3.3}$$

$$B_{dc} = \mu \cdot H = \frac{\mu_0 \cdot N \cdot I_{DC}}{2\alpha \times 10^{-3}} \quad \text{Equation 3.4}$$

V = Maximum supply voltage

t = on time, μs

N = Number of turns

A_e = Area of core, mm^2

$\mu_0 = 4\pi \times 10^{-7}$ H/m

I_{DC} = Average DC current

α = air gap, mm

The B-H curve is temperature dependent. *Figure 3.4* shows the B-H curves of the inductor core at 25°C and 100°C. However both temperatures are unlikely to be the working temperature of this battery equalising system. The working temperature of the converter depends on the allocation of the converter, and along the EV3 the warmest area will be the engine bay. During the operation, the temperature of the engine bay would be around 40°C. By allowing 20°C temperature rises on the inductor, the core temperature would be 60°C, which means the saturation level of the core would be around 375mT.

At the initial stage, if the maximum supply voltage V is set as 13Volts, the on time $t = 5\mu\text{s}$, number of turns $N = 10$, and the A_e is equal to 96 mm^2 . The B_{ac} can be calculated as 67.7mT .

To calculate the B_{dc} , the number of turns N and the average current I_{DC} were assumed as 10 and 2A. The air gap size α was calculated from Step 4, which is 0.5mm. Therefore the dc flux density is calculated as 25.1mT . The total flux density is equal to 92.8mT , which is well under the maximum allowable flux density of 350mT .

B - The planar inductor

Since 25 24W buck-boost converters need to be built and ideally located in a recess in the top of each battery, the manufacturing process for a low profile design has to be as simple as possible. The disadvantage of the conventional inductor is that it has a relatively large physical size. Therefore if 25 converters have to be installed into the EV3, they would occupy too much space and create a mounting problem. To overcome this mounting issue, the planar inductor and the integrated inductor technologies were investigated.

A planar inductor is constructed using either one E and one I core or two E cores, and the actual winding is made up by the loops of printed circuit board (pcb) tracks, where higher inductance can be achieved by multiple loops of a multilayer pcb. The biggest advantage of the use of the planar inductor is that since the windings are made up by the pcb tracks, the inductor can be made in a low profile, high precision and easily manufactured format. The constructions of the planar inductor are shown in *Figure 3.5*.

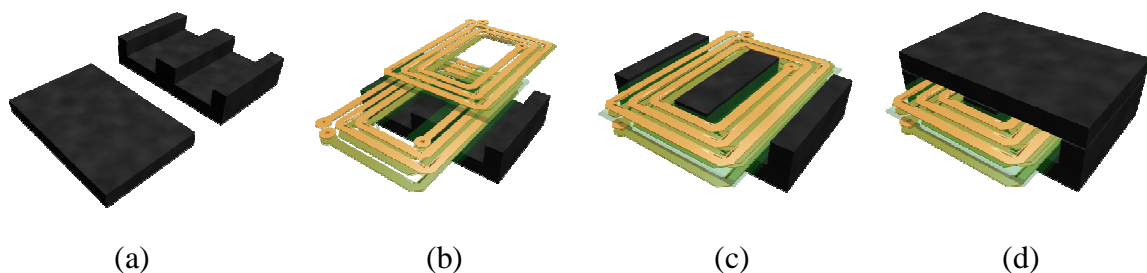


Figure 3.6a. E core and I core

3.6.b. Fitting two multilayer pcb into the E core

3.6.c. Interconnecting the two pcb together

3.6.d. Putting the I core on then completing the player inductor

A major problem of the planar inductor is that if the pcb contains more than two layers, any intermediate windings would not have as much heat dissipating capacity as the top and bottom layers. Therefore, as the current flows through the winding, the pcb temperature will build up, then winding resistance and conducting losses will increase. To overcome this problem, a wider pcb track can be used to reduce the winding resistance and hence increase the current capacity and reduce the conduction losses from the inductor. The trade off by using the wider pcb track is the allowable numbers of turns per layer would be decreased. To emphasise the idea, *Figure 3.6* shows how the pcb temperature can be varied by changing the track width.

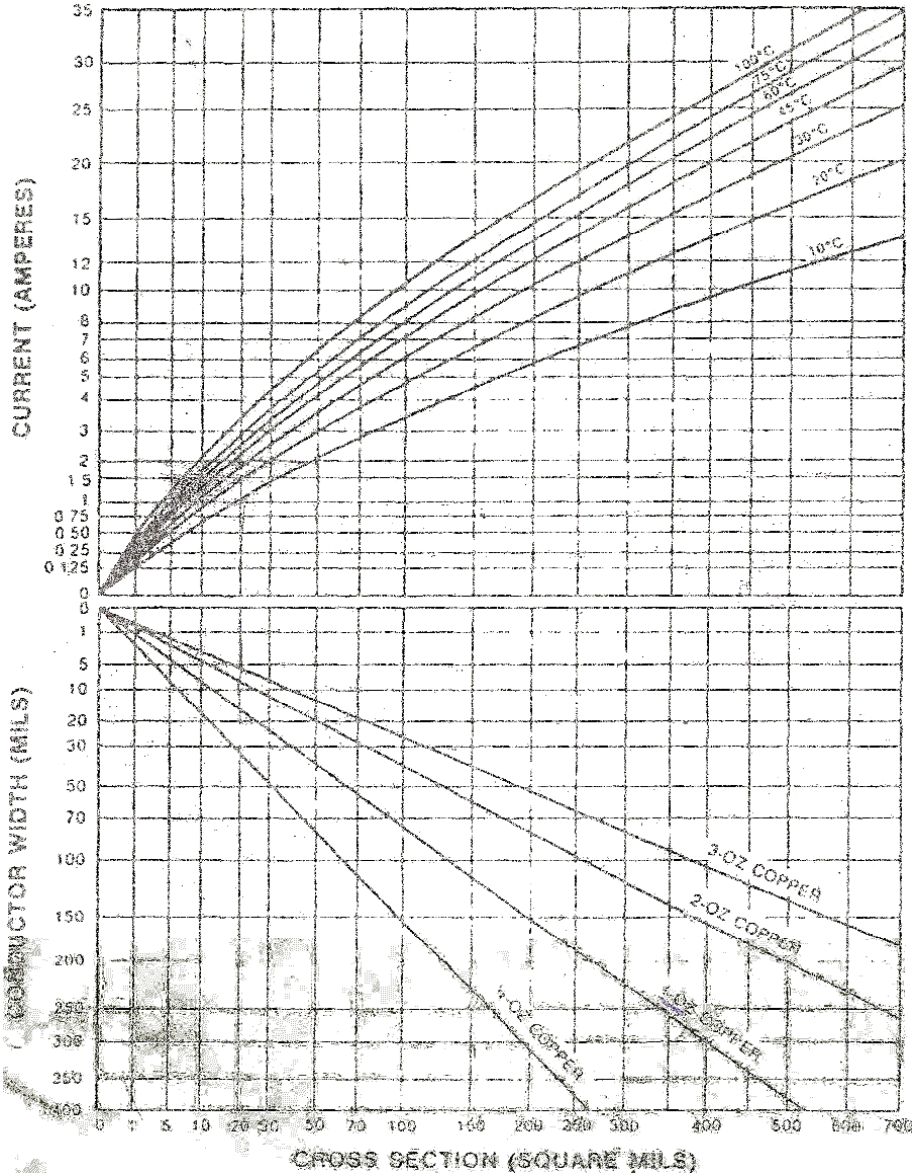


Figure 3.7. The track width versus temperature rise diagram

C – The Integrated Inductor

The integrated inductor is an inductor that has the form of an integrated circuit. Unlike the plastic package from the standard integrated circuit, the whole package of the integrated inductor is the inductor core, which has a built in air-gap. The leads of the package are the partial windings of the inductor, and the inductor is completed by the pcb wiring. The construction of the integrated inductor is shown in *Figure 3.7*.

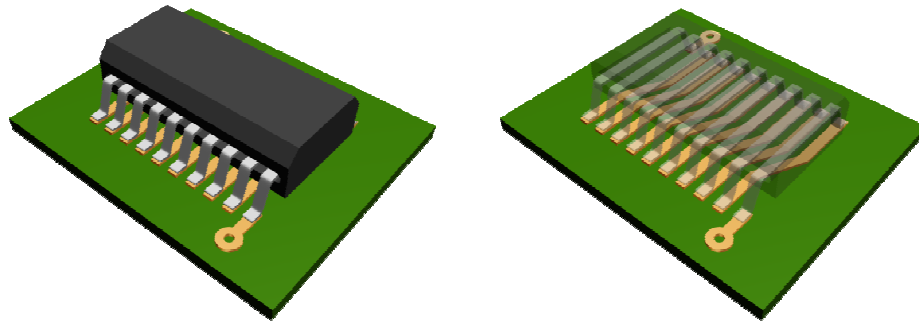


Figure 3.8. The construction of the integrated inductor

Compared with the standard inductor and the planar inductor, the integrated inductor has the advantages of the smallest physical size, and because there is no multi-layer pcb required, the pcb manufacture also becomes relatively simpler compared with the others. However, apart from these advantages, there are two disadvantages of this integrated inductor. The first drawback is due to this compact core size; the maximum inductance from a single integrated inductor can only be made around $5\mu\text{H}$, which means the converter requires 250kHz or higher switching frequency. The second drawback is the cross section area of the pin out. The cross section area of the lead is 0.18mm^2 , which is eight times smaller than the litz wire that can be used on the RM core. The smaller cross section area brings higher dc resistance, which means the conduction loss from the inductor would be eight times higher.

D - MOSFET selection

To select an appropriate MOSFET for the 24W buck-boost converter, there are four main considerations - voltage rating, current rating, on resistance $R_{\text{ds-on}}$ and switching loss.

The voltage rating tells how much voltage MOSFET can handle between Drain and Source. For the buck-boost converters, the voltage between drain and source V_{ds} would be equal to twice the supply voltage; therefore, the voltage rating of the MOSFET must be at least two times the supply voltage plus 20 percent of margin. Ideally the current rating is defined by the MOSFET peak operational current. However, in the converter design the pulse current also needs to be considered. Therefore, the continuous current and the pulse current determine that MOSFET rating.

The R_{ds-on} is the on resistance when the MOSFET is in the on state. The low R_{ds-on} MOSFET has low conducting loss and in most cases is proportional to the voltage rating of the MOSFET. Therefore, it is not wise to select a high voltage rating MOSFET and operate it under low voltage conditions.

Ideally, higher switching frequency requires less inductance to maintain continuous conduction. Unfortunately, the high switching frequency means larger switching loss. The switching losses are created as a result of the simultaneous exposure of a MOSFET to high voltage and current during the transition between the open and closed states [3]. The fast transient requirement pushes us towards possibly high switching frequencies, which in turn increases the relative importance of the switching losses[3].

In reality it is difficult and uneconomical to manufacture and purchase the MOSFET, which has both low R_{ds-on} and low switching loss. The low R_{ds-on} MOSFET is normally made up of a larger silicon area to reduce the on resistance, and the switching speed of MOSFETs is limited by the gate capacitance on the silicon, which is called the gate charge. The gate charge is the gate capacitance that needs to be charged or discharged during the on or off switching transition. The drawback of this larger silicon area is the creation of a larger gate capacitance. That makes the MOSFETs need more energy to be turned on, hence increasing the switching time and the switching loss. Therefore the compromise between the conducting loss and the switching loss has to be considered.

In this equalisation system, the overall battery string is divided into four banks. The first bank contains 8 batteries. The second, the third and the fourth banks each contains 6 batteries. So the required number of 24W buck-boost converters for each bank is 7 for the first bank, and 5 for the second, the third and the fourth bank. Therefore the total number

for the required 24W buck-boost converters is 22. In each 24W buck-boost converter, each converter requires two MOSFETs, therefore the cost becomes a significant concern. In general, the price of the MOSFET is dominated by two factors; the voltage rating and R_{ds-on} . By allowing 20 percent allowance on both voltage and current signal, the voltage and current rating could be set to 29V and 2.4A. Then any MOSFET, which has a voltage rating higher than 29V and has a reasonably low R_{ds-on} and price can be considered.

The gate charge defines whether the MOSFET has low switching loss or not. It determines the gate capacitance of the MOSFET, and it is mainly related to the Gate to Source voltage and is slightly affected by the Drain to Source voltage. In practice, the logic MOSFETs normally have lower gate charge because they only need 5V to be switched on instead of the 9 to 10V of the standard MOSFETs. Therefore by considering the factors of cost, conduction loss and switching loss, the logic MOSFET SUD35N05-26L is chosen for the 24W buck-boost converter and more details on this MOSFET will be discussed in chapter 5.

3.2. The 192W buck-boost converter

The 192W buck-boost converter is for transferring energy between the adjacent banks. The design procedure of the 192W buck-boost converter is similar to the previous 24W version, but there are three exceptional concerns that need to be considered. First, due to the input voltage is higher than the 24W buck-boost converter, so the selected MOSFETs should have higher voltage ratings. Second, since the power rating of this buck-boost converter is higher than the previous 24W version, a larger inductor core is required for storing larger energy. Third, assuming 90 percent efficiency is achieved, the total power loss from the converter would be 19.2W. Due to the majority of power loss being caused by the MOSFETs, heatsinks for each MOSFET are required in order to prevent overheating the MOSFET.

The input voltage of this 192W buck-boost converter is eight times higher than the previous 24W version. Minimising the switching loss becomes important. From the design of the 24W buck-boost converter, it mentions that minimising the switching loss can be done by either using the low gate charge MOSFETs or reducing the switching frequency. However,

the problem brought from choosing low gate charge MOSFETs and how to compromise between the low R_{ds-on} or the low gate charge was also detailed. Then the result tells that reducing the switching frequency is the better option to minimising the switching loss from the 192W buck-boost converter. In order to meet the electrical specification and minimising the cost, IRF740 is chosen for the 192W buck-boost converter.

The inductor design procedure is identical to the inductor design of the 24W buck-boost converter. However because the power rating of the converter has been increased, a larger inductor core is used. According to the RM core power rating curve from *Figure 3.4*, the minimum inductor core size for the 192W buck-boost converter would be RM14.

Alternatively the planar inductor core can also be used in this 192W buck-boost converter. According to the cross section area and the material, the E42 planar core would also be suitable for this application. However, due to the insufficient core size and the wiring space, the integrated inductor can not be used on this converter.

Reducing the switching frequency requires larger inductance to maintain the continuous conduction. By repeating the inductor design procedure in the design of the 24W buck-boost converter, if the switching frequency is reduced from 100kHz to 50kHz, and the duty-cycle and the allowable current ripple remain unchanged, the minimum inductance can be calculated as 192 μ H for the 192W buck-boost converter.

3.3. The 192W flyback converter

The flyback converter can provide an electrical isolation between two battery banks. Therefore, it is used for transferring energy between the top and the bottom banks. The schematic of the design flyback converter is shown in *Figure 3.8*.

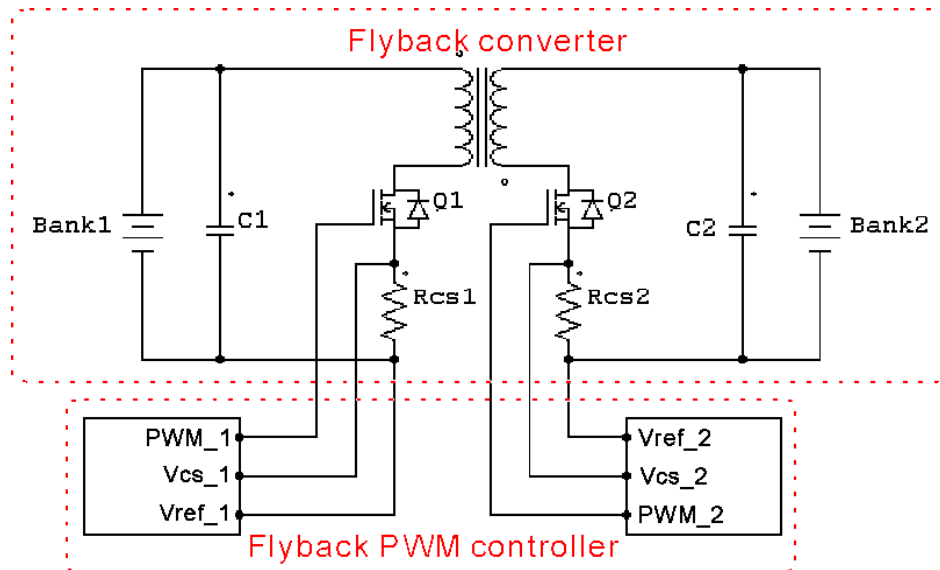


Figure 3.9. The flyback converter

This flyback converter is also designed for bi-directional energy transformation, and 2A of average operational current. In *Figure 3.12*, each side of the flyback transformer has its own PWM controller. Bank 1 represents the top bank and Bank 2 represents the bottom bank of the battery string; therefore, the reference voltage V_{ref_1} would be 216V higher than the V_{ref_2} because there are 18 batteries between these two reference points. The two R_{cs} are used for current sensing purposes, and the sensed current signal would be fed into V_{cs} , which is the current sensing input of the PWM controller. Then the PWM controller would adjust the duty-cycle to switch the MOSFETs.

3.3.1. PWM controller for the 192W flyback converter

The PWM controller for this 192W flyback converter is similar to the buck-boost PWM controller. The control strategies of both controllers are by sensing the pulse by pulse current signal then convert it into a dc voltage, and then the SG3526 PWM controller to adjust the duty-cycle of the PWM signal. However, there are two differences between these two controllers. The first difference is that each controller only needs to drive one MOSFET, which makes the switching control strategy simpler than the buck-boost controller. The second difference is since the current sensing resistor is connected to the reference point of the battery bank, the differential amplifier used in the buck-boost controller is not required. Instead of the differential amplifier, a negative feedback amplifier

is used to sense the current signal and then the amplified current signal would be sent to the SG3526. The schematic of the flyback PWM controller is shown in *Figure 3.9*.

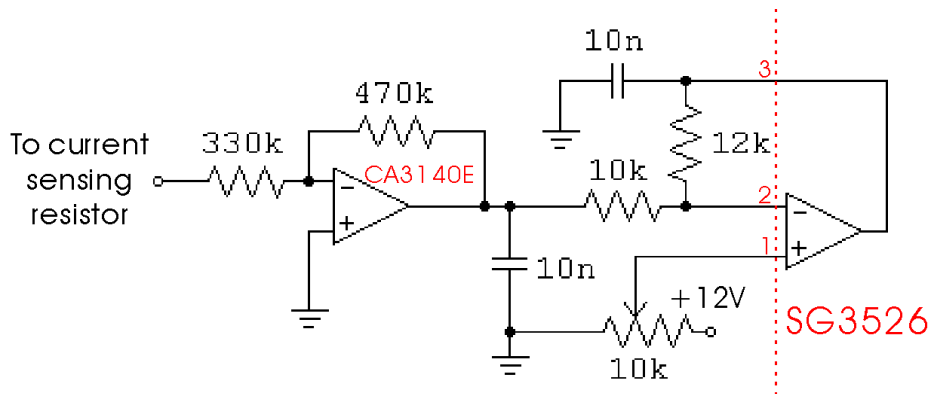


Figure 3.10. The PWM controller for the 192W flyback converter.

3.3.2. 192W flyback transformer

The key design of the flyback converter is the flyback transformer. The flyback transformer is used for storing and transferring energy from one side of the transformer to the other. Therefore, to design an appropriate flyback transformer becomes the most important factor of the flyback converter design. The construction of the flyback transformer can be seen as the combination of two inductors. Therefore, the inductor design procedure from the buck-boost converter is again used; moreover, the primary and secondary inductances can not be treated individually. Then some reiterative calculation would be required in order to make both primary and the secondary turns meet the electrical requirement, and the detailed transformer design procedure is shown below.

Step 1, Core selection

The core size depends on how much power the converter needs to deal with. From the design of the 192W buck-boost converter, the RM14 core was selected. According to the identical power rating, the RM14 core can also be used in this flyback transformer design.

Step 2, Calculating minimum primary inductance

The minimum inductance is required to maintain the continuous conduction of the converter when the maximum input voltage is applied. Assuming the switching frequency and the duty-cycle are 50kHz and 50 percent, the average battery voltage inside the bank

and the allowable current ripple are 13V and 6A. The minimum primary inductance can be calculated again from *Equation 3.1*, and the value of the minimum primary inductance is 174 μ H.

Step 3, Selecting maximum “on” period

In order to maintain the constant power flow, the maximum “on” period will occur at minimum input voltage and maximum load.[3] Assuming the input voltage is dropped to 11.5V, and the rest of the parameters from Step 2 remain unchanged, the maximum on period can be calculated as 57% from *Equation 3.1*.

Step 4, Select ac flux density swing

From *Figure 3.4*, the maximum allowable flux density is 350mT. The flux density swing also consists of both ac and dc flux densities, and from *Figure 3.4*, the ac flux density swing is initially selected as 250mT.

Step 5, calculate minimum primary turns

After the ac flux density is selected. By rearranging *Equation 3.3*, the minimum number of primary turns is shown in *Equation 3.5*, and according to the manufacture’s datasheet [4] of the RM14 core, the effective area of the centre leg is 198mm².

$$N_{\min} = \frac{V \cdot t}{\Delta B_{ac} \cdot A_e} \quad \text{Equation 3.5}$$

N_{\min} = minimum primary turns

V = applied dc voltage = 12 \times 8 = 96V

t = “on” times, μ s = 10 μ s

ΔB_{ac} = maximum ac flux density, T. Assuming ΔB_{ac} = 250mT

A_e = minimum cross-section area of core, mm². A_e = 198 mm².

Therefore the minimum primary turns N_{\min} can be calculated as 20.

Step 6, Calculate secondary turns

The output voltage of the transformer has the nominal voltage of 72V (6 \times 12V batteries). Therefore, the secondary turns can be calculated by *Equation 3.6*, which converts the primary turns into volts per turn, then calculates the required secondary turns.

Primary volts per turn $V/N = V_p/\text{primary turns} = 96/20 = 4.8 \text{ V/N}$

$$\begin{aligned} \text{And then the secondary turn } N_s &= \frac{V_s \cdot N_p}{V_p} && \text{Equation 3.6} \\ &= \frac{72 \cdot 20}{96} = 15 \end{aligned}$$

Where V_s = secondary voltage

N_s = secondary turns

The secondary inductance can be calculated by Equation 3.7.

$$L = Al \cdot N^2 \quad \text{Equation 3.7}$$

L is the value of the inductance

Al is the equivalent quantity of the inductance

N is the numbers of turn

Al is the equivalent quantity of the inductance in mH with a winding of 1000turns, which can be calculated from the primary turn and primary inductance, and the calculated Al is 3×10^{-7} . Then the secondary was calculated as $67.5 \mu\text{H}$.

Step 7, Calculating the air gap size

The air gap calculation is very important in the flyback transformer design. An insufficient air gap would saturate the core, hence reduce the converter efficiency. Alternatively, if the air gap is too large, the inductance would become too small, which may lead to the inductor working under discontinuous conduction, and thus decrease the converter efficiency. The air gap can be calculated as 0.24mm from Equation 3.2.

Step 8, Check core flux density and saturation margin

The overall flux density of this flyback converter consists of the ac flux and the dc flux, and they can also be calculated by Equation 3.3 and 3.4. At this stage, the supply voltage V is made up by eight 12Volts batteries, which makes up a total voltage of 96 Volts. Assuming 50% duty-cycle, the on time $t = 10 \mu\text{s}$, and from Step 4, the primary number of turns N is 20; and the effective area A_e of the E43 core is 198 mm^2 . Therefore, the ac flux density is calculated as 240mT.

To calculate the dc flux density, the number of turns N and the average current I_{dc} were assumed as 20 and 2A. The air gap size α was also calculated as 0.23mm. Therefore the dc flux density is calculated as 109mT. The total flux density is equal to 349mT, which is under the maximum allowable flux density of 350mT.

In the buck-boost converter design, the planar core was introduced to improve the manufacturability. However, in the flyback converter design, due to the manufacturability, it is very difficult to make a pcb that has greater than four layers. Therefore, the planar core was not considered.

3.3.3. Reducing the voltage stress on MOSFETs

The voltage stress is the Drain voltage to overshoot during the turn-off edge, caused by the transformer leakage inductance.[3] Since the current flowing through the inductor can not be stopped instantaneously at the time that the MOSFET is switched off, the small amount of leakage inductance and this residual current would result in an overshoot across the drain and source of the MOSFET.

To overcome this effect, the voltage overshoot problem is best dealt with by ensuring that the leakage inductance is as small as possible, then clamping the tendency to overshoot by dissipative or energy recovery methods.[3] Minimising the leakage inductance can be made by shortening the wiring distance from the transformer to the other components. To achieve this, it is better to place the other components close to the transformer.

The flyback converter with the voltage clamping circuit is shown in *Figure 3.10*. The idea of this clamping circuit is when MOSFET Q1 is turned on, the reverse polarity of the clamping diode Dc1 makes the clamping circuit act like an open circuit. However, during the instant when the MOSFET is turned off, due to the current flow through the inductor it can not be instantaneously turned off. Therefore, the current from leakage inductance from the primary inductance would try to keep flowing through Q1, and then cause a voltage spike. The Clamping circuit 1 provides an alternative path for the primary inductance to dissipate remaining energy from the primary leakage inductance.

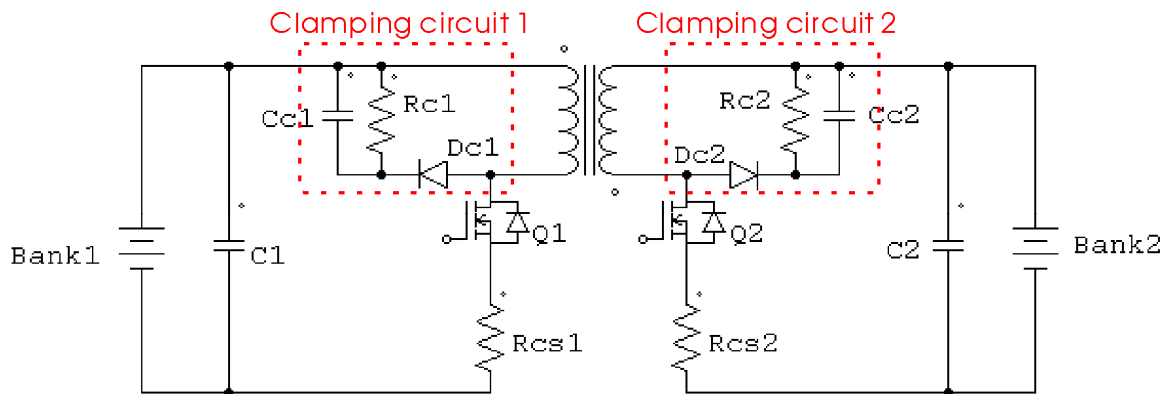


Figure 3.11 Flyback converter with clamping circuit

In *Figure 3.15*, the flyback converter with the clamping circuit is displayed, and it shows each clamping circuit consists of three components, a diode D_c , a capacitor C_c and a resistor R_c . The diode is used to provide a current flow path for the energy stored in the leakage inductance. Therefore, when the MOSFET is turned off, the energy from the leakage inductance can flow into the clamping circuit. Then the R_c and C_c inside the clamping circuit would dissipate the energy from the leakage inductance.

There is no rule for selecting the value of the R_c and C_c . The values of R_c and C_c depend on how fast the energy from the leakage inductance needs to be dissipated. If the RC time constant is large, less voltage stress appears on the MOSFET. However, the drawback of the clamping circuit is that during the off state the voltage across the MOSFET is equal to the sum of the input voltage and the voltage across the flyback transformer. Therefore, if large clamping resistance and capacitance are used, the clamping circuit would require more time to charge the clamping capacitor C_c , which increases the MOSFET turn off time, hence increases the switching loss.

Increasing the value of R_c and C_c can significantly reduce the voltage stress, but it is undesirable to make the clamp voltage too low, as the flyback overshoot has a useful function. It provides additional forcing volts to drive current into the secondary leakage inductance during the flyback action. This results in a more rapid increase in flyback current in the transformer secondary, improving the transfer efficiency and reducing the losses incurred in the clamp resistor R_c [3].

3.4. Summary

In this chapter, the design procedures of three different converters - 24W buck-boost, 192W buck-boost and 192W flyback converters were detailed. The PWM controllers for all three types of converters are very similar. However there are two exceptional design considerations. First, as there is only one switching device on the 192W flyback converter and the MOSFET is connected to the reference point via the current sensing resistor. Therefore, there is no high-side drive required for this converter. Second, unlike the buck-boost converter, the current sensing resistor of the flyback converter is not sitting on the voltage source like the buck-boost converter does. So the additional op-amp for providing wide common mode range is not needed.

In the next chapter, the simulations of each converter will be made by Pspice simulator. The component values calculated in this chapter are also applied into these simulation tests. The simulation results include the detailed equalisation process and the switching waveforms on each key component, and finally it shows the energy between the two batteries can be successfully balanced by the designed converter.

References:

- [1] Data sheet of SG3526
- [2] Philips inductor core material
- [3] Keith Billings, "Switchmode power supply handbook second edition", 1999
- [4] Andy Chow, Chief Design Engineer, J. W. Miller Magnetics, Gardena, Calif. "Inductor Core Material: The Heart of an Inductor"

4. Converters Simulations

In this Chapter the results from the simulations of each converter making up the chosen voltage equaliser topology are discussed. The simulation models include one 24W non-isolated buck-boost converter, one 192W non-isolated buck-boost converter and one 192W isolated flyback converter. The simulations were carried out by Pspice simulator and in these simulations two rechargeable batteries or banks of batteries were modelled as two 1F capacitors, and the battery internal resistance and the wiring resistances were modelled as two 100m Ω resistors.

Before the simulation, a series connected battery discharging test at a rate of 30A for 60 minutes through a resistive load was done in order to measure what the nominal voltages from each battery would be after the batteries have been discharged. In the EV3 there are 26 batteries connected in series. Drawing energy from each battery at a rate of 30A is equal to drawing 10kW of energy, which is roughly equal to the power consumption of standard city driving. In this battery discharging test, eight sealed lead-acid batteries were first parallel connected and equally charged, and then connected in series, and the discharging result is shown in *Table 4.1*.

| | Batt 1 | Batt 2 | Batt 3 | Batt 4 | Batt 5 | Batt 6 | Batt 7 | Batt 8 | Average voltage |
|---|--------|--------|--------|--------|--------|--------|--------|--------|-----------------|
| Starting voltage | 12.62 | 12.78 | 12.74 | 12.76 | 12.65 | 12.72 | 12.71 | 12.76 | 12.72 |
| End voltage | 11.34 | 11.64 | 11.5 | 11.5 | 10.87 | 10.76 | 10.88 | 11.72 | 11.28 |
| Difference from the average end voltage | +0.06 | +0.36 | +0.22 | +0.22 | -0.41 | -0.52 | -0.40 | +0.44 | |

Table 4.1. The open-circuit voltages of each battery after 30A of 60 minutes discharge

In *Table 4.1*, the result shows that after an hour of discharge, the open-circuit voltages from these batteries end up between 10.76 and 11.72 volts, which means after an hour of driving, the voltage difference from each battery could be as high as 1V. Therefore, for the

following simulations, the initial voltage of the source and the target batteries will have 1 volt difference.

4.1. 24W buck-boost converter

The voltage equaliser based on the 24W non-isolated buck-boost converter is shown in *Figure 4.1*. In this configuration, C1 represents the higher voltage battery and C2 is the battery required to be recharged, and the initial voltage these batteries are set to 12.5V and 11.5V respectively. In this simulation, the switching frequency was set to 100kHz, the inductor wiring resistance R3 is 15m Ω and the inductance value is set to 18 μ H, which is the minimum inductance value to maintain continuous conduction.

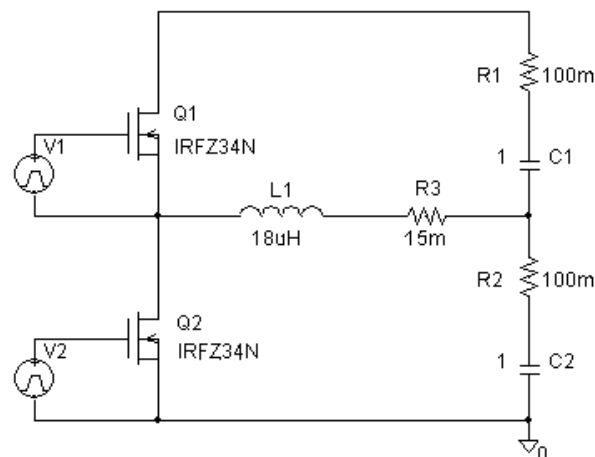


Figure 4.1. 24W non-isolated buck-boost converter

The aim of this simulation is to transfer the energy from C1 to C2, and the detailed switching waveforms of the MOSFET and the inductor are shown in *Figure 4.2*. In these simulation results, the PWM switching signal is represented by the switching signal V1. Vds indicates the drain to source voltage of Q1. I_{C1} and I_{C2} show the current flow from the source and target batteries C1 and C2. Finally, I_L represents the current flow through the inductor L1.

When the PWM switching signal V1 of this equaliser is high, Q1 turns on, then inductor L is charged by C1 via R1 and Q1. Later when V1 is switched low, Q1 turns off, the current stops flowing from C1, the inductor current keeps circulating and the stored energy in the inductor is discharged into C2 through R2 and the internal diode of Q2 without any additional control.

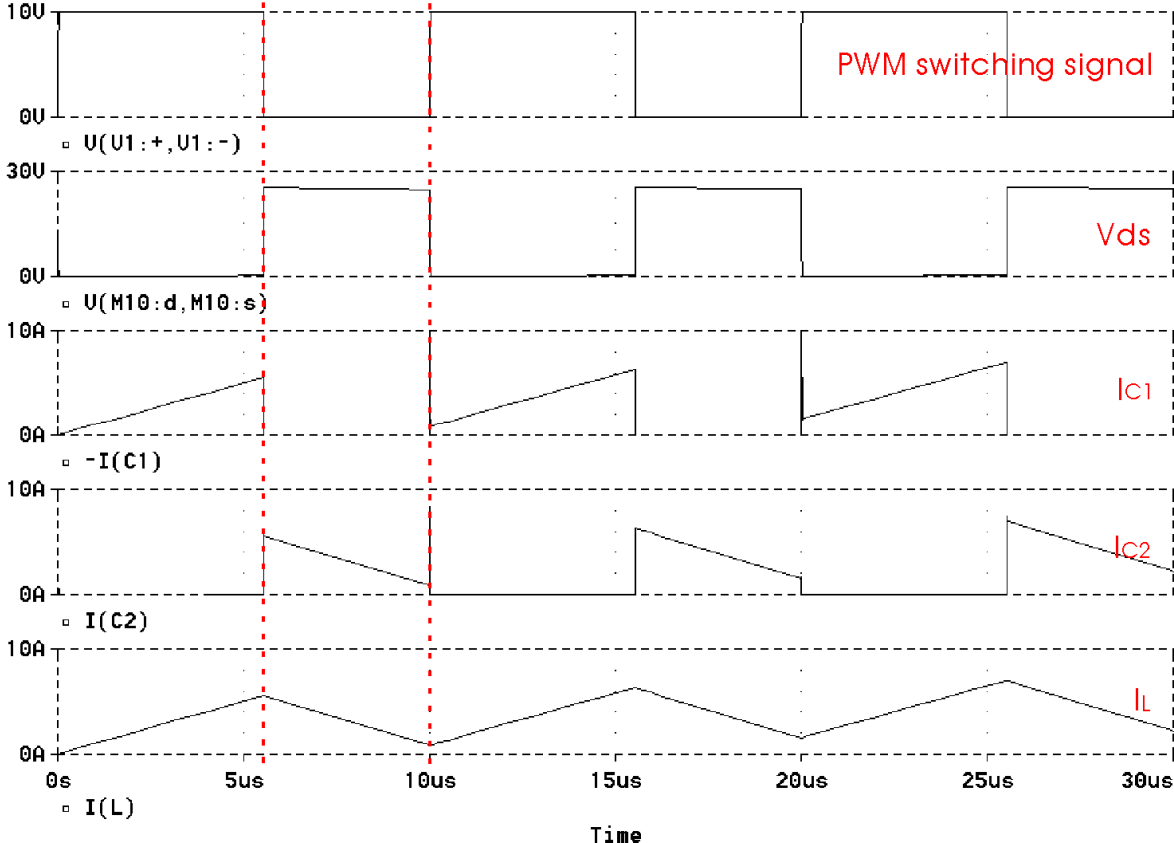


Figure 4.2. The switching waveforms of the 24W buck-boost converter.

The charge level of the lead acid battery is proportional to its open-circuit voltage. By measuring the open-circuit voltages across both C1 and C2, the charge level of each battery can be monitored. The voltage equalisation result of this 24W buck-boost converter is shown in *Figure 4.3*, which demonstrates that in principle the battery voltages can be balanced. However the test result that is shown in *Figure 4.3* is the accelerated version of the voltage equalisation process. In the real world application, the voltage equalisation speed would be much slower than this.

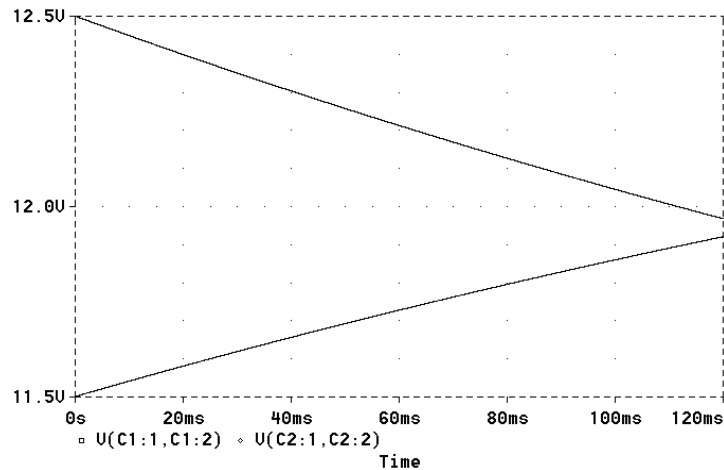


Figure 4.3. 24W buck-boost converter equalisation.

4.2. 192W buck-boost converter

The setup configuration of this 192W Buck-boost converter simulation is similar to the 24W version. However, there are four changes required. First, in this simulation the source and the target banks are made up of 8 and 6 batteries connected in series. Therefore, the initial voltage for the source and the target banks are set as 100V ($12.5V \times 8$) and 69V ($11.5V \times 6$). Second, because the operational voltage has been increased, the switching frequency is reduced to minimise the switching loss, and in this simulation the switching frequency is set to 50kHz. Third, in Chapter 3.2, the minimum required inductance to maintain the continuous conduction for 50kHz switching frequency was calculated as $192\mu\text{H}$. Moreover a larger inductance requires more turns, therefore, the dc resistance of the inductor will also be increased, and in this simulation the inductor dc resistance is set to $70\text{m}\Omega$. Fourth, the MOSFETs have to be changed to handle larger the input voltage, and so in this converter the IRF740 was chosen. The schematic of the 192W buck-boost converter is shown in *Figure 4.4*.

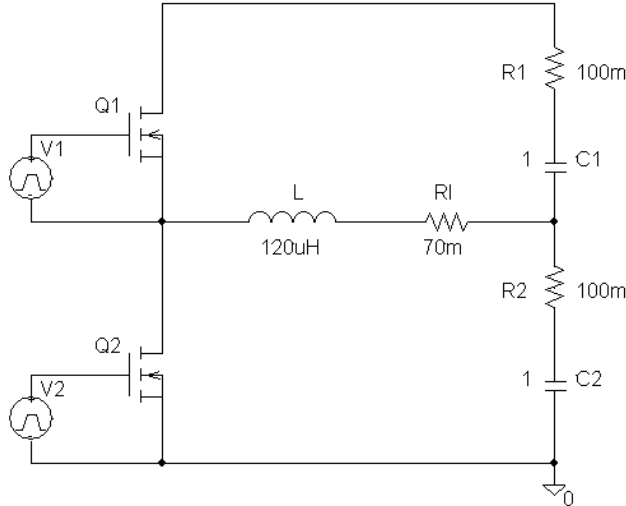


Figure 4.4. 192W buck-boost converter

In the simulation results, the PWM switching signal is represented by the switching signal V1. Vds indicates the drain to source voltage of Q1. I_{C1} and I_{C2} show the current flow from the source and target batteries C1 and C2. Finally, I_L represents the current flow through the inductor L. The operation principle of the 192W buck-boost converter is identical to the 24W version. This assumed, C1 has a higher voltage than C2, and the detailed operational waveforms are shown in *Figure 4.5*.

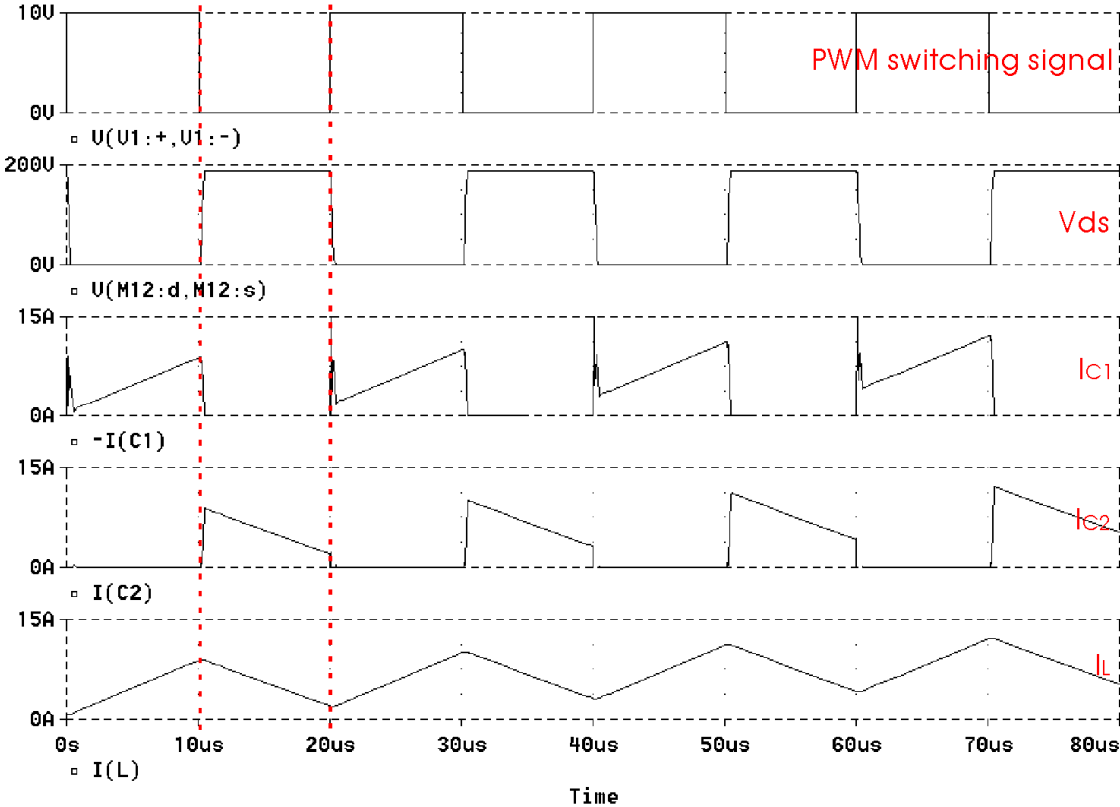


Figure 4.5. 192W buck-boost converter switching waveforms.

From *Figure 4.5*, the shape of the switching waveform of the 192W buck-boost converter is similar to the 24W version. The only difference is due to the input voltage being eight times higher than the 24W buck-boost converter, the required MOSFET drain to source voltage V_{ds} also becomes eight times higher. In *Figure 4.5*, the current waveform from the source battery has a large current overshoot during the transition from off to on period. This is caused by the reverse recovery of the body diode in Q2 which has been conducting immediately prior to Q1, and then creates the current overshoot. The voltage equalisation result of the 192W buck-boost converter is shown in *Figure 4.6*, which demonstrates in principle that battery bank voltage can also be balanced.

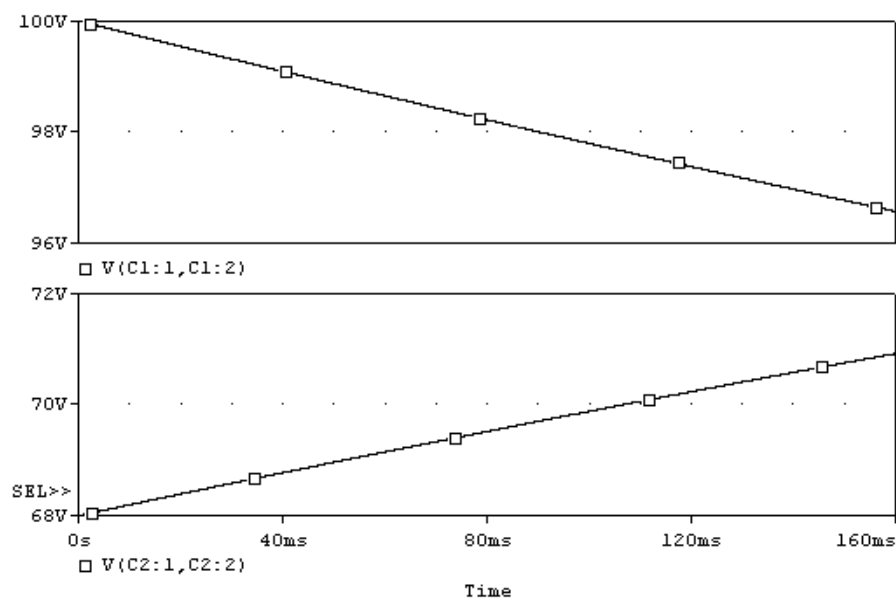


Figure 4.6. 192W buck-boost converter equalisation.

4.3. 192W flyback converter

The use of the flyback converter is to provide both electrical insulation between the top and the bottom battery banks and to balance the voltage of those bank. The schematic of the single switch flyback converter is shown in *Figure 4.7*. In this simulation the initial voltage of each bank is set to 100V ($12.5V \times 8$) and 69V ($11.5V \times 6$), and the switching frequency is set to 50kHz. In Chapter 3.3, the primary and secondary inductances were calculated as $174\mu\text{H}$ and $98\mu\text{H}$ respectively. To simulate the clamping circuit, the primary and the secondary leakage inductances were estimated as $2\mu\text{H}$ and $1\mu\text{H}$ respectively. The

transformer primary and secondary wiring resistances in this simulation were estimated as 50mΩ and 25mΩ respectively.

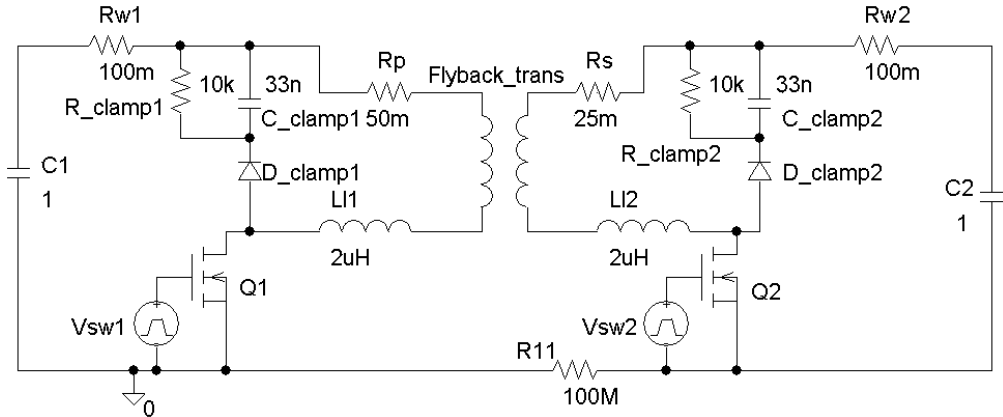


Figure 4.7. The schematic of the 192W flyback converter

In the simulation, C1 was assigned has higher charge level than C2. To transfer the energy from C1 to C2, the switching signal diagrams of this flyback converter are shown in *Figure 4.8*. In the simulation results, the PWM switching signal is represented by the switching signal V_{SW1} . V_{ds} indicates the drain to source voltage of Q1. I_{C1} and I_{C2} show the current flow from the source and target batteries C1 and C2. I_d specifies the current flow through the MOSFET Q1 and finally I_{d_clamp} symbolises the current flow through the clamping diode $D_{_clamp1}$.

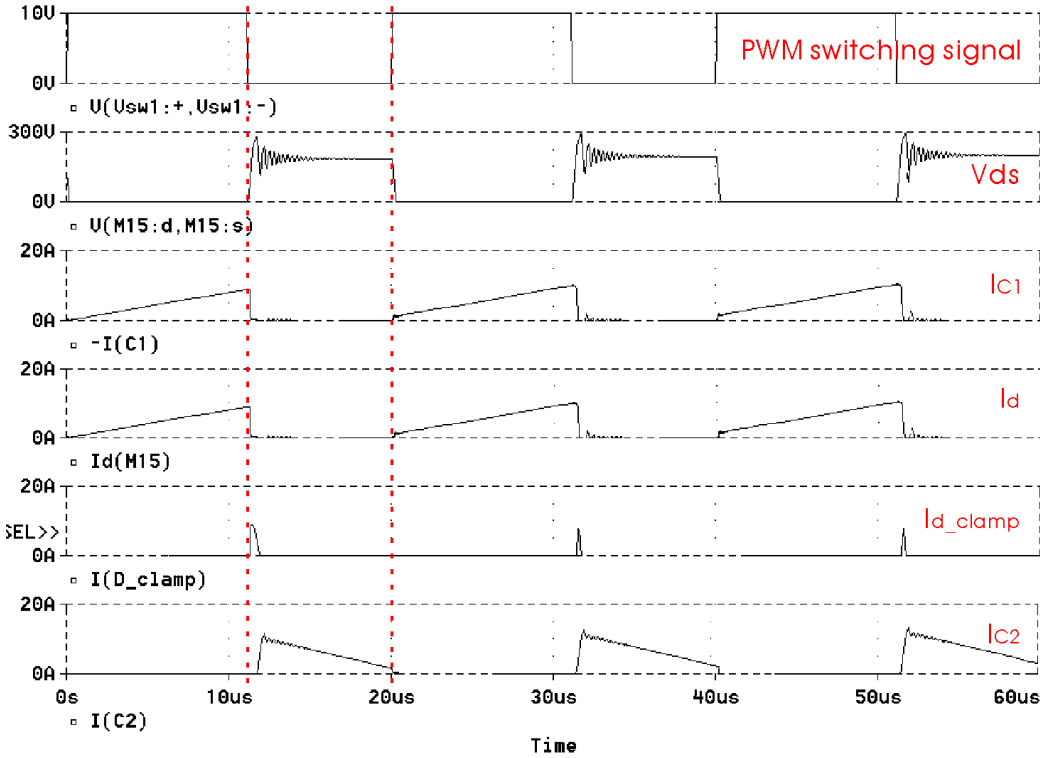


Figure 4.8. 192W flyback converter switching waveforms.

As Figure 4.8 indicates for the flyback converter, when the switch V_{SW1} is high, Q1 turns on. The primary inductance is charged by C1. During this period, because the clamping diode D_clamp1 polarity is reversed, the clamping circuit is inactive. When V1 turns low, the leakage inductance energy flows into the clamping circuit and the power dissipating component C_clamp1 and R_clamp1 dissipates this energy. Then the stored energy from the primary inductance is transferred to the secondary inductance. During this turn off state, the current flow at the secondary side goes through the internal diode of Q2 to C2 to complete one equalisation cycle without any additional control. During this turn off period, clamping circuit 2 does not do anything because it only functions when energy is taken from C2 to C1. The result of this simulation is shown in *Figure 4.9*, which demonstrates in principle that the battery bank voltages at either end of the battery string can be balanced.

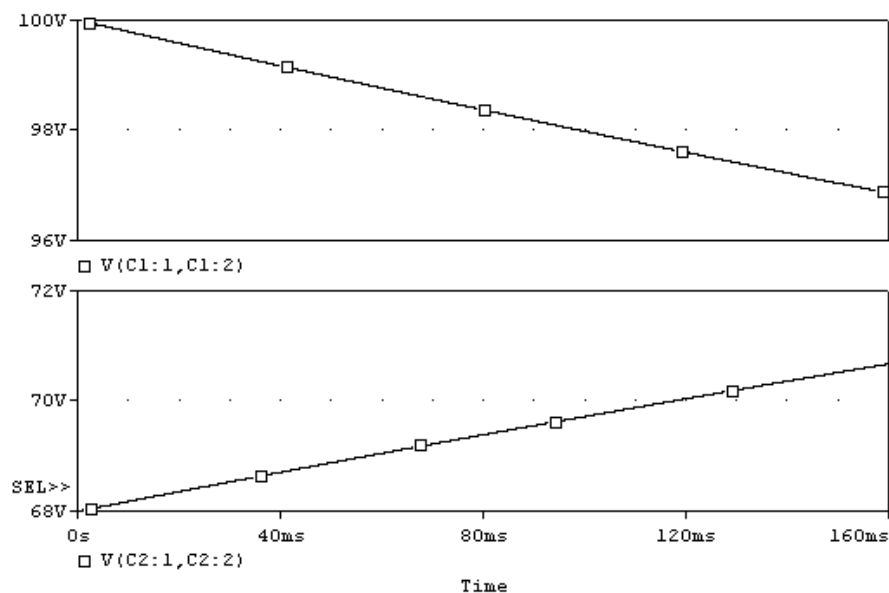


Figure 4.9. 192W flyback converter equalisation.

4.4. Summary

In this Chapter, three different power converters 24W buck-boost, 192W buck-boost and 192W flyback converters were simulated by PSpice simulator. The calculated component values for each converter were obtained in Chapter 3. The detailed switching waveforms for each converter were also described, and the simulation results show that the energy equalisation between each individual battery and between banks of batteries can be achieved. In the next chapter, the construction of each converter are detailed.

5. The system construction

In Chapters 3 and 4, the design procedures and the simulations of this voltage equaliser were detailed. In this chapter, the construction procedures of the 24W buck-boost converter, the 192W buck-boost converter, and the 192W flyback converter are described. The concept of the system's construction is to make each converter compact, light weight, easy to manufacture and highly efficient, with the target efficiency for each converter at 90%.

For the 24W buck-boost converter, the main design concentrates on the performance investigation of the different inductor cores: the RM core, the planar core and the integrated inductor. Then the investigation results are applied to the design of the 192W buck-boost converter. In the design of the 192W buck-boost converter, due to the converter structure being identical to the 24W version, the design procedure would be focused on minimising the power losses of the converter. In the design of the 192W flyback converter, investigating the frequency response of the flyback converter will be first discovered. Then the clamping circuit will be made to reduce the voltage stress on the MOSFET from the leakage inductance of the chosen flyback transformer.

To turn each equaliser on and off easily, two 4N35 optical couplers are employed on each PWM controller to enable and disable PWM control. This makes the PWM controllers easier to interface with the micro-controller. However, in order to minimise the component count and accelerate the construction process, the current mode control circuits are built on a separate board, which would be connected to the equaliser when the converter is required to be turned on.

5.1. The 24W Buck-boost converter

The overall voltage equalisation system requires twenty-two 24W buck-boost converters. To minimise the weight and size, a heatsinkless design is essential. To achieve this, the right MOSFET and right switching frequency have to be carefully selected in order to improve the converter efficiency.

5.1.1. Inductor design

In Chapter 3, the three different types of inductors, RM, planar and integrated inductors were introduced, and their advantages and disadvantages were also discussed. In this section, the performance analysis of these inductors is measured.

For this performance test, three buck-boost converters were built based on these three types of inductor. In order to accurately compare the performance of each inductor, each converter used an identical MOSFET, and had identical pcb layouts. For this test, the switching frequency was set from 100kHz to 200kHz, and the maximum current swing was set to 6A. The required minimum inductance of 12 μ H was calculated from *Equation 3.1*.

The first inductor was based on a RM core, and it was wound with 1.2mm diameter litz wire. The number of turns and the air gap were 8 and 0.8mm respectively. The inductance and the dc resistance of this inductor were recorded as 16 μ H and 33m Ω . The second inductor was based on an E32 planar core. This planar inductor was made up of two double layer pcbs, and the width of the pcb track was 95mil. The inductance and the dc resistance of this inductor were recorded as 16 μ H and 59m Ω respectively. The third inductor was the integrated inductor. Due to the core size of the integrated inductor, each integrated inductor can only provide 5 μ H of inductance. Therefore in this performance test, three integrated inductors were connected in series to make up a 15 μ H inductor, and the efficiency comparison of the three inductors is shown in *Figure 5.1*.

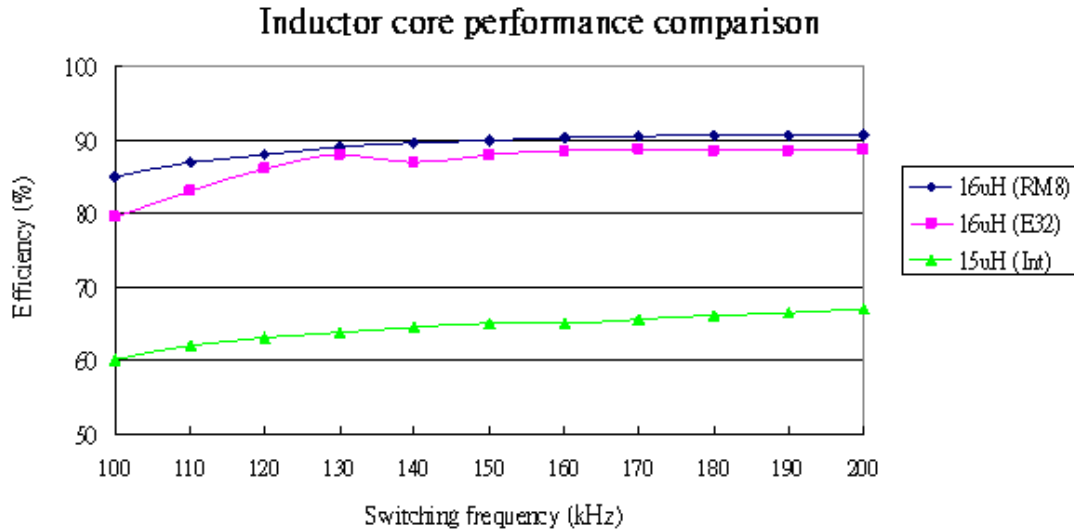


Figure 5.1. RM, planar inductor and integrated inductors efficiency comparison

This efficiency measurement is made by applying a constant input voltage 12 Volts and constant input current 2A into the converter. Then varying the switching frequency from 100kHz to 200kHz, and then measure the output voltage and output current from the resistive load and calculate the output power to determine the efficiency.

The experimental results in *Figure 5.1* show the efficiency of the converter that uses the planar inductor is typically around 1.5 ~ 2% lower than the inductor wound on the RM core. This extra loss from the planar inductor is caused by the higher winding resistance; whereas the litz wire that was used in the RM cored inductor has a much larger cross section area compared to the pcb track. The advantage gained by using a planar inductor to produce a low profile pcb outweighs the small loss in efficiency. However, by looking at the efficiency of the integrated inductor, its performance is unsatisfactory. Due to the track width of the integrated inductor being much narrower than the others; it ends up with the highest dc resistance and the worst efficiency. Therefore, from considering the performance, ease of construction and cost, the planar inductor was chosen.

The chosen planar inductor core for the 24W Buck-boost converter was Philips 3C90 E32 core. Due to the manufacturability, it is difficult to make more than two layers per pcb. Therefore, the inductor was made by connecting two double layer pcb to achieve a total four layer board.

In the power converter design, minimising the temperature rise on the pcb is important for reducing the conducting loss from the pcb tracks. The pcb track material used in this project is 1oz copper. According to the temperature rise versus track width diagram shown on *Figure 3.6*, for the single side pcb and the average current of 2A, the temperature rise can be maintained under 20°C if the track width is wider than 50 mils. The same theory can also be applied to the double side pcb; by having an identical operational current and 20°C limitation on temperature rise, the minimum pcb width would be 100 mils.

In the E32 planar inductor, the winding space allows two turns of 110 mils wide pcb tracks per layer. Therefore, for two double layer pcbs, eight turns in total were achieved in this E32 planar inductor, and by adding the 0.8mm air gap, the inductance was measured as 35 μ H. The photo of the inductor is shown in *Figure 5.2*.

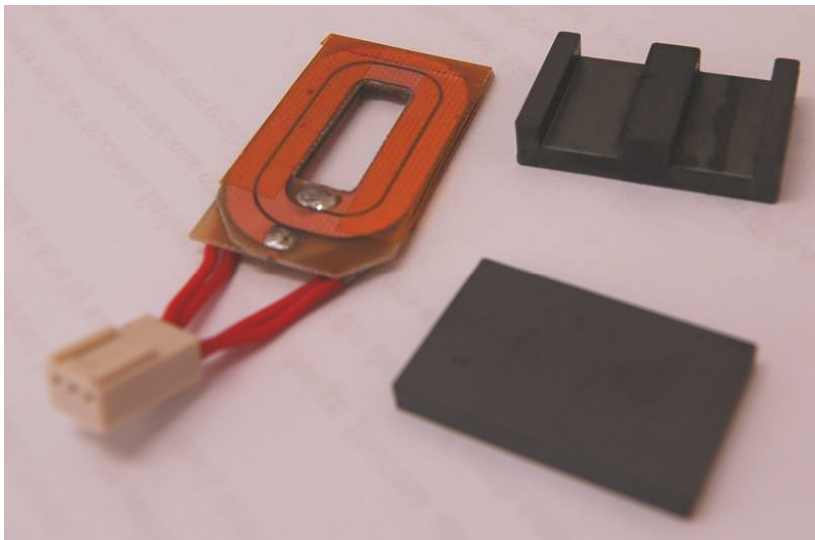


Figure 5.2. The inductor for the 24W buck-boost converter

5.1.2. MOSFET selection

In this battery equalisation system, 22 24W buck-boost converters need to be built, and in Chapter 3 the requirements of the MOSFET were detailed. Ideally, to achieve a heatsinkless design, the MOSFETs have to have low on-resistance to minimise the conduction loss, and low gate charge to reduce the switching loss. However, due to the concerns of the cost and the availability, it is not practical to select a MOSFET that has both low on-resistance and gate charge.

To minimise the power losses for this 24W buck-boost converter, the logic MOSFET was chosen. The logic MOSFET is designed for low power converter use, and it normally has the slightly lower gate charge than the standard MOSFET. Therefore, it can be switched as low as 5V compared with 10V from the standard MOSFET. However, applying higher switching voltage to the logic MOSFET can reduce the charging time on the gate capacitance, which results a quick switching transition, and then reduces the switching loss.

The MOSFET used in this 24W buck-boost converter was SUD35N05-26L. The SUD35N05-26L is a logic type MOSFET, which has the voltage rating of 55V and the average current rating of 25A. When switching at 12V gate signal, the R_{ds-on} is 20m Ω and the gate charge is 22nC. It is also a surface mount component; therefore, the converter can be made in low profile format. The final design of the 24W Buck-boost converter is shown in *Figure 5.3*, and according to the experimental results, the maximum efficiency was recorded as 92% when switching at 70kHz. Since the power loss from this converter is only 2W, the heatsink is not required in this converter.

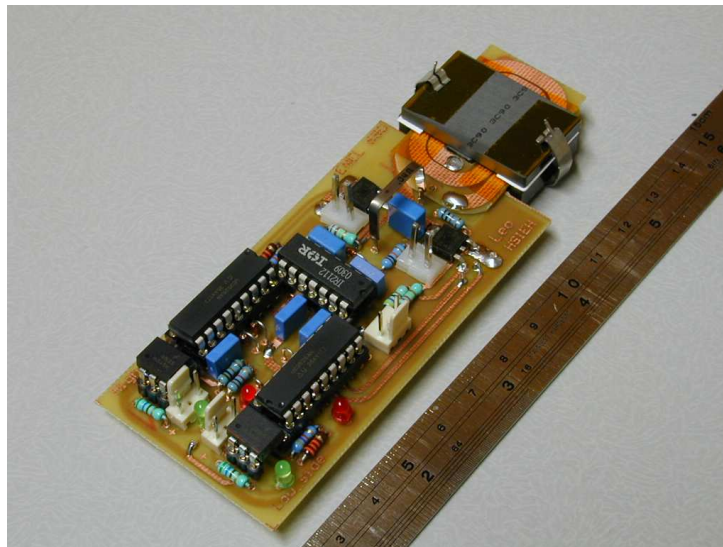


Figure 5.3. The photo of the 24W Buck-boost battery equaliser

The measured switching signal of the design's 24W buck-boost converter is shown in *Figure 5.4*. It includes the waveforms of the PWM signal from the PWM controller, the MOSFET drain to source voltage and the inductor current waveforms. The PWM controller generates a 70kHz switching signal. When the switching signal is high, MOSFET turns on and then the inductor is charged by the source battery; therefore, the inductor current ramps

up. Then when the switching signal is low, MOSFET turns off, and then the stored energy in the inductor discharges the stored energy into the lower charged battery.

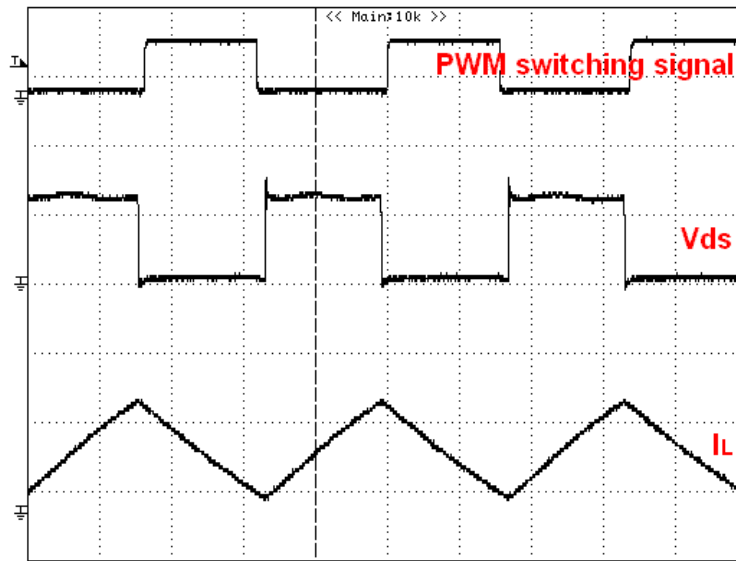


Figure 5.4. 24W buck-boost converter action waveforms

5.2. The 192W Buck-boost converter

The design procedure of the 192W buck-boost converter is identical to the 24W buck-boost converter. In the design of the 192W buck-boost converter, the Philips E43 planar inductor was selected. In Chapter 3.2, the required inductance for this 192W buck-boost converter was calculated as $166\mu\text{H}$. Comparing with the previous inductor from the 24W buck-boost converter, the larger inductance requires more turns to be made up, thus it requires increasing the wiring resistance of the inductor. In this inductor, the wiring pcb was also constructed by 2 double layer pcbs, but each layer has 3 turns, and the track width is 135 mil to increase the inductance and reduce dc resistance. The required air gap was calculated as 0.4mm, and the inductance was measured as $191\mu\text{H}$. Then, assuming input voltage equals 96V, the ripple current is 6A and 50% duty-cycle, the minimum switching frequency is calculated as 50.4kHz. by *Equation 3.1*.

The chosen MOSFET for this 192W buck-boost converter was IRF740. The voltage and the current ratings of this MOSFET are 400V and 10A respectively. The on-resistance R_{ds-on} and the gate charge of this MOSFET are 0.55Ω and $36nC$, therefore the conducting loss from the higher on resistance and the switching loss from the higher gate capacitance and higher input voltage would result a larger power loss than the 24W buck-boost converter.

In order to dissipate the power losses from the MOSFETs, the heatsinks were required in this 192W buck-boost converter. According to the experimental results, the best efficiency was recorded as 90% when the switching frequency was 60kHz. A photo of the 192W buck-boost converter is shown in *Figure 5.5*.

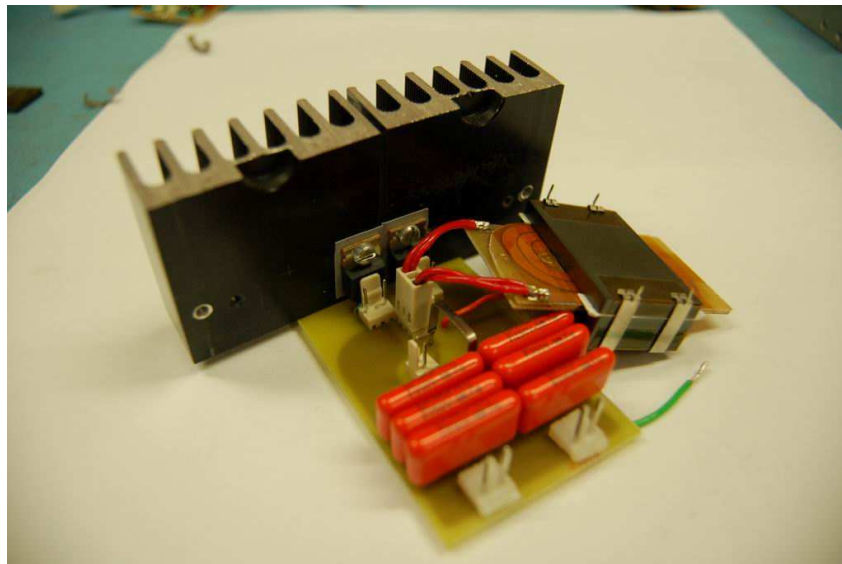


Figure 5.5. The 192W buck-boost converter

5.3. The 192W Flyback converter

In this 192W flyback converter, the required voltage and current rating are identical to the 192W buck-boost converter. Therefore, IRF740 was selected in this converter. The use of the flyback converter is to provide an electrical isolation between the source and the load. Therefore, the design of this flyback converter would be focused on the flyback transformer design and reducing the voltage stress of the MOSFET.

In Section 5.1 and 5.2, the inductors for both 24W and 192W buck-boost converters are constructed based on the planar inductors, which result in an overall design with high productivity, low profile and low cost. However due to the manufacturability and the concern for the converter efficiency, the flyback transformer was wound on the standard RM core, and in order to improve the transformer efficiency and experimental frequency capability, litz wire was used.

The design procedure of the flyback transformer is described in Chapter 3.3. By making different flyback transformers for different switching frequencies, the frequency response curve was made to find the maximum efficiency point and the efficiency curve is shown in *Figure 5.6*.

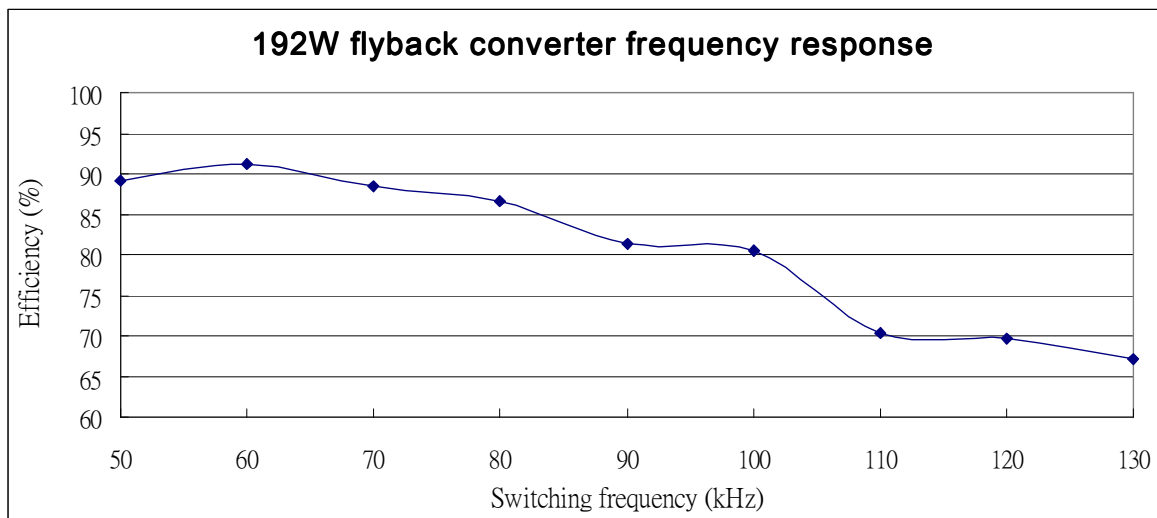
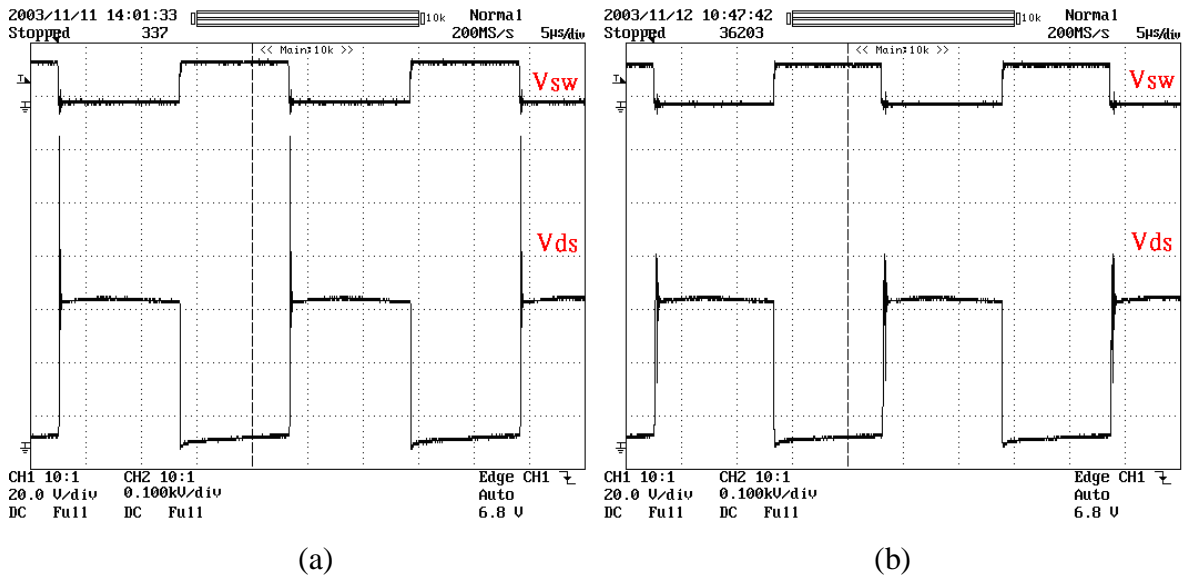


Figure 5.6. The frequency response curve of the 192W flyback converter.

In this efficiency test, the converter reaches the highest efficiency at 60kHz. At this frequency, the flyback transformer was designed to have 20 turns on the primary winding and 16 turns on the secondary winding.

In this performance test, the converters were made without the clamping circuit. As mentioned in Chapter 3.3, the clamping circuit is designed to reduce the voltage stress on the MOSFET, hence improving the safety of the converter. However, due to the clamping circuit slows down the MOSFET turn off time, the increased turn off time will decrease the converter efficiency.

To design the clamping circuit for this flyback transformer, the leakage inductances of the primary and secondary windings were measured as $1.9\mu\text{H}$ and $1.2\mu\text{H}$. To select the value of power dissipating components R_c and C_c in the clamping circuit, the clamping voltage has to be defined. In general practice, the clamping voltage can be set up to 30% higher than 2 times the input voltage without affecting the converter efficiency too much. Therefore, in this design, a $1\text{k}\Omega$ resistor and a 3.3nF capacitor were chosen. In *Figure 5.7* the switching waveforms show the switching signal of the MOSFET.



(a) Switching and drain to source signals without clamping circuit.
 (b) Switching and drain to source signals with clamping circuit.

Finally, this 192W flyback converter was made, and the photo of the converter is shown in *Figure 5.8*. The maximum efficiency was recorded as 89% at the switching frequency of 60kHz

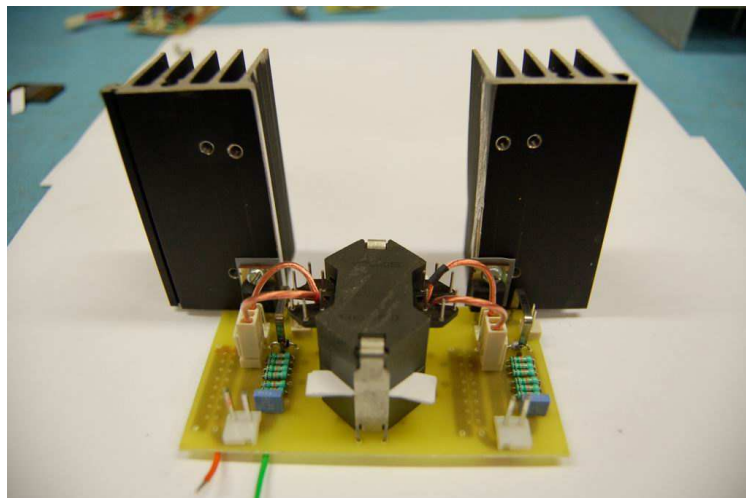


Figure 5.8 The photo of the 192W flyback converter

The switching waveform of this 192W flyback converter is shown in *Figure 5.9*. It shows when the primary switching signal is high, the primary MOSFET turns on and then the primary inductor is charged by the source battery. Then when the primary switching signal is low, the primary MOSFET turns off. The flyback action would transfer the stored energy to the secondary side and then flow through the internal diode of the secondary side MOSFET to recharge the load battery.

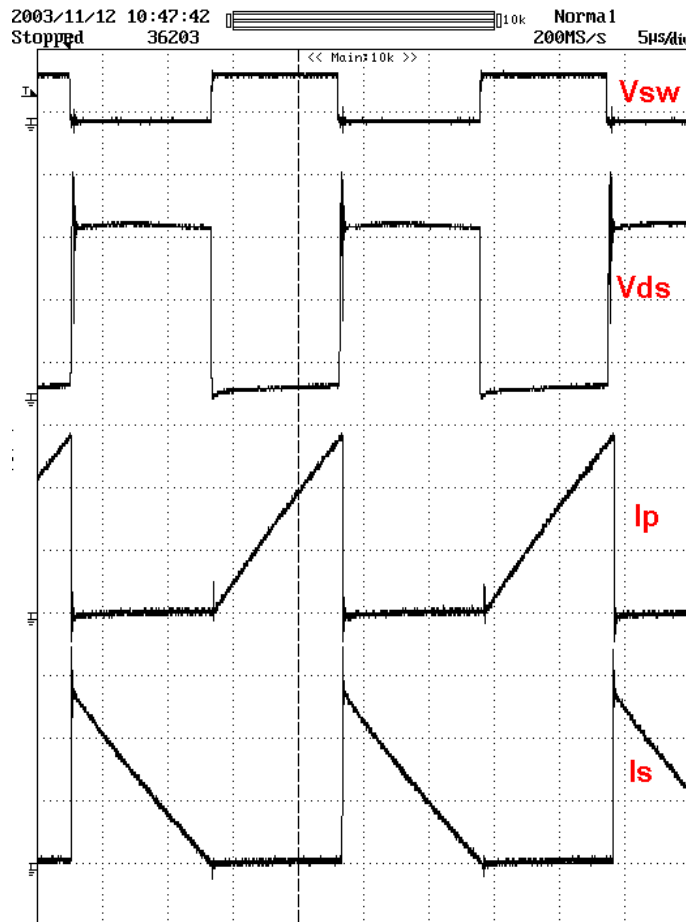


Figure 5.9. The switching waveform of the 192W flyback converter

In this Chapter, the construction procedures of each converter were described. In the design of the 24W buck-boost converter, the investigation of several of inductor cores was made, and the result shows the planar inductor becomes the better solution for this application in terms of the construction and the efficiency. Further, the logic level surface mount type MOSFET was used to reduce the switching loss and then making the construction of the converter into a low profile, heatsinkless format. In the design of the 192W buck-boost converter, the planar core was also chosen. However, because higher operating power and

larger power loss was involved, the surface mount type MOSFET was not suitable and the heatsink was required in this 192W buck-boost converter. In the design of the 192W flyback converter, due to the difficulty on making the multi-layer pcb and the concern for the energy efficiency, the RM core was chosen to make the flyback transformer.

5.4. Summary

In this chapter, the efficiencies from each converter were also measured. In both 24W and 192W buck-boost converters, the efficiency were recorded as 92 and 90% respectively. In the design of the 192W flyback converter, due to the voltage clamping circuit was implemented to improve the safety of the converter, the increased switching time also increases the switching loss. Then the efficiency was recorded as 89%.

In the next chapter, experimental battery equalisation tests using these converters are detailed. The equalisation process will be done by equalising series connected batteries after the batteries have been discharged at rate of 30A for an hour, and the required time for equalising the entire battery string will be measured.

6. Performance Records

In Chapters 3, 4 and 5, the designs, the simulations and the construction of each converter making up the proposed battery equaliser topology are detailed and operational tests are described. To confirm the correct operation of the overall equaliser topology, experimental measurements of the battery equalisation on two banks of $4 \times 12\text{V}$ batteries can provide a reasonably clear indication, and with this configuration, the designed 192W converters, which have already been tested to their rated capacities in Chapter 5 will be tested under 96W of load. These equalisation test results are given in this chapter.

The overall test was divided into two parts, the equalisation using the 192W non-isolated buck-boost converter and equalisation using the 192W isolated flyback converter, which are shown in *Figure 6.1*. In the first equalisation test, using the 192W non-isolated buck-boost converter, two banks of batteries were connected in series. Within each bank, the four batteries were equalised using three 24W non-isolated buck-boost converters. In the second equalisation test, the two banks were isolated from each other, and the bank equalisation was done using the 192W flyback converter. However, within each bank, the four series connected batteries were still equalised by three 24W non-isolated buck-boost converters.

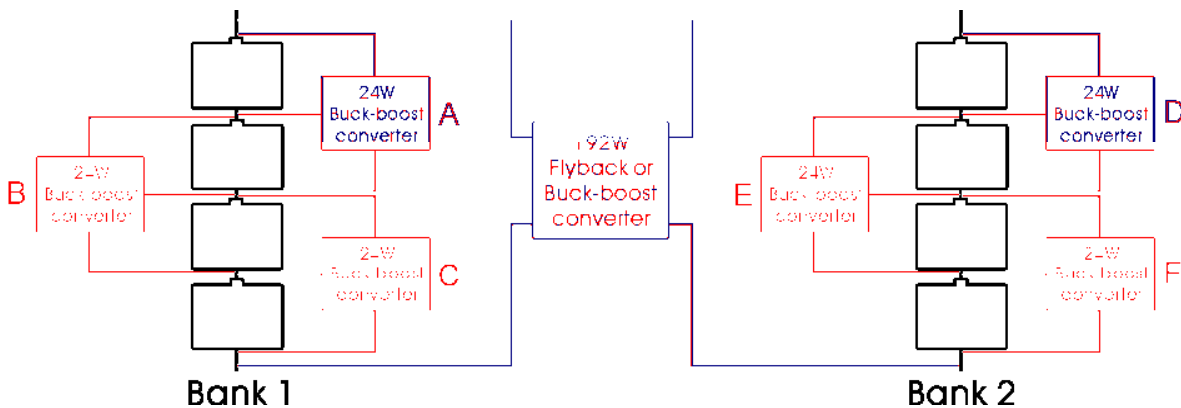


Figure 6.1. The equalisation setup

For these equalisation tests, each battery is rated 76Ahr, which is three times higher than the batteries used in the EV3. Because of this, the equalisation speed will also be three times slower. Before each equalisation test, all eight batteries were connected in parallel and equally charged to around 13.5V. After that, these batteries were disconnected, settled for three hours, and then reconnected into two banks of four series connected batteries and

their open-circuit voltages are recorded. At this stage, four older batteries were intentionally grouped into one bank to deliberately make the bank perform like a weak battery bank, and the other four batteries were formed into a stronger battery bank. Since old batteries always draw energy faster than newer ones, separating the old and the new batteries can make a clear voltage difference between the two banks. Next, these two banks of batteries were connected in series and then discharged by a carbon resistor at a rate of 30A for an hour, which is approximately the average power consumption that is equal to the EV3 being driven in the city area in an hour. After that, the whole battery string was left to settle for three hours, and then the open-circuit voltage from each battery was recorded again.

During equalisation, the decision to turn on or off on each converter is not straightforward. Because, for the open circuit battery monitoring measurement, the rate of change of voltage on each battery is different. Besides, the rate of change of voltage on each battery when it approaches full charge or nears the under charge condition are also different. Therefore a comprehensive control system is required to accurately and efficiently turn on or off each converter. Such control would be necessary when the equalisation system was installed in the EV3. However the design of the control system for the equaliser was not part of the brief for this project, because extensive testing of the system would be required first to ascertain an appropriate control strategy. For the purposes of these results, each converter was controlled manually according to a set of rules, which are described by *Figure 6.2*.

The rules for this equalisation process are simply when the open-circuit voltage between any two adjacent batteries is greater than 0.2V, the 24W buck-boost converter will be activated to balance these two batteries, or if the bank voltage difference is greater than 0.6V, the bank equalisation will start. Because the measured open-circuit voltage during the equalisation process is much higher than its settled open-circuit voltage, the target battery would be charged until its open-circuit voltage becomes 0.3 to 0.5V higher than the source battery.

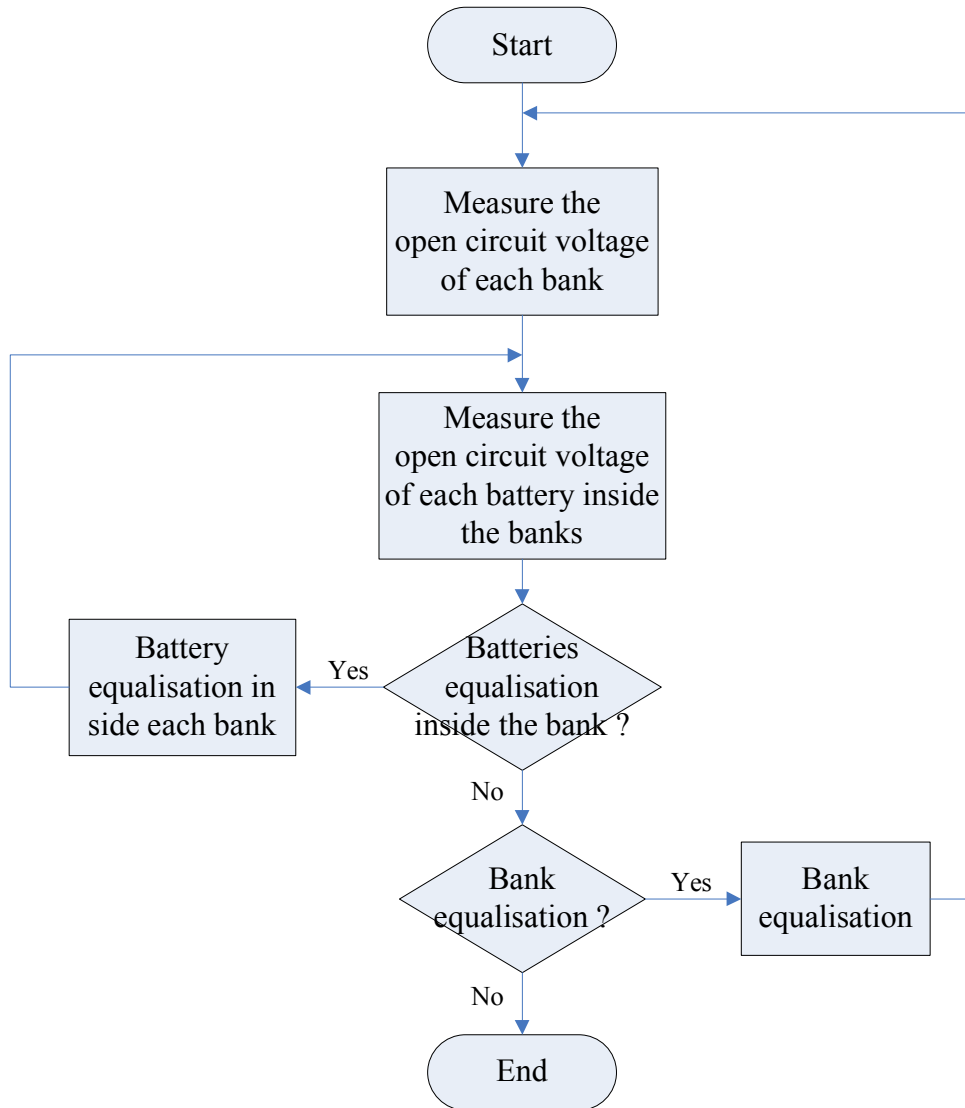


Figure 6.2. Equalisation procedure

6.1. Battery equalisation between non-isolated banks

The first battery equalisation test was set up to balance two series-connected battery banks, which were formed by four series connected batteries in each bank. Within each bank, three 24W buck-boost converters were used to equalise two adjacent batteries, and the set up diagram is shown in *Figure 6.3*. After the entire battery string has been discharged at rate of 30A, the open-circuit voltages from each battery are recorded in *Table 6.1*.

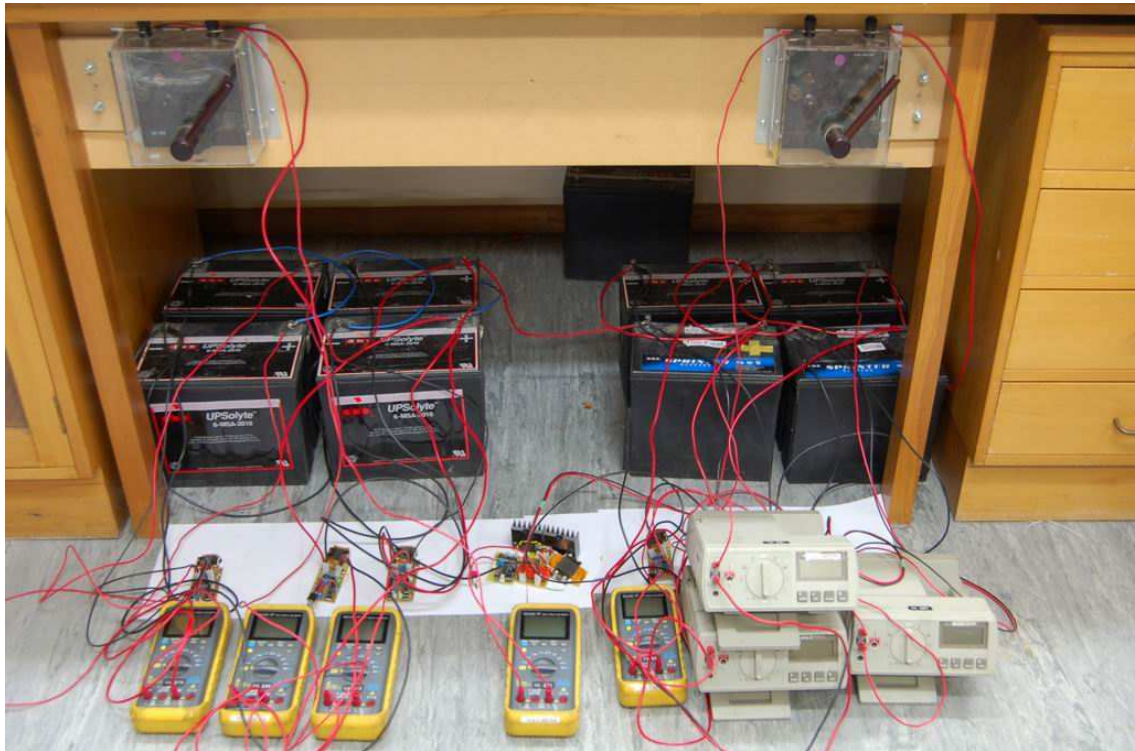
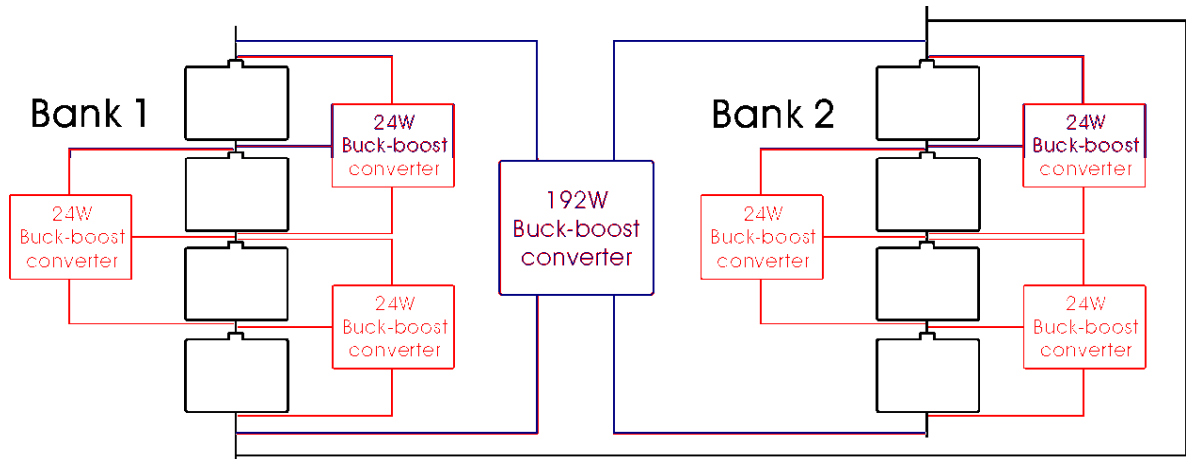


Figure 6.3. The setup diagram for non-isolated bank equalisation

| | Batt1 | Batt2 | Batt3 | Batt4 | Batt5 | Batt6 | Batt7 | Batt8 |
|--------------------------|-------|-------|-------|-------|-------|-------|-------|-------|
| Voltage before discharge | 13.52 | 13.67 | 13.54 | 13.57 | 13.58 | 13.57 | 13.55 | 13.62 |
| Voltage after discharge | 11.05 | 11.08 | 11.09 | 11.2 | 11.45 | 11.57 | 11.59 | 11.42 |

Table 6.1. The measured battery open-circuit voltages

In *Table 6.1*, Batt 1 to 4 was formed by four older batteries to make up the first battery bank. Batt 5 to 8 was formed by four newer batteries to make up the second battery bank. The following steps detail the battery equalisation process, which was based on the 192W and 24W buck-boost converter, and the equalisation results are shown in *Figure 6.4*.

Equalisation starts – Bank 1 voltage = 44.42V, Bank 2 voltage = 46.03V.

No battery equalisation required inside each bank.

Bank 2 starts transferring to Bank 1 by 192W buck-boost converter

Interval 1 – Bank 2 transfers energy to Bank 1 by 192W buck-boost converter

Point A – Bank 2 stops transferring energy to Bank 1 (Bank 1 idles)

Batt7 starts transferring energy to Batt8 by 24W buck-boost converter

Interval 2 – Batt7 transfers energy to Batt8 by 24W buck-boost converter

Point B – Batt7 stops transferring energy to Batt8

Bank 2 starts transferring energy to Bank 1 by 192W buck-boost converter

Interval 3 – Bank 2 transfers energy to Bank 1 by 192W buck-boost converter

Point C – Bank 2 stops transferring energy to Bank 1 (Bank 2 idles)

Batt2 starts transferring energy to Batt3 by 24W buck-boost converter

Interval 4 – Batt2 transfers energy to Batt3 by 24W buck-boost converter

Point D – Batt2 stops transferring energy to Batt3

Bank 2 starts transferring energy to Bank 1 by 192W buck-boost converter

Interval 5 – Bank 2 transfers energy to Bank 1 by 192W buck-boost converter

Point E – Bank 2 stops transferring energy to Bank 1 (Bank 2 idles)

Batt4 starts transferring energy to Batt3 by 24W buck-boost converter

Interval 6 – Batt4 transfers energy to Batt3 by 24W buck-boost converter

Point F – Batt7 starts transferring energy to Batt8 by 24W buck-boost converter

Interval 7 – Batt4 transfers energy to Batt3 by 24W buck-boost converter

Batt7 transfers energy to Batt8 by 24W buck-boost converter

Point G – Batt4 stops transferring energy to Batt3

Batt1 starts transferring energy to Batt2 by 24W buck-boost converter

Interval 8 – Batt7 transfers energy to Batt8 by 24W buck-boost converter

Batt1 transfers energy to Batt2 by 24W buck-boost converter

Point H – Batt7 stops transferring energy to Batt8 (Bank 2 idles)

Interval 9 – Batt1 transfers energy to Batt2 by 24W buck-boost converter

Point I – Batt1 stops transferring energy to Batt2. Bank 1, Bank 2 idle. Equalisation Ends

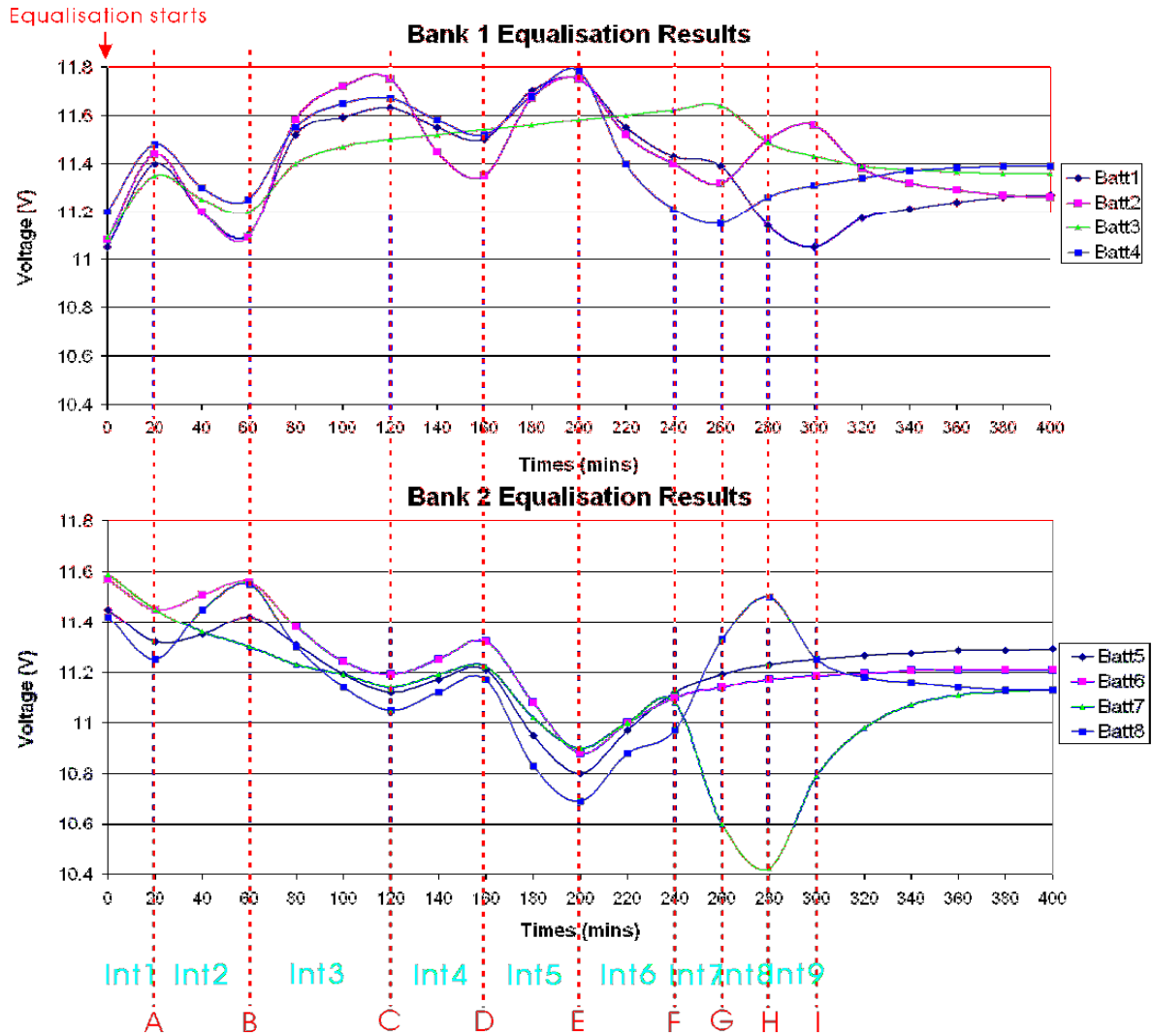


Figure 6.4. Battery equalisation process for an eight series connected batteries

In this equalisation test, two banks of battery were connected in series, and this equalisation process shows these two banks can be successfully equalised by the combination of the 192W and 24W buck-boost converters.

6.2. Battery equalisation between isolated banks

The second battery equalisation test was set up to balance two isolated battery banks. Inside each bank there were four batteries connected in series. In this equalisation test, the bank equalisation was done by the 192W flyback converter and the individual battery inside each bank was balanced by the 24W buck-boost converter. The set up diagram is shown in *Figure 6.5*.

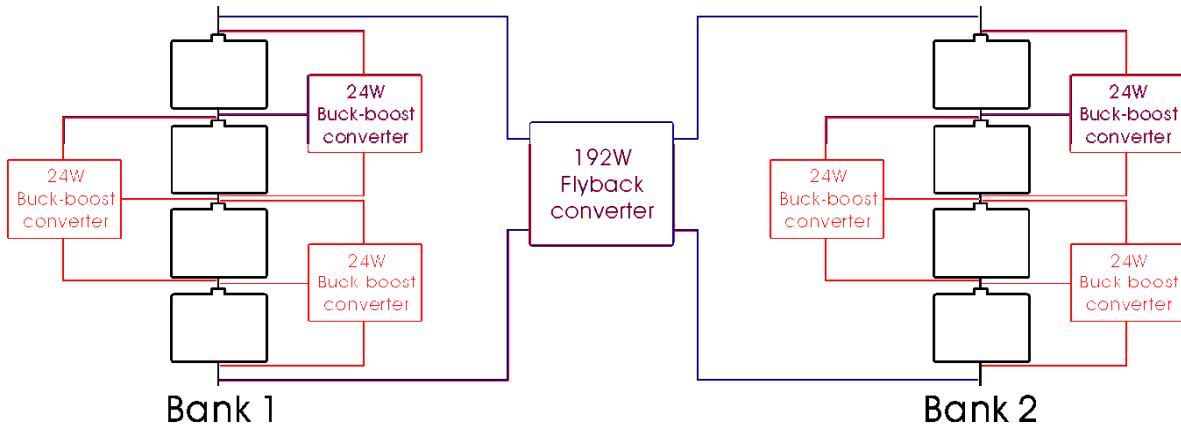


Figure 6.5. The setup diagram for isolated bank equalisation

Again, a battery discharging process has done before the equalisation process, and the measured open-circuit voltage are recorded in *Table 6.2*.

| | Batt1 | Batt2 | Batt3 | Batt4 | Batt5 | Batt6 | Batt7 | Batt8 |
|--------------------------|-------|-------|-------|-------|-------|-------|-------|-------|
| Voltage before discharge | 13.76 | 13.77 | 13.74 | 13.68 | 13.75 | 13.73 | 13.7 | 13.79 |
| Voltage after discharge | 11.76 | 11.74 | 11.92 | 11.71 | 12.01 | 11.88 | 11.79 | 11.9 |

Table 6.2. The measured battery open-circuit voltages

The following steps detail the battery equalisation process, which was based on the 192W flyback converter and 24W buck-boost converters, and the equalisation results in *Figure 6.6* shows two isolated battery bank can be successfully balanced.

Equalisation starts – Batt3 starts transferring energy to Batt4 by 24W buck-boost converter
 Batt5 starts transferring energy to Batt6 by 24W buck-boost converter
 Batt8 starts transferring energy to Batt7 by 24W buck-boost converter

Interval 1 – Batt3 transfers energy to Batt4 by 24W buck-boost converter
 Batt5 transfers energy to Batt6 by 24W buck-boost converter
 Batt8 transfers energy to Batt7 by 24W buck-boost converter

Point A – Batt8 stops transferring energy to Batt7

Interval 2 – Batt3 transfers energy to Batt4 by 24W buck-boost converter
 Batt5 transfers energy to Batt6 by 24W buck-boost converter

Point B – Batt5 stops transferring energy to Batt6

Interval 3 – Batt3 transfers energy to Batt4 by 24W buck-boost converter

Point C – Batt3 stops transferring energy to Batt4
 Bank 2 starts transferring energy to Bank 1 by 192W flyback converter

Interval 4 – Bank 2 transfers energy to Bank 1 by 192W flyback converter

Point D – Bank 2 stops transferring energy to Bank 1

Interval 5 – System idle

Point E – Batt3 starts transferring energy to Batt2 by 24W buck-boost converter

Interval 6 – Batt3 transfers energy to Batt2 by 24W buck-boost converter

Point F – Batt6 starts transferring energy to Batt7 by 24W buck-boost converter

Interval 7 – Batt3 transfers energy to Batt2 by 24W buck-boost converter
 Batt6 transfers energy to Batt7 by 24W buck-boost converter

Point G – Batt3 stops transferring energy to Batt2

Batt6 stops transferring energy to Batt7

Equalisation ends

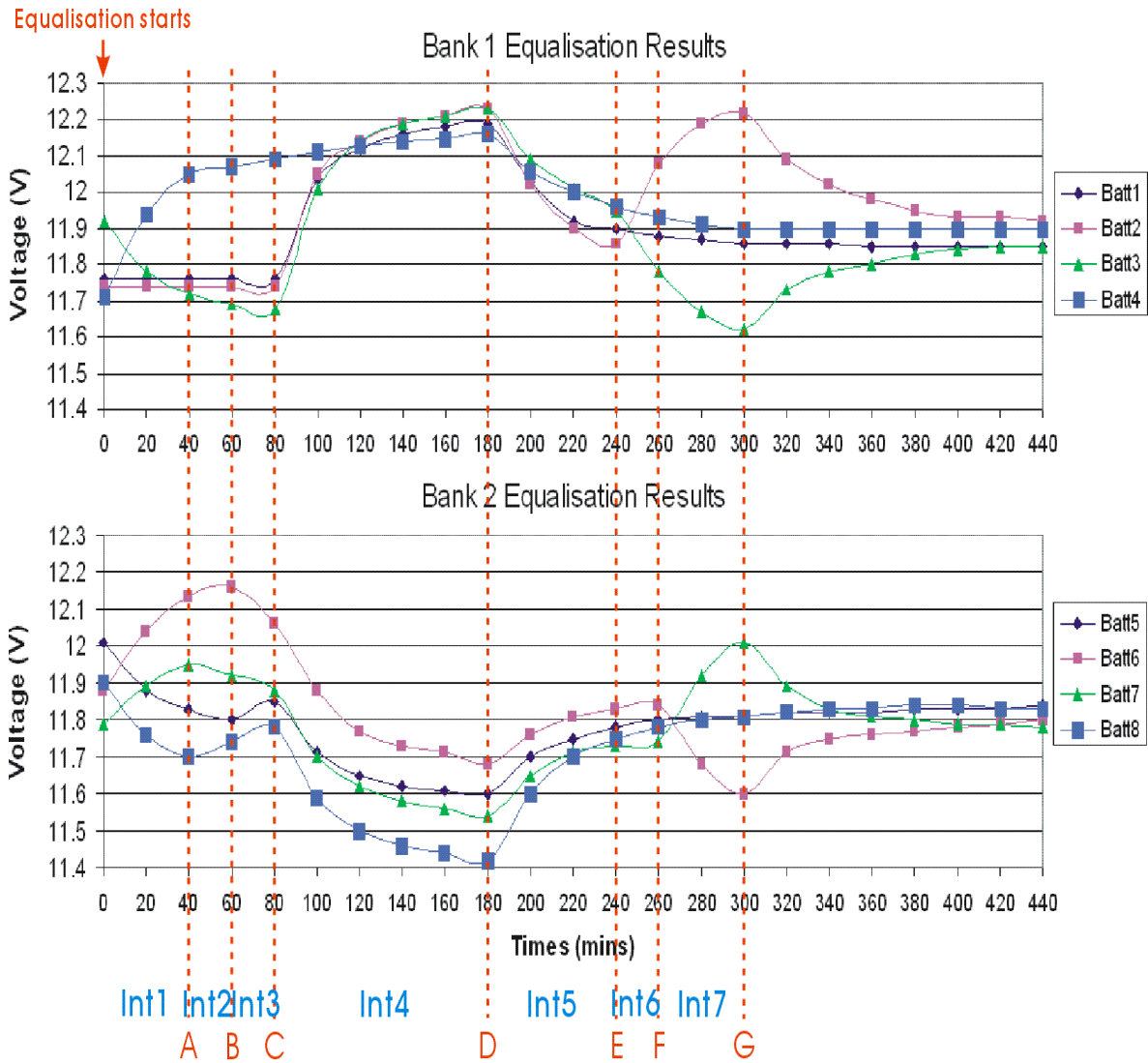


Figure 6.6. Equalisation process for the isolated battery banks

6.3 Summary

In this chapter, two battery equalisation tests are detailed and the results indicate that each individual battery can be successfully equalised to adjacent batteries. However, there was one disadvantage found during the test. That is, when the 192W converter is turned on, the 24W converters have to be off. Otherwise the 192W and the 24W converters would affect each other, and making the overall system unstable. When two banks are equalised by the 192W converter, the rest of 24W converters have to wait until the 192W converter finishes the bank equalisation. To solve this problem, reducing the number of batteries per bank can increase the chance of multiple banks working at the same time. However by doing this, the system would require more converters to do the bank equalisation, which increases the cost and increases the size and weight of the system. Within each bank, multiple 24W converters can be turned on at the same time without any problem. Therefore how to configure the number of converters required to equalise the bank, the batteries inside the bank and the future expansion become an important future consideration.

Additionally, in this chapter, each converter was turned on or off manually, but an automatic control scheme is required in the real world application. A possible solution could be a microprocessor-based control system with an intelligent control algorithm to monitor the condition of each battery and then give commands to each converter. However, this controller needs to accurately measure how much charge each battery has and how long the charging process needs to be done.

7. Conclusion

A prototype battery equalisation system has been designed, constructed and tested for the EV3, which is powered by 26 series-connected lead acid batteries divided into four banks. This prototype battery equalisation system is based on the ring equaliser topology. The overall system requires three different types of converters, each designed to operate under average current mode control at a rate of 2A. The three types are the 24W buck-boost converter, the 192W buck-boost converter and 192W flyback converter. The 24W and the 192W buck-boost converters are non-isolated converters and are designed for transferring energy between any two adjacent batteries or banks. The 192W flyback converter is an isolated converter that links the top and bottom battery banks to complete the ring structure.

Simulations of the designed equaliser were performed using a PSpice simulator. In the simulation section, two rechargeable batteries or banks of batteries were modelled as two 1F capacitors, and the battery internal resistance and the wiring resistances were modelled as two 100m Ω resistors. To determine the suitable initial nominal voltage for each battery and the voltage variation from each battery, a 30A, one hour battery discharge test over eight equally charged series connected batteries was done. Drawing energy from each battery at a rate of 30A is equivalent to drawing 10kW of energy from the EV3, which is approximately equal to the power consumption of standard city driving. In the simulation test, each converter was also designed to operate at a rate of 2A, and the simulation results showed that two rechargeable batteries can be successfully equalised by the proposed converter.

The aim of the design and construction is for each converter to have an efficiency of at least 90% and to be physically compact, light-weight and of a low profile format. To achieve a high efficiency at a reasonably low cost, the switching frequency and the MOSFET for each converter were carefully selected. In the design of the 24W and 192W buck-boost converters, the planar inductor was introduced to improve the manufacturability and to enable the converter to be made in a low profile format without significant efficiency reduction.

However, planar technology is not the universal solution for all inductor design. In the design of the flyback converter, the required numbers of turns for both primary and secondary winding are much higher than the number of turns used in the buck-boost converter. Therefore, in order to make the pcb track wide enough to minimise the dc resistance and at the same time fit a greater numbers of turns into a limited area, the multi-layer pcb is essential. However, due to the difficulties of making a multi-layer pcb, the planar technology was abandoned in the flyback converter design, and instead, a RM core was used and the primary and secondary windings were wound with litz wire to improve frequency capability and reduce the dc resistance.

Correctly sensing the current is the most important part in the buck-boost converter design. The current sensing resistor is not connected to the voltage reference point like the flyback converter. Therefore, to make the current sensing function work, a differential amplifier had to be used to sense the voltage difference across the current sensing resistor. A differential amplifier, which has a wide common mode range, is required. Most modern op-amps can be used in the 24W buck-boost converter, but the op-amp selection for the 192W buck-boost is very limited. The reason for this is the controller is powered by 12V, but the current sensing resistor is sitting on top of and connected to the 72V battery bank. Therefore, if the common mode range of the op-amp is not high enough, the current sensing will not work properly or will become less sensitive to the current signal.

In the 192W flyback converter design, the biggest challenge was the design of the voltage clamping circuit. The voltage clamping circuit consists of a diode, a resistor and a capacitor, and the use of this was to reduce the voltage stress on the MOSFET during the transition of the turn off time. To ensure the voltage can be clamped under the expected value, the expected turn off speed, the converter efficiency, the amounts of leakage inductance and leakage power need to be considered. The component value used in this flyback converter may not be the most suitable value, but it significantly reduced the MOSFET voltage stress with only 2% efficiency reduction.

Overall, a prototype of a battery equalisation system for the EV3 has been successfully designed, built and tested. The equalisation results show series-connected batteries can be equalised by either the combination of 24W buck-boost converters and a 192W buck-boost converter, or the combination of 24W buck-boost converters and a 192W flyback converter. However, there are two disadvantages found during these equalisation tests. First, because there is not any control system to accurately measure the open-circuit voltage from each battery and calculate how much time does the equalisation is required. Manual control the action of each converter is impractical. Second, since the 192W and the 24W converters can not be turned on at the same time, or any two 24W converters can not operate from the same battery at the same time. The time consumed on waiting for the other converter to complete their part of the equalisation process may be significant, which contributes to overall system inefficiency.

To improve the system capability, a microprocessor-based control system and a high accuracy battery monitoring system need to be implemented, and hence provide a more flexible control strategy and bring about a more efficient equalisation processes. Overall, this project gives a clear indication on how the designed battery equalisation system can be used on a series-connected battery string and what are the design considerations required.

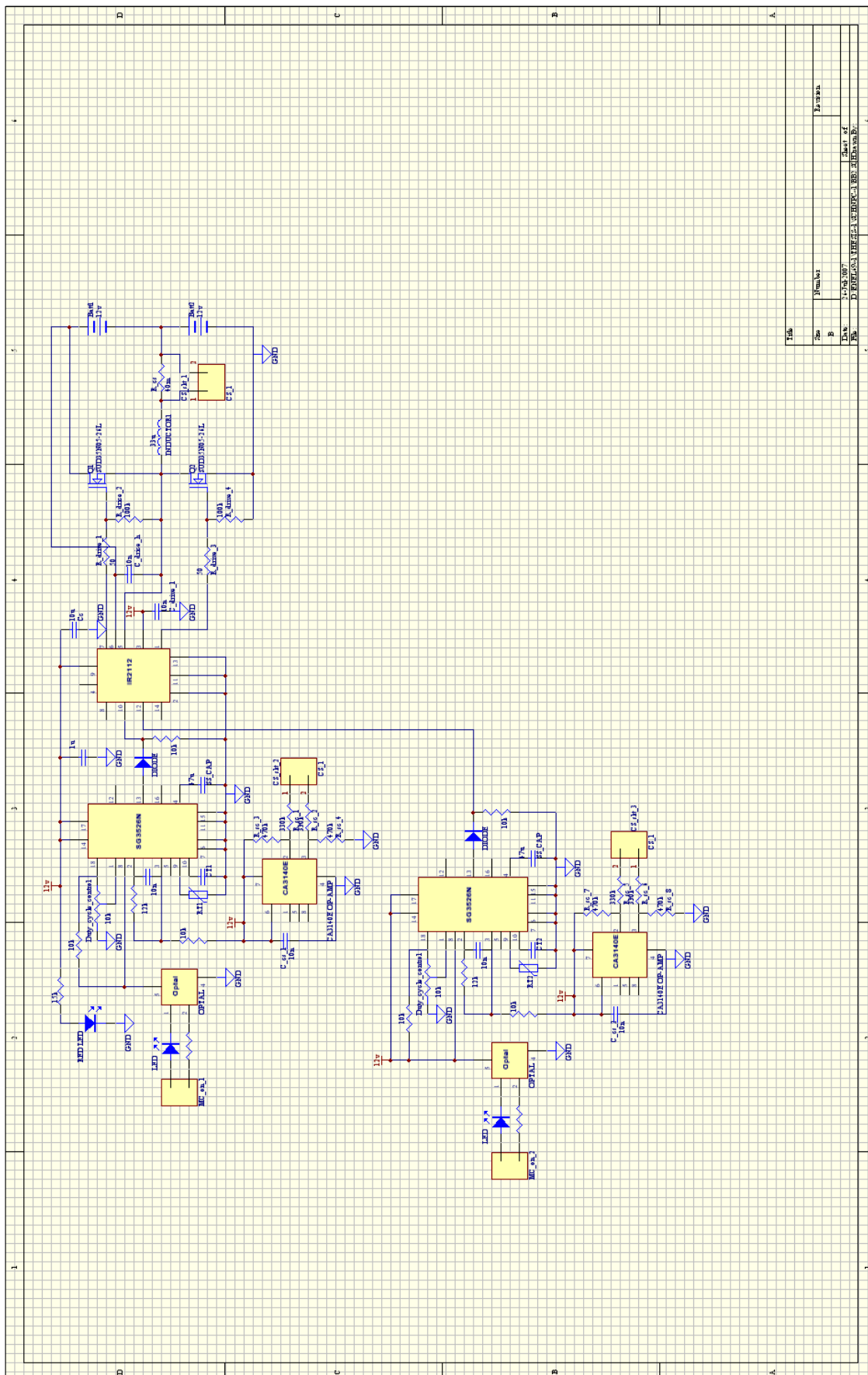
Appendix

The schematics of 24W buck-boost converter
192W buck-boost converter
192W flyback converter

The PCB of 24W buck-boost converter
192W buck-boost converter
192W flyback converter

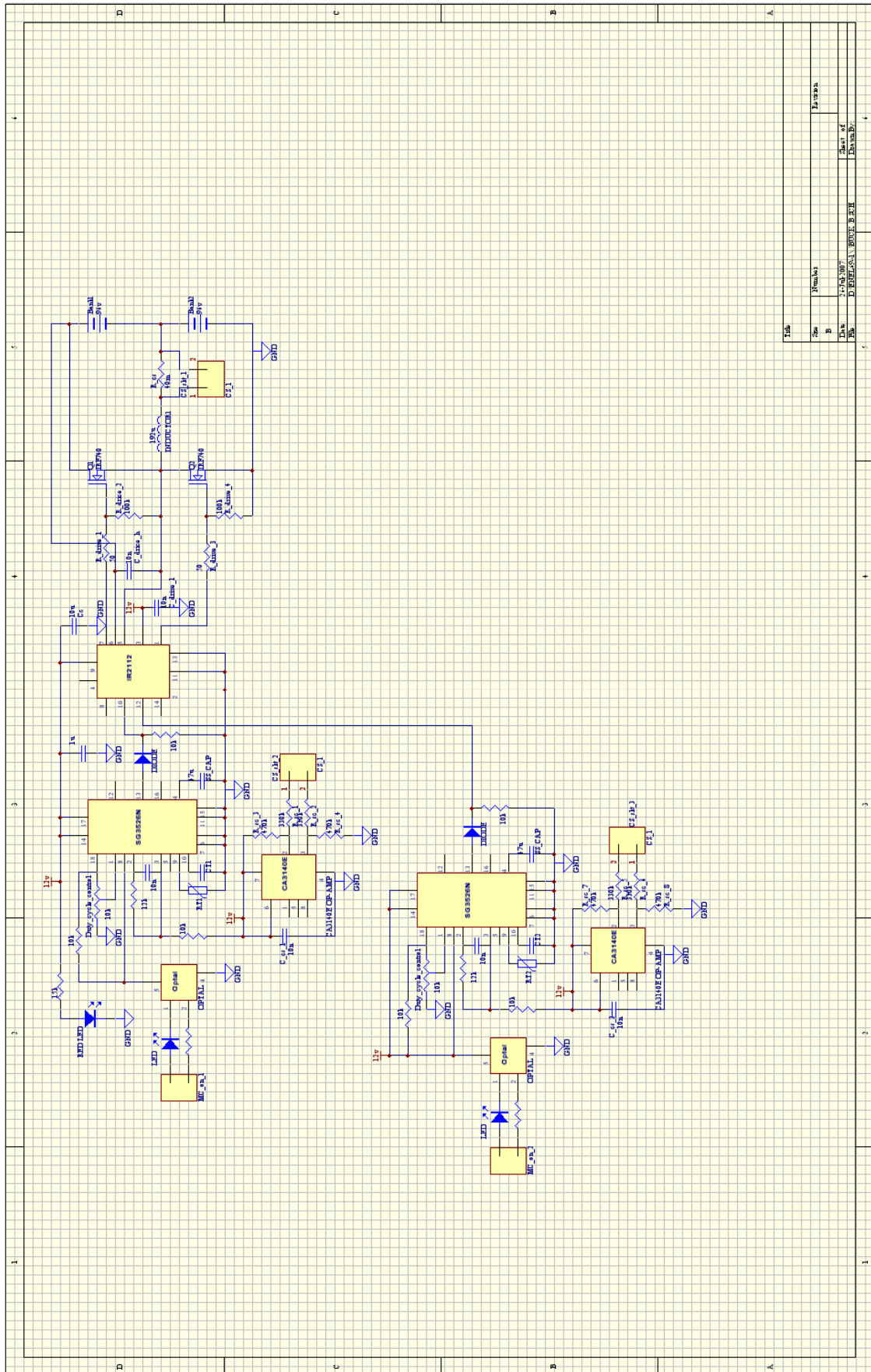
The data sheet of E32 planar inductor
E43 planar inductor
SUD35N05-26L MOSFET
IRF740 MOSFET

The schematics of 24W buck-boost converter



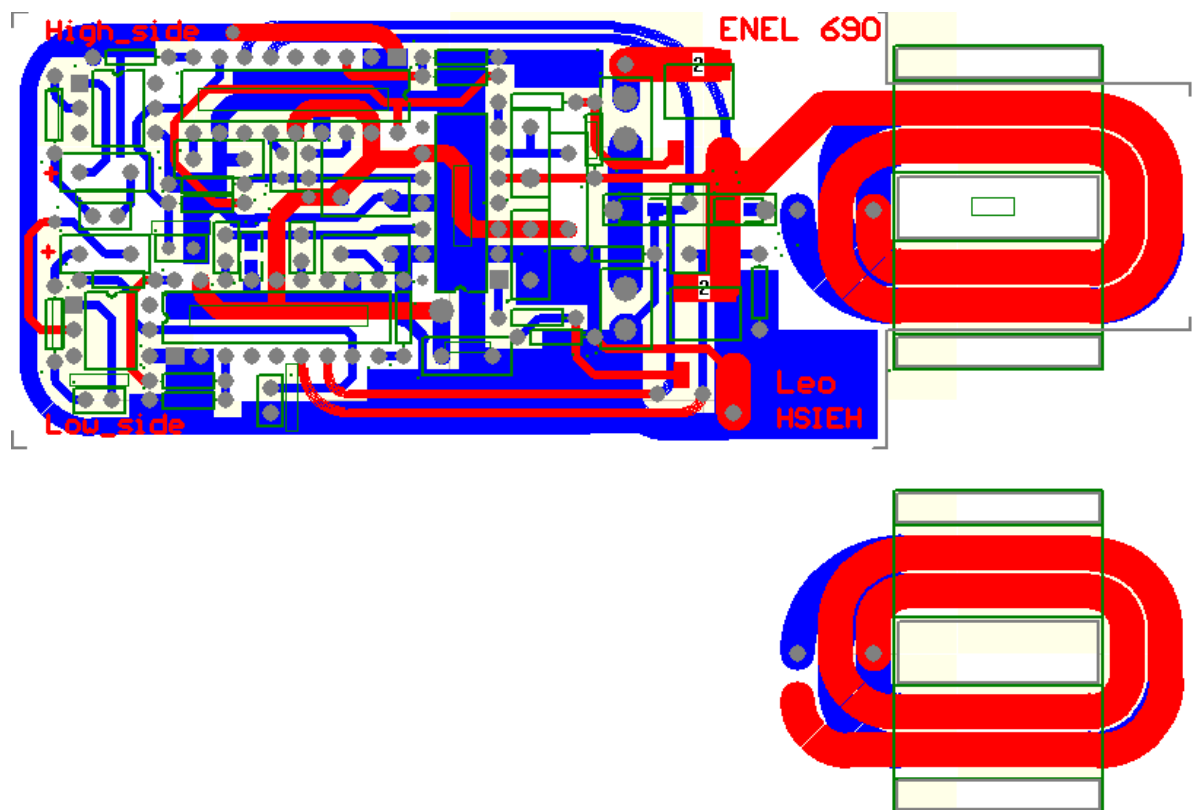
| Tab | Number | Part |
|-----|--------|-------|
| 1 | 1 | 12V |
| 2 | 1 | 100nF |
| 3 | 1 | 10μF |
| 4 | 1 | 100μF |
| 5 | 1 | 10k |
| 6 | 1 | 100k |
| 7 | 1 | 100Ω |
| 8 | 1 | 10k |
| 9 | 1 | 1k |
| 10 | 1 | 100k |
| 11 | 1 | 100Ω |
| 12 | 1 | 100k |
| 13 | 1 | 100Ω |
| 14 | 1 | 100k |
| 15 | 1 | 100Ω |
| 16 | 1 | 100k |
| 17 | 1 | 100Ω |
| 18 | 1 | 100k |
| 19 | 1 | 100Ω |
| 20 | 1 | 100k |
| 21 | 1 | 100Ω |
| 22 | 1 | 100k |
| 23 | 1 | 100Ω |
| 24 | 1 | 100k |
| 25 | 1 | 100Ω |
| 26 | 1 | 100k |
| 27 | 1 | 100Ω |
| 28 | 1 | 100k |
| 29 | 1 | 100Ω |
| 30 | 1 | 100k |
| 31 | 1 | 100Ω |
| 32 | 1 | 100k |
| 33 | 1 | 100Ω |
| 34 | 1 | 100k |
| 35 | 1 | 100Ω |
| 36 | 1 | 100k |
| 37 | 1 | 100Ω |
| 38 | 1 | 100k |
| 39 | 1 | 100Ω |
| 40 | 1 | 100k |
| 41 | 1 | 100Ω |
| 42 | 1 | 100k |
| 43 | 1 | 100Ω |
| 44 | 1 | 100k |
| 45 | 1 | 100Ω |
| 46 | 1 | 100k |
| 47 | 1 | 100Ω |
| 48 | 1 | 100k |
| 49 | 1 | 100Ω |
| 50 | 1 | 100k |
| 51 | 1 | 100Ω |
| 52 | 1 | 100k |
| 53 | 1 | 100Ω |
| 54 | 1 | 100k |
| 55 | 1 | 100Ω |
| 56 | 1 | 100k |
| 57 | 1 | 100Ω |
| 58 | 1 | 100k |
| 59 | 1 | 100Ω |
| 60 | 1 | 100k |
| 61 | 1 | 100Ω |
| 62 | 1 | 100k |
| 63 | 1 | 100Ω |
| 64 | 1 | 100k |
| 65 | 1 | 100Ω |
| 66 | 1 | 100k |
| 67 | 1 | 100Ω |
| 68 | 1 | 100k |
| 69 | 1 | 100Ω |
| 70 | 1 | 100k |
| 71 | 1 | 100Ω |
| 72 | 1 | 100k |
| 73 | 1 | 100Ω |
| 74 | 1 | 100k |
| 75 | 1 | 100Ω |
| 76 | 1 | 100k |
| 77 | 1 | 100Ω |
| 78 | 1 | 100k |
| 79 | 1 | 100Ω |
| 80 | 1 | 100k |
| 81 | 1 | 100Ω |
| 82 | 1 | 100k |
| 83 | 1 | 100Ω |
| 84 | 1 | 100k |
| 85 | 1 | 100Ω |
| 86 | 1 | 100k |
| 87 | 1 | 100Ω |
| 88 | 1 | 100k |
| 89 | 1 | 100Ω |
| 90 | 1 | 100k |
| 91 | 1 | 100Ω |
| 92 | 1 | 100k |
| 93 | 1 | 100Ω |
| 94 | 1 | 100k |
| 95 | 1 | 100Ω |
| 96 | 1 | 100k |
| 97 | 1 | 100Ω |
| 98 | 1 | 100k |
| 99 | 1 | 100Ω |
| 100 | 1 | 100k |

The schematics 192W buck-boost converter

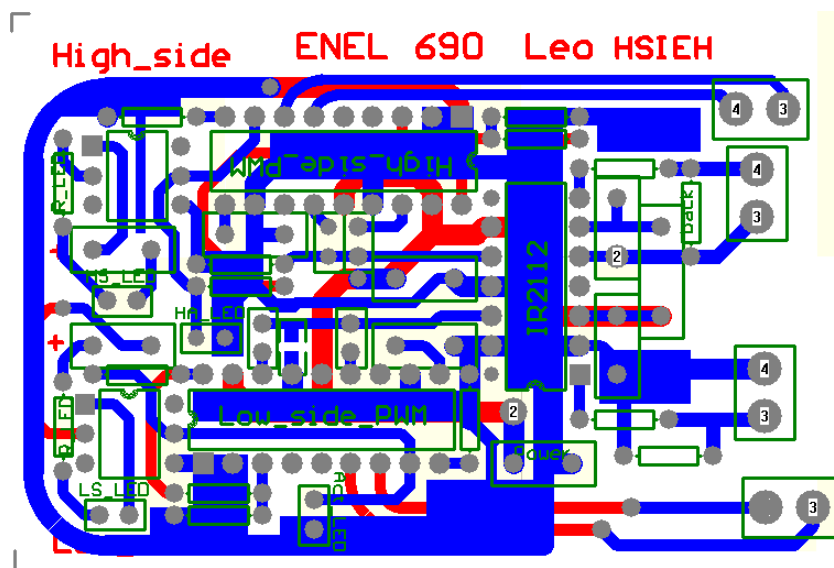


| Title | | Revision | |
|------------|--------|------------|--------|
| Rev | Number | Date | By |
| 1 | 1 | 11/03/2007 | W.H.P. |
| Date | | Drawn By | |
| 11/03/2007 | | W.H.P. | |

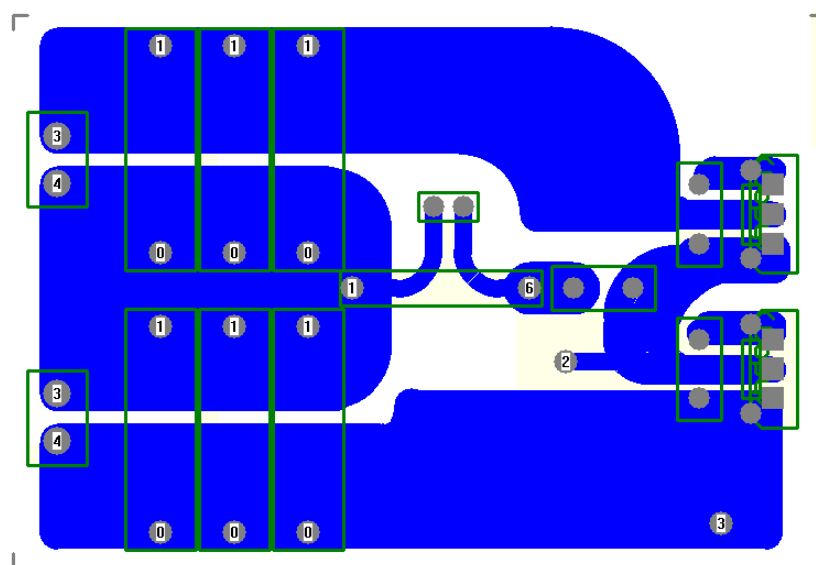
The PCB of 24W buck-boost converter



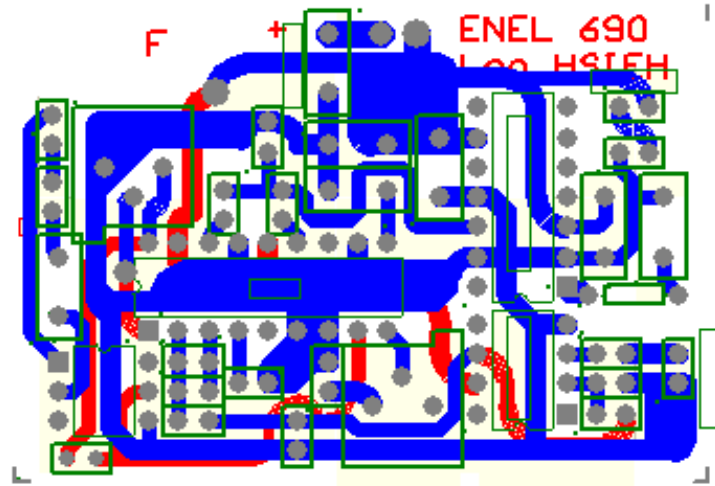
The PCB of 192W buck-boost converter



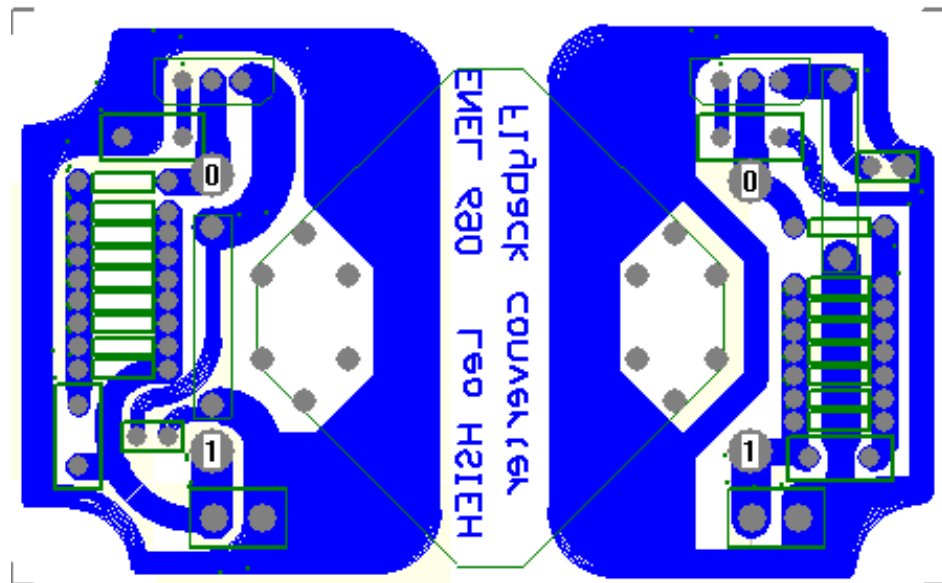
192W buck-boost controller



The PCB of 192W flyback converter



192W Flyback controller



192W Flyback power converter

The data sheet of E32 planar inductor

Ferroxcube

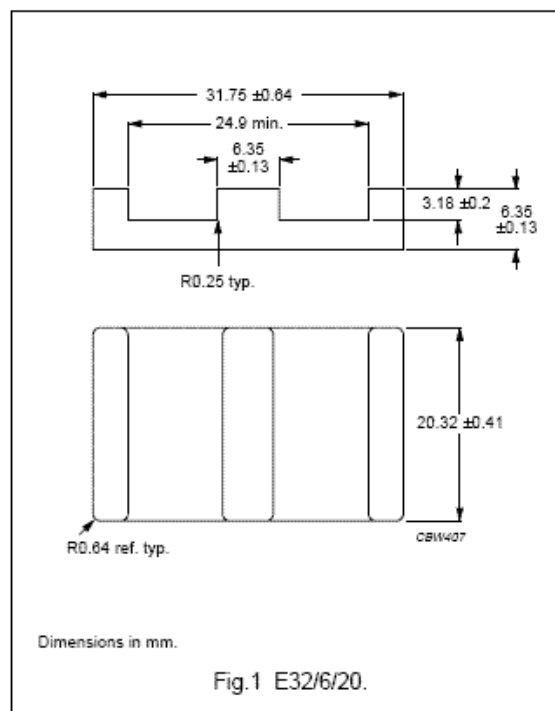
Planar E cores and accessories

E32/6/20

CORES

Effective core parameters of a set of E cores




| SYMBOL | PARAMETER | VALUE | UNIT |
|---------------|-------------------|-------|------------------|
| $\Sigma(l/A)$ | core factor (C1) | 0.323 | mm ⁻¹ |
| V_e | effective volume | 5380 | mm ³ |
| l_e | effective length | 41.4 | mm |
| A_e | effective area | 130 | mm ² |
| A_{min} | minimum area | 130 | mm ² |
| m | mass of core half | ≈ 13 | g |

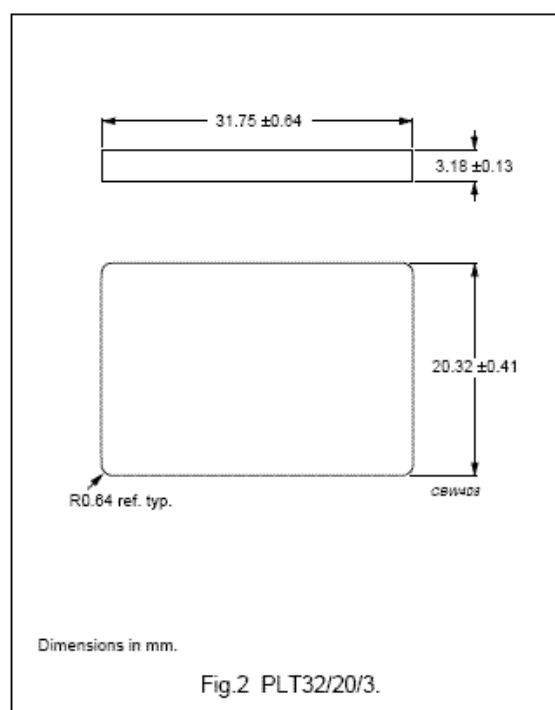


Effective core parameters of an E/PLT combination

| SYMBOL | PARAMETER | VALUE | UNIT |
|---------------|------------------|-------|------------------|
| $\Sigma(l/A)$ | core factor (C1) | 0.278 | mm ⁻¹ |
| V_e | effective volume | 4560 | mm ³ |
| l_e | effective length | 35.1 | mm |
| A_e | effective area | 130 | mm ² |
| A_{min} | minimum area | 130 | mm ² |
| m | mass of plate | ≈ 10 | g |

Ordering information for plates

| GRADE | TYPE NUMBER |
|--|-----------------|
| 3C90 | PLT32/20/3-3C90 |
| 3C94  | PLT32/20/3-3C94 |
| 3C96  | PLT32/20/3-3C96 |
| 3F3 | PLT32/20/3-3F3 |
| 3F4  | PLT32/20/3-3F4 |



The data sheet of E43 planar inductor

Ferroxcube

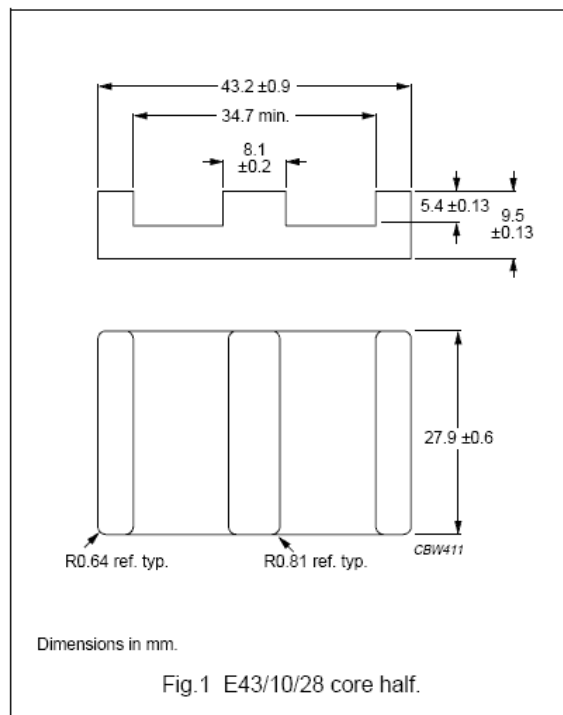
Planar E cores and accessories

E43/10/28

CORES

Effective core parameters of a set of E cores

| SYMBOL | PARAMETER | VALUE | UNIT |
|---------------|-------------------|-------|------------------|
| $\Sigma(I/A)$ | core factor (C1) | 0.276 | mm ⁻¹ |
| V_e | effective volume | 13900 | mm ³ |
| l_e | effective length | 61.1 | mm |
| A_e | effective area | 229 | mm ² |
| A_{min} | minimum area | 229 | mm ² |
| m | mass of core half | ≈ 35 | g |

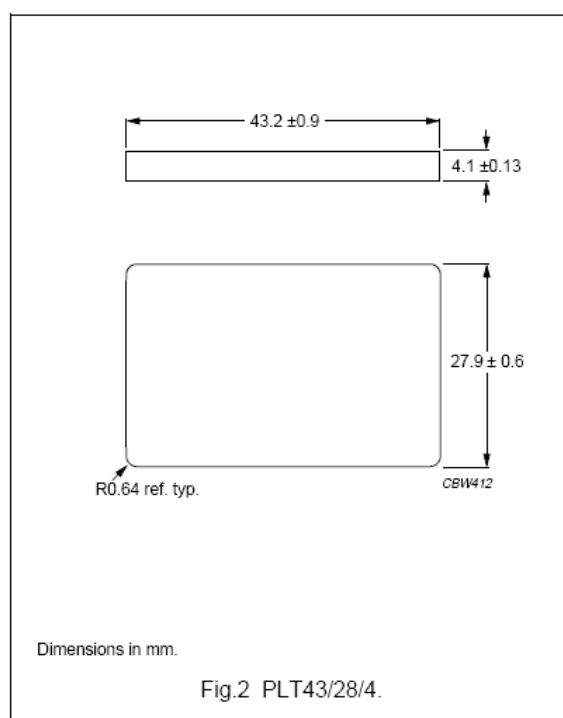


Effective core parameters of an E/PLT combination

| SYMBOL | PARAMETER | VALUE | UNIT |
|---------------|-------------------|-------|------------------|
| $\Sigma(I/A)$ | core factor (C1) | 0.226 | mm ⁻¹ |
| V_e | effective volume | 11500 | mm ³ |
| l_e | effective length | 50.4 | mm |
| A_e | effective area | 229 | mm ² |
| A_{min} | minimum area | 229 | mm ² |
| m | mass of core half | ≈ 24 | g |

Ordering information

| GRADE | TYPE NUMBER |
|-------------------------|-----------------|
| 3C90 | PLT43/28/4-3C90 |
| 3C94 <small>des</small> | PLT43/28/4-3C94 |
| 3F3 | PLT43/28/4-3F3 |
| 3F4 <small>des</small> | PLT43/28/4-3F4 |



The data sheet of SUD35N05-26L MOSFET



New Product

SUD35N05-26L

Vishay Siliconix

N-Channel 55-V (D-S) 175°C MOSFET

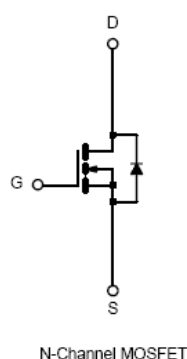
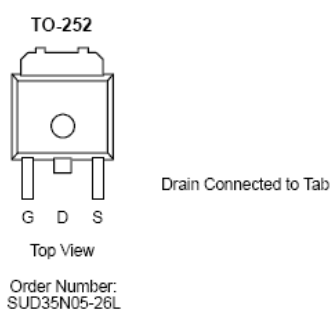
| PRODUCT SUMMARY | | |
|-----------------|---------------------------|------------------------|
| V_{DS} (V) | $r_{DS(on)}$ (Ω) | I_D (A) ^a |
| 55 | 0.020 @ $V_{GS} = 10$ V | 35 |
| | 0.026 @ $V_{GS} = 4.5$ V | 30 |

FEATURES

- TrenchFET® Power MOSFETS
- 175°C Rated Maximum Junction Temperature
- Low Input Capacitance

APPLICATIONS

- Automotive Fuel Injection Systems
- Automotive Wipers
- Automotive Door Modules



| ABSOLUTE MAXIMUM RATINGS ($T_A = 25^\circ\text{C}$ UNLESS OTHERWISE NOTED) | | | |
|---|----------------|---------------------------|------------------|
| Parameter | Symbol | Limit | Unit |
| Drain-Source Voltage | V_{DS} | 55 | V |
| Gate-Source Voltage | V_{GS} | ± 20 | |
| Continuous Drain Current ($T_J = 175^\circ\text{C}$) ^b | I_D | $T_C = 25^\circ\text{C}$ | A |
| | | $T_C = 100^\circ\text{C}$ | |
| Pulsed Drain Current | I_{DM} | 80 | |
| Continuous Source Current (Diode Conduction) ^a | I_S | 35 | |
| Maximum Power Dissipation | P_D | $T_C = 25^\circ\text{C}$ | W |
| | | $T_A = 25^\circ\text{C}$ | |
| Operating Junction and Storage Temperature Range | T_J, T_{stg} | -55 to 175 | $^\circ\text{C}$ |

| THERMAL RESISTANCE RATINGS | | | | |
|----------------------------------|------------|-----------------|---------|--------------------|
| Parameter | Symbol | Typical | Maximum | Unit |
| Junction-to-Ambient ^b | R_{thJA} | $t \leq 10$ sec | 17 | $^\circ\text{C/W}$ |
| | | Steady State | 50 | |
| Junction-to-Case | R_{thJC} | 2.5 | 3.0 | |
| Junction-to-Lead | R_{thJL} | 5.0 | 6.0 | |

Notes

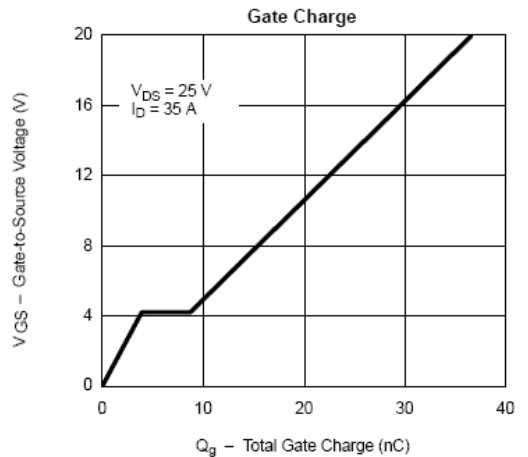
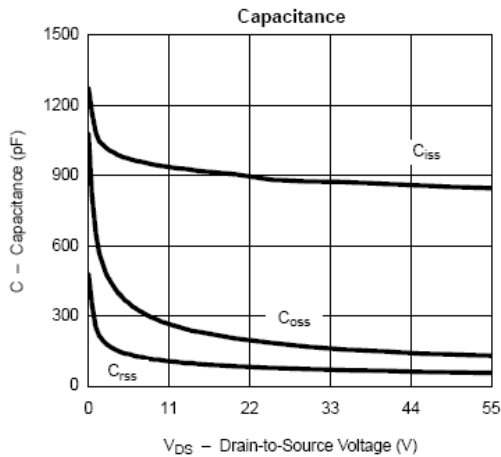
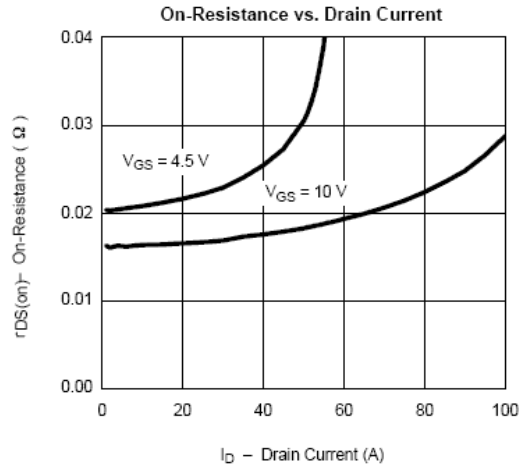
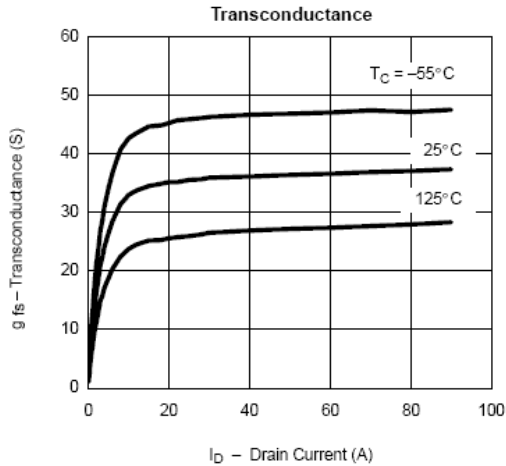
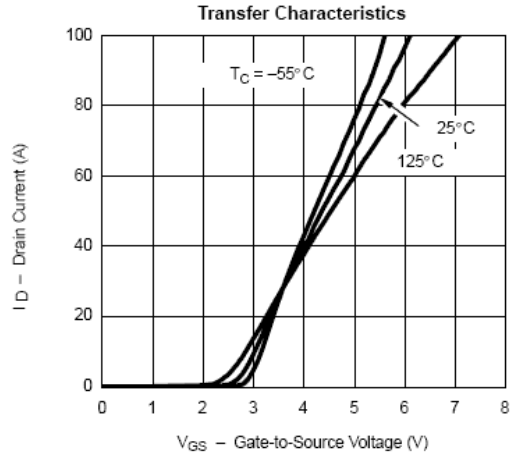
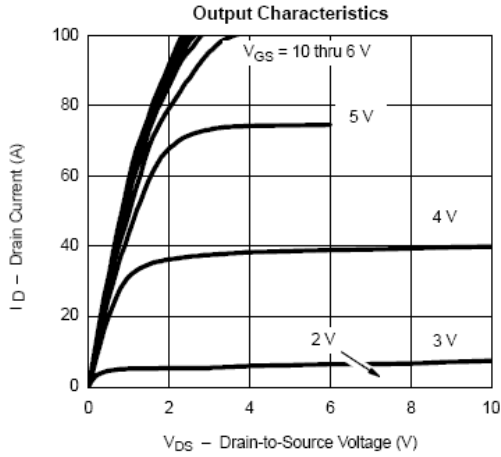
- Package Limited.
- Surface Mounted on 1" x 1" FR4 Board, $t \leq 10$ sec.
- See SOA curve for voltage derating.



New Product

SUD35N05-26L
Vishay Siliconix

TYPICAL CHARACTERISTICS (25°C UNLESS NOTED)



The data sheet of IRF740 MOSFET



IRF740

N-CHANNEL 400V - 0.46Ω - 10A TO-220
PowerMESH™II MOSFET

| TYPE | V _{DSS} | R _{DS(on)} | I _D |
|--------|------------------|---------------------|----------------|
| IRF740 | 400 V | < 0.55 Ω | 10 A |

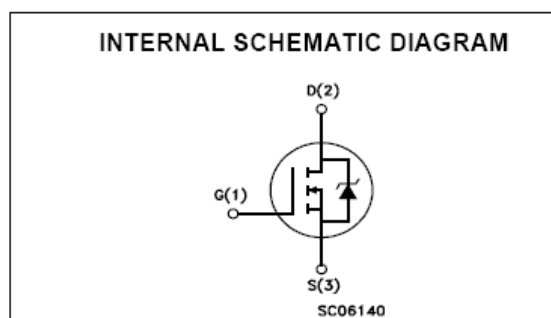
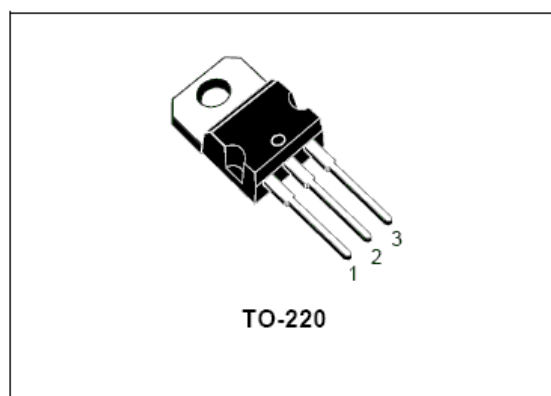
- TYPICAL R_{DS(on)} = 0.46Ω
- EXCEPTIONAL dv/dt CAPABILITY
- 100% AVALANCHE TESTED
- LOW GATE CHARGE
- VERY LOW INTRINSIC CAPACITANCES

DESCRIPTION

The PowerMESH™II is the evolution of the first generation of MESH OVERLAY™. The layout refinements introduced greatly improve the Ron*area figure of merit while keeping the device at the leading edge for what concerns switching speed, gate charge and ruggedness.

APPLICATIONS

- HIGH-EFFICIENCY DC-DC CONVERTERS
- UPS AND MOTOR CONTROL



ABSOLUTE MAXIMUM RATINGS

| Symbol | Parameter | Value | Unit |
|---------------------|--|-------------|------|
| V _{DS} | Drain-source Voltage (V _{GS} = 0) | 400 | V |
| V _{DGR} | Drain-gate Voltage (R _{GS} = 20 kΩ) | 400 | V |
| V _{GS} | Gate- source Voltage | ± 20 | V |
| I _D | Drain Current (continuous) at T _C = 25°C | 10 | A |
| I _D | Drain Current (continuous) at T _C = 100°C | 6.3 | A |
| I _{DM} (●) | Drain Current (pulsed) | 40 | A |
| P _{TOT} | Total Dissipation at T _C = 25°C | 125 | W |
| | Derating Factor | 1.0 | W/°C |
| dv/dt(1) | Peak Diode Recovery voltage slope | 4.0 | V/ns |
| T _{stg} | Storage Temperature | - 65 to 150 | °C |
| T _j | Max. Operating Junction Temperature | | |

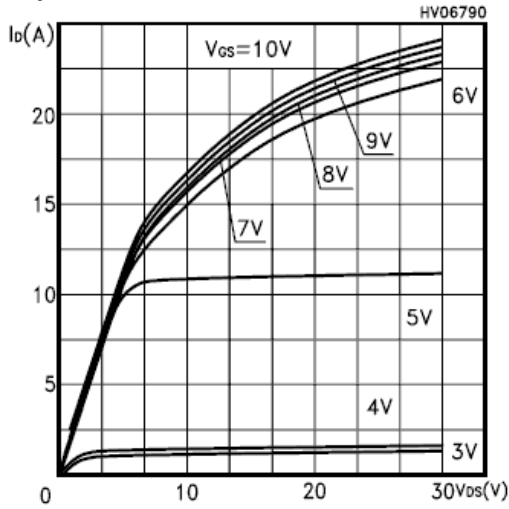
(●) Pulse width limited by safe operating area

(1) I_{SD} ≤ 10A, di/dt ≤ 120A/μs, V_{DD} ≤ V_{(BR)DSS}, T_j ≤ T_{JMAX}.

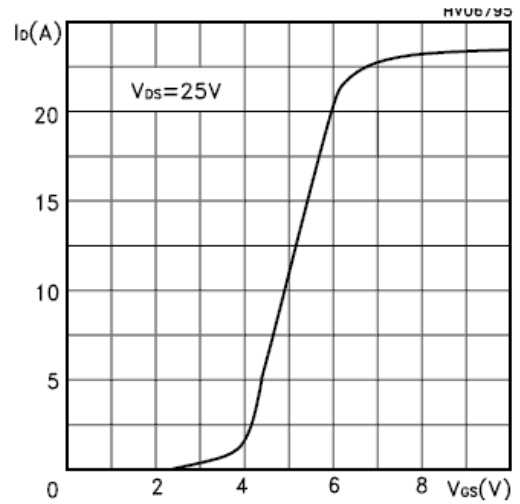
June 2002

IRF740

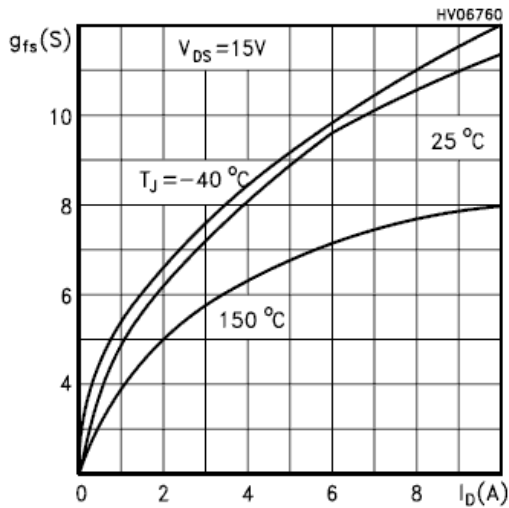
Output Characteristics



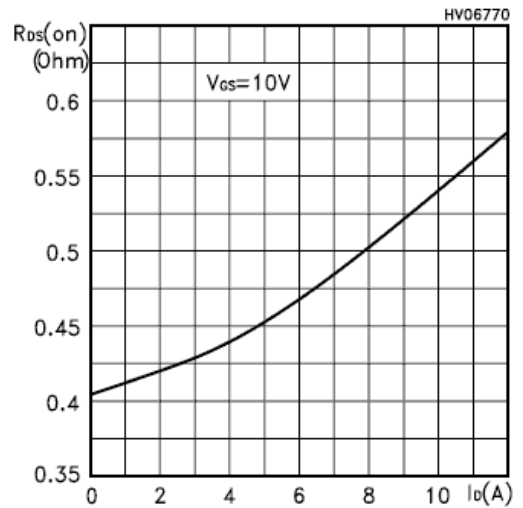
Transfer Characteristics



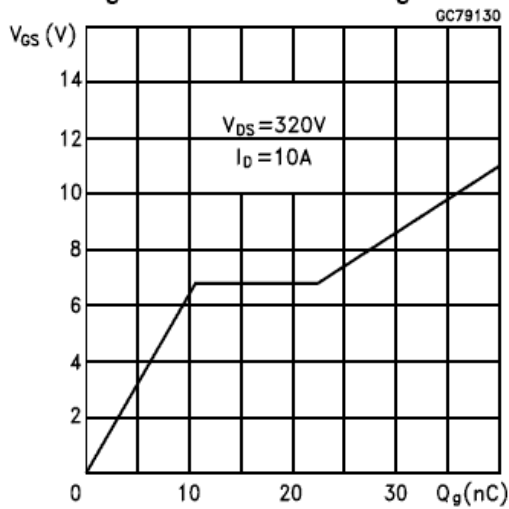
Transconductance



Static Drain-source On Resistance



Gate Charge vs Gate-source Voltage



Capacitance Variations

